COMMISSIONING OF A REFRIGERANT TEST UNIT AND ASSESSING THE PERFORMANCE OF REFRIGERANT BLENDS

Ndlovu Phakamile

B. Eng. (Hons) NUST Zimbabwe

Submitted in fulfilment of the Academic Requirements for the Awards of the Master of Science Degree in Engineering at the School of Chemical Engineering, University of KwaZulu-Natal.

December 2017

Supervisor: Prof Paramespri Naidoo.

Co-supervisors: Prof Deresh Ramjugernath, Prof J.D Raal and Dr Caleb Narasigadu

As the candidate's supervisor I agree to the submission of this thesis:

Prof. P. Naidoo Date

Declaration

I, Ndlovu Phakamile, student number 216074625 declare that:

(i) The research reported in this dissertation, except where otherwise indicated or acknowledged, is my original work.

(ii) This dissertation has not been submitted in full or in part for any degree or examination to any other university.

(iii) This dissertation does not contain other persons' data, pictures, graphs or other information unless specifically acknowledged as being sourced from other persons.

(iv) This dissertation does not contain other persons' writing unless specifically acknowledged as being sourced from other researchers. Where other written sources have been quoted, then:

a) Their words have been rewritten but the general information attributed to them has been referenced.

b) Where their exact words have been used, their writing has been placed inside quotation marks, and referenced.

(v) This dissertation is primarily a collection of material, prepared by myself, published as journal articles or presented as a poster and oral presentations at conferences. In some cases, additional material has been included.

Signed: Date:

Acknowledgements

I would like to thank God, the one "*in whom we live and move and have our being*" Acts 17 vs 28, who made it possible for me accomplish this feat. To my mother and father, thank you very much for grooming a man in me. My brothers and sister, dreams do come true.

I would express my gratitude to my supervisors, Prof Deresh Ramjugernath, Prof Paramespri Naidoo, Prof J.D Raal and Dr Caleb Narasigadu, for their invaluable knowledge they imparted, their academic guidance and support throughout my study. My academic life has been revolutionised because of learning from such academic giants.

I would like to thank Pelchem SOC, Fluorochemical Expansion Initiative and the NRF for financial assistance, as well as the Thermodynamics Research Unit's administrators, laboratory technicians, and the department's workshop technicians. Special thanks to A Khanyile for taking time to assist me in the equipment handling.

To my friends and colleagues at Chemical Engineering, I am forever grateful for the friendship and helpful criticism namely: Zibusiso L, Fredrick C, Obert M, Sandile N, Deliwe M, Emmanuel G, Thandiwe M, Tauheedah A and Dr Samuel I.

Finally, to Alisha Shadrach, we have finally achieved what you set out to do. The refrigerant unit is functioning perfectly, you did a great job in the design of the refrigerant unit.

Abstract

This study has two major purposes; to commission and to demonstrate that a new refrigerant test rig can be used for investigating the performance of different refrigerants and refrigerant blends. The motivation for this work is the need for testing new refrigerants or refrigerant blends to replace current refrigerants which are on the verge of being phased out due to environmental concerns (Montreal and Kyoto protocols). These protocols seek to implement refrigerants without any environmental impacts such as global warming potential and ozone depletion. In literature, several refrigerant test rigs that have been assembled and used in the investigation of different refrigerants are outlined, but there is limited coverage of refrigerant blends due to technical difficulties associated with the use of blends. Consequently, this places restrictions on their application, necessitating further research into properties, operating procedures, and equipment development.

A refrigerant test rig was designed and assembled at the University of KwaZulu-Natal to operate on the following cycles; simple vapour compression cycle, two-stage vapour – compression cycle, cascade system and vapour –compression cycle with a suction-line heat exchanger. In this study, the simple vapour compression cycle was used, with the refrigerant R134a being employed to validate the reliability and reproducibility of the refrigerant test rig. The main components of the cycle were the evaporator, the condenser, the compressor and the throttle valve. Water was used as the heat load and heat sink medium in the evaporator and the condenser, respectively. The temperature was measured by thermocouples and; pressure transducers were used for the measurement of pressure, and their combined expanded uncertainties were 0.1 ℃ and 0.026 MPa respectively. Commercial blends R507a and R413a, as well as a laboratory synthesised blend R134a/R125 in the ratio (66/34) and (50/50) by wt-%, were used in the investigation. The simulation of the refrigeration cycles was carried out using the Reference Fluid Properties Package **(**REFPROP**)** property method, which is a component within Aspen Plus ® V8.6. This software package allowed the prediction of the theoretical performance of the refrigerants, and refrigerant blends studied.

One objective of this study was to compare the performance of the test rig against the simulated results to assess the extent of the deviation between the practical and theoretical (ideal) results. Mollier charts were used to analyse experimental data. Refrigerant blend R507 displayed the best performance when compared to the refrigerants investigated in this study, with a coefficient of performance (COP) value of 5.00, while R413a had the lowest COP value of

4.00. Considering environmental aspects, R134a/R125 (66/34 wt %) with COP value of 4.88 has the least negative impact. The deviation between the theoretical and experimental values was within the experimental uncertainty, with a notable difference occurring in the evaporator inlet temperature. The results show that the test rig is fit for use in refrigeration experimental work. Furthermore, refrigerant blends showed good performance on the vapour compression cycles employed in this study proving that it is feasible to use the test rig in the investigation of refrigerant blending.

Nomenclature

English letters

b. p	boiling point
Cv	flow coefficient
e	specific exergy
E	exergy
f_x	Equivalent substance reducing ratios for the mixture
F_l	pressure recovery factor
gz	Specific potential energy [J/kg]
h	Specific enthalpy [J/kg]
h_x	Equivalent substance reducing ratios for the mixture
H	Enthalpy
I	exergy destruction rate [watts]
k_{ij}	Binary interaction parameter and are nonzero when $i \neq j$.
l_{ij}	Binary interaction parameter and are nonzero when $i \neq j$.
$\dot{m}$	Mass flow rate of the refrigerant [kg/s]
MPa	Mega Pascal
q	Heat transfer per unit mass [J/kg]
$\dot{Q}$	Rate of heat transfer between the control volume and its surroundings [J/s]
$\dot{Q}_{in}$	Refrigeration capacity [W]
R	gas constant (0.083144711bar mol^{-1} $K^{-1)}$
S	Entropy
T	Temperature
W	Energy crossing the boundary of a closed system/Energy transfer [J]
w	Work done per unit mass of the system
x_i	Concentration of component i in the mixture
x_j	Concentration of component j in the mixture
X_t	Pressure differential ratio factor
z^r	Residual compressibility factor

Greek Letters

η	Refrigeration efficiency
ρ	Density
τ	Reduced temperature (T_c / T)
δ	Reduced density (ρ/ρ_c)

Subscript

HEE	heat exchanger evaporator
HEC	heat exchanger condenser
i	inlet state
o	outlet state
in	quantities entering the system
out	quantities leaving the system
dew	dew point
bub	bubble point
Surr	Surroundings
r	residual fluid behavior

Superscript

c	critical point
”	inch

Abbreviations/Acronyms

AB	Alkylbenzene
ANSI	American National Standards Institute
ASME	American Society of Mechanical Engineers
CFC	Chlorofluorocarbon
cRIO	Compact Reconfigurable Input and Output unit
CV	Control volume
CSU	Combined standard uncertainty

COP	Coefficient of Performance
EPA	Environmental Protection Agency
EX	Expansion valve
GWP	Global Warming Potential
HCFC	Hydrochlorofluorocarbons
HFC	Hydrofluorocarbons
HFO	Hydrofluoroolefin
HP	High pressure cycle
HT	High-temperature circuit
HTF	Heat transfer fluids
HTC	Heat transfer coefficients
LCCP	Life cycle climate performance
LCA	Life-cycle assessment
LP	Low-pressure cycle
LT	Low temperature
mBWREOS	modified Benedict-Webb-Rubin Equation of State
MT	Medium temperature
NIST	National Institute of Standards and Technology
ODP	Ozone Depleting Potential
POE	Polyol ester oil
RE	Refrigeration effect
REFPROP	Reference fluid properties package
RTD	Resistance Thermometer Detectors
SLHX	Suction line heat exchanger
SWEOS	Schmidt-Wagner Equation of State
TEWI	Total Equivalent Warming Impact
UV	Ultra-violet
VCC	Vapour Compression Cycle
VCRS	Vapour Compression Refrigeration System

Table of Contents

Declaration.....i

Acknowledgements.....ii

Abstract.....iii

Nomenclature.....v

List of Figures.....xii

List of Tables.....xiv

Chapter 1.....1

1 Introduction.....1

1.1 Environmental Impact of Refrigerants.....1

1.2 Background to the Study.....3

1.3 Thesis Overview.....4

Chapter 2.....6

2 Principles of Refrigeration.....6

2.1 Refrigeration Cycles.....6

2.1.1 Vapour Compression Refrigeration Cycle.....6

2.1.2 Multistage Refrigeration Cycles.....10

2.1.3 Cascade Refrigeration Systems.....12

2.2 Energy Analysis.....14

2.3 Exergy Analysis.....18

Chapter 3.....23

3 Refrigerant and Refrigerant Blends.....23

3.1 Refrigerant Properties.....24

3.1.1 Evaporator thermodynamic features.....27

3.2 Refrigerant Blends.....27

3.2.1 Types of Refrigerant Blends.....28

3.2.2 Behavior of Blends.....29

3.3 Review of the Performances of Refrigerants and Refrigerant Blends.....29

Chapter 4.....36

4 Equipment Review.....36

4.1 Equipment Setups presented in literature.....36

Chapter 5.....45

5 Equipment Description.....45

5.1 Original Design.....45

5.2 Refrigerant Cycles in the Test rig.....48

5.3 General Unit Description 48
5.3.1 Piping 48
5.4 Component Specification 50
5.4.1 Expansion Valve 50
5.4.2 Heat Exchangers 50
5.4.3 Evaporator 51
5.4.4 Condenser 51
5.4.5 Suction Line Heat Exchanger 52
5.4.6 Compressor 52
5.4.7 Suction Accumulator 53
5.4.8 Moisture Indicator 54
5.4.9 Filter Dryer 54
5.4.10 Liquid Receivers 55
5.5 Instrumentation 55
5.5.1 Compact reconfigurable input and output (CRio) 55
5.5.2 Variable Frequency Drive (VLT) 57
5.6 Water Circuits 57
5.7 Design Modifications carried out in this work. 58
5.7.1 Valves 58
5.7.2 Evaporator water bath 59
5.7.3 Evaporator Rotameter 59
5.7.4 Condenser Chiller Bath 59
5.7.5 Addition of Temperature Probes 61
5.7.6 Charging Gauge 61
5.7.7 Insulation 61
5.7.8 Mass Balance 61
Chapter 6 65
6 Experimental Procedure 65
6.1 Preparation 65
6.2 Leak Testing and Detection 65
6.3 Start-Up 66
6.3.1 Vacant System 66
6.3.2 Charged System 67
6.4 Recovery of refrigerant Blends 68
6.5 Calibrations 69

6.5.1 Temperature 69
6.5.2 Pressure 70
6.5.3 Flowrate 70
6.5.4 Experimental Uncertainty Measurements 70
Chapter 7 73
7 Results and Discussions 73
7.1 Chemical Purity and Physical Properties of Refrigerants 73
7.2 Uncertainty in Measurements 74
7.2.1 Uncertainty Analysis for Refrigeration Systems 76
7.3 Commissioning of unit using R134a 77
7.3.1 Variables Investigated 79
7.3.2 Comparison of experimental results to literature. 84
7.4 Performance analysis of refrigerants R413a, R507a and R134a. 86
7.4.1 Variation of Compressor Work with COP 87
7.4.2 Variation of Evaporator Temperature with COP 87
7.4.3 Variation of Condenser Temperature with Compressor Work 89
7.4.4 Variation of Condenser Temperature with COP 90
7.4.5 Variation of Cooling Effect with COP 91
7.4.6 Variation of Condenser Water Flowrate effect with COP 92
7.4.7 Variation of Condenser water flowrate with Discharge Temperature 92
7.4.8 Variation of Refrigerant Charge with Discharge Temperature 93
7.4.9 Variation of Refrigerant Charge with Compressor Efficiency 94
7.4.10 Variation of Condenser and Evaporator water flowrate with Evaporator Refrigerant Temperature 95
7.5 Simulations for the Vapour Compression Cycle 96
7.5.1 Components Selection for the vapour compression cycle 97
7.5.2 Thermodynamics models employed in the study 97
7.5.3 Specifications of Simulation Parameters 100
7.5.4 Analysis of the simulated results 102
Chapter 8 109
8 Conclusions 109
Chapter 9 111
9 Recommendations 111
References 112
Appendices 119

Appendix A: Temperature Glide.....119
Appendix B: Technical Information of the Equipment Components 121
Appendix C: Refrigeration Cycle.....123
Appendix D: Uncertainty in Measurements.....130
Appendix E: Simulation results.....133
Appendix F: Simulation Procedure.....139
Appendix G: Lists of Refrigerants utilised in this study.....141

List of Figures

Figure 2-1: Components of Vapour-Compression Refrigeration Cycle. 7
Figure 2-2 : T-S diagram of an ideal vapour- compression cycle.(Extracted from Moran and Shapiro, 2006).....8
Figure 2-3: T-S diagram for a real simple vapour compression cycle.....9
Figure 2-4 : Multistage Compression Refrigeration System with a Flashing Chamber. 11
Figure 2-5 : Temperature-entropy diagram of a Multi-stage Compression System.(Extracted from Çengel and Boles, 2006). 12
Figure 2-6 : Two-Stage Cascade Refrigeration Cycle. 13
Figure 2-7 : Temperature-entropy diagram for Cascade Refrigeration system (Extracted from Çengel and Boles, 2006).....14
Figure 2-8 : Flowchart for the Exergy Analysis for a VCRS with two-Evaporators (Extracted from Yataganbaba et al., 2015).....22

Figure 3-1 : Comparison of Pressures of Lower Boiling and Higher Boiling Refrigerants at given Evaporator and Condenser Temperature. (Extracted from Arora, 2009). 25
Figure 3-2 : An (a) azeotropic refrigerant and (b) near-azeotropic refrigerant blend at a given pressure as they boil (Extracted from Whitman et al., 2013). 28

Figure 4-1 : Experimental set-up for R12, R134a, and R290/600a investigation (Extracted from Mani and Selladurai, 2008).....36
Figure 4-2 : The breadboard heat pump (Extracted from Jung et al., 2000).....38
Figure 4-3 : Schematic of the refrigeration unit (Extracted from Halimic et al., 2003). 39
Figure 4-4 : Schematic representation of the air/air heat pump test unit (Extracted from Sami and Desjardins, 2000). 40
Figure 4-5 : Schematic of the experimental setup for the performance test of CO_2/propane mixture (Extracted from Kim et al., 2007). 41
Figure 4-6 : Schematic of the multi-cycle R744 test rig (Extracted from Chesi et al., 2012).42
Figure 4-7 : Layout of the thermal load management system (Extracted from Chesi et al., 2012). 43

Figure 5-1 : Original schematic of the test unit (Produced by Shadrach, 2014).....47
Figure 5-2 : Stainless Steel vibration eliminator (Extracted from Heldon, 2009b). 49
Figure 5-3: Flow diagram of a single-pass counter flow arrangement (Extracted from Kakac et al., 2012). 51
Figure 5-4 : A Cross-sectional view of a Suction Accumulator (Extracted from Heldon, 2009a). 53
Figure 5-5 : Schematic Design of Modified test unit.....64

Figure 6-1 : Recovery Unit and the refrigeration system (Extracted from Dennis et al., 2010). 69

Figure 7-1 : Compressor Work vs. Coefficient of performance (COP). (*) R507, (▲) R413a, (●) R134a.....87

Figure 7-2 : Evaporating Temperature vs. Coefficient of performance (COP), (*) R507, (▲) R413a, (●) R134a.....88
Figure 7-3 : Condensing Temperature vs. Compressor Work, (▲) R413a, (●) R134a.....89
Figure 7-4 : Condensing Temperature vs. Coefficient of performance (COP), (▲) R413a, (●) R134a. 90
Figure 7-5 : Cooling effect vs. Coefficient of performance (COP), (*) R507, (▲) R413a, (●) R134a 91
Figure 7-6 : Condenser Water flowrate vs. Coefficient of performance (COP), (▲) R507, (●) R134a 92
Figure 7-7 : Condenser water flowrate vs. Compressor discharge temperature, (▲) R507, (●) R134a. 93
Figure 7-8 : Refrigerant charge vs. compressor discharge temperature, (▲) R413a, (●) R134a 94
Figure 7-9 : Refrigerant charge vs Compressor Efficiency, (▲) R413a, (●) R134a.....94
Figure 7-10 : Condenser and Evaporator water flowrate vs Evaporator Refrigerant Temperature. (right (●) R134a), left (▲) R507) 95
Figure 7-11 : Flowsheet of a single vapour compression cycle with Hot and Cold fluid cycles.....96

Figure A.1 : Temperature profiles of heat exchanger during the phase change of (a) pure refrigerant, (b) zeotropic refrigerant mixture with glide matching. (Rajapaksha, 2007).....119
Figure A.2 : Pressure and temperature profile for condensation of a non-azeotropic mixture. (Jung et al., 2003).....121

Figure C.1 : Simple VC configuration. 125
Figure C.2 : VC configuration using two compressors. 126
Figure C.3 : Configuration for VC with suction line heat exchanger. 127
Figure C.4 : Cascade VC cycle configuration 128
Figure C.5 : Two-stage VC cycle configuration. 129

List of Tables

Table 3-1 : Summarised Properties of an ideal Refrigerant (Compiled from Arora, 2009; Sapali, 2009; Mohanraj et al., 2011).....26
Table 3-2: A Review of Studies published on Refrigerants and Refrigerant Blends.....30
Table 5-1 : Geometric Specifications of the Heat Exchangers. 52
Table 5-2 : Specifications of Instruments 57
Table 7-1 : Details of the chemicals used in this study. 73
Table 7-2 : Thermodynamic Properties of Refrigerants.....74
Table 7-3 : Temperature Sensors Calibration Details. 75
Table 7-4 : Pressure Transducers Calibration Details. 75
Table 7-5 : Uncertainties in measurements related to this study.....76
Table 7-6 : Results during commissioning of unit using R134a. 78
Table 7-7 : Effects of the Condenser Flowrate on system. 80
Table 7-8 : Effects of Refrigerant Mass on the system. 81
Table 7-9 : Comparison of Effects of Power Settings on the system.....82
Table 7-10 : Comparison of Refrigerant Properties at different degrees of throttling. 83
Table 7-11 : Comparison of Experimental results to literature for R134a with Evaporator (4-5 ^{o}C) and Condenser (40 ^{o}C).....85
Table 7-12 : Specification of Simulation Variables. 101
Table 7-13 : Comparison of Simulated COP results for refrigerants and refrigerant blends. 102
Table 7-14 : Comparison of the experimental and simulated results for R134a. 103
Table 7-15 : Comparison of the Experimental and simulated results for R507. 104
Table 7-16 : Comparison of the experimental and simulated results for R413a. 105
Table 7-17 : Comparison of simulated results for R134a, R125, and R134a/R125 blends. .107

Table A.1: Azeotropic Refrigerant blends temperature glide for selected CFCs/HCFCs replacements determined at 100kPa. (Rajapaksha, 2007). 119

Table B.1 : Compressor Specifications 122
Table B.2 : Valves Specifications (Swagelok Company, 2013). 122

Table E.1 : Simulation Results for R413a 133
Table E.2 : Simulation Results for R134a 134
Table E.3 : Simulation Results for R134a/R125 (50/50 wt %).....135
Table E.4 : Simulation Results for R134a/R125 (66/34 wt %).....136
Table E.5 : Simulation Results for R507 137
Table E.6 : Simulation Results for R125 138

Table G.1 : List of Refrigerants used in this study 141

Chapter 1

1 Introduction

Until recently, contemporary refrigeration technology used for temperature regulation within built structures and the preservation of perishables, was dependent largely on chlorofluorocarbons and hydrochlorofluorocarbons as refrigerants. This dependence was due to their excellent physical and thermodynamic properties. However, these refrigerants are being phased out from the market due to their adverse environmental impact.

This project is in line with the ongoing global research on refrigerants and refrigerant blends. It seeks to come up with the most fitting substances to replace chlorofluorocarbons (CFCs) and hydrochlorofluorocarbons (HCFCs). The application of CFC-free refrigerant blends also provides a means of assisting air-conditioning and refrigeration industries in complying with the CFC phase-out provision, (Szymurski (2005) and Goetzler et al. (2014)), under the Montreal Protocol, without harming the interests of end users.

This study which investigates new refrigerant blends and use of fluorochemicals, also concurs with the South African Fluorochemicals Expansion Initiative (FEI) research which seeks to explore the use of fluorochemicals and fluorine products in various areas across multiple market sectors (Pelchem, 2014). The program was launched by the Government in 2008 (South African Government Press Release, 2009), through Pelchem, a chemical division of the Nuclear Energy Corporation of South Africa. These include fluorocarbons which can be converted to refrigerants and refrigerant blends, consequently tapping into the fluorspar reserves which are abundant in the country. Utilisation and beneficiation of the fluorspar reserves will promote the economic development of the nation.

1.1 Environmental Impact of Refrigerants

Molina and Rowland (1974), stated that the chlorine ion in chlorofluorocarbons (CFCs) was responsible for the destruction of the stratosphere's ozone layer. The ozone layer protects the earth surface by absorbing the sun's UV rays. CFCs have a long lifespan (Satyanarayana and Kotaiah, 2012). Therefore, a single chlorine molecule in the stratosphere repeatedly reacts with, and causes deterioration of ozone molecules, leading to a "hole" in the ozone layer (Angell, 1988; Sivasakthivel and Reddy, 2011). The discovery of the hole in the ozone layer marked

the beginning of the decline in the widespread use of CFCs and HCFCs, which in turn, provides the motivating factor for research into alternative refrigerants.

By the 1980s, the destruction of ozone by refrigerants caught the attention of the international community leading to a number of international agreements which affected the refrigeration industry. In the year 1987, 27 nations convened in Montreal Canada, and signed a global environment treaty. Under this agreement, industrialised countries were obliged to begin phasing out CFCs by 1993, and to achieve a 50% reduction relative to 1986 consumption levels, by 1998 (United Nations Montreal Protocol, 1987). At meetings in London (1990) Copenhagen (1992), Vienna (1995), Montreal (1997) and Beijing (1999) amendments were adopted with the intention of speeding up the phasing out of ozone-depleting substances (United States EPA, 2007). In the year 2014, a proposal, by Mexico, Canada, and the United States, was made to amend the Montreal Protocol to cut the production and use of hydrofluorocarbons (HFCs) by 85% in the period 2016-2035 for industrialised countries (United Nations EPA, 2014).

Due to the adverse effects of climate changes, and the escalation of greenhouse gases in the atmosphere from uncontrolled emissions, 192 nations convened in Kyoto Japan in 1997 and penned a concord, which became known as the Kyoto Protocol (Baxter et al., 1998). Under this agreement, countries were to reduce the discharge of greenhouse gases (by 5% by the year 2012 relative to the 1990 emission levels) and lessen the use of global warming potential (GWP) substances (Breidenich et al., 1998). All halocarbon refrigerants are categorised as GWP substances, and their presence in the atmosphere contributes to global warming. A total equivalent warming index (TEWI) method was developed to quantify and analyse the greenhouse effect caused by the emission of refrigerants' from a refrigeration system (Bitzter, 2014). Also, the environmental impact of the refrigerant over the entire life cycle of the fluid and the equipment was evaluated with the life cycle climate performance (LCCP) formula. The lower the LCCP for a refrigerant the lesser is its environmental impact, hence, the more desirable it will be for refrigeration applications (Abdelaziz et al., 2012).

As a result of the current environmental regulations, based upon scientific findings, stipulations have been made that refrigerants must be; substances with lower global warming potential, zero ozone depletion potential (ODP), and comply with requirements for safety, material compatibility, and suitability (Calm, 2008). Hydrochlorofluorocarbon (HCFC) refrigerant mixtures and hydrofluorocarbons (HFCs) have proven to be suitable replacements possessing most of the required properties (Akintunde, 2013). Hydrofluorocarbon mixtures and

hydrocarbons have a short atmospheric lifetime making them attractive for use in air conditioning and refrigeration systems (Sekiya and Misaki, 2000). Hydrocarbon refrigerants such as isobutene, propane and *n*-butane are considered for refrigeration due to the ODP and GWP effects of the current refrigerants. However, the main shortcoming of hydrocarbons in refrigeration is their high flammability (Mani et al., 2013).

1.2 Background to the Study

The motivation to design the refrigerant unit in this study was driven by the need to be able to test different refrigerants and refrigerant blends over a wide range of operating conditions using different refrigeration cycle configurations. Furthermore, it seeks to address the practical aspect of the theoretical study carried out by Satola (2014) within the Thermodynamics Research Unit. Satola worked on a predictive tool to enable development of suitable refrigerant combinations which are environmental friendly for use in refrigeration applications. This was performed using computational software ASPEN Plus ® along with Dortmund Data Bank (DDB) imported into Visual Basic for Applications (VBA) project. In his work, he proposed many refrigerant blends which can be utilised as replacements for R22 refrigerant.

The refrigeration test rig utilised in this study was designed and built in the Thermodynamics Research Unit in 2012 by Ms Alisha Kate Shadrach a MSc. Eng. Student under the supervision of Professors J.D Raal, P Naidoo, and D Ramjugernath. While the unit was assembled in 2014, it was not commissioned. Shadrach did not overcome the issues of sealing in achieving very low pressures/vacuum in the refrigeration system. Hence further test measurements could not be performed. There were also various problems encountered in the piping and location and/or installation of key units.

In this study, major modifications were performed to deem the unit suitable for experimental measurements. These included overcoming the challenge of pressure loss in the experimental unit. This pressure loss was mainly due to leaks in the condenser seals, vibration eliminators and in many loose joints in the unit. To achieve the throttling effect there was also a need to remove the metering valve due to its small orifice which was a hindrance to the passage of the liquid refrigerant to the expansion valve. Furthermore, there was a need to replace the water baths at the condenser and evaporator with larger ones to meet the duties of these two heat exchangers.

The unit was designed to operate in several thermodynamic (refrigeration) cycles namely: the simple vapour compression cycle, two-stage vapour compression cycle, cascade system and vapour compression cycle with a suction-line heat exchanger. The novelty of the design is the selection of compressors with variable drive motors used to vary the operating conditions over a wide range and thus enabling the operator to adjust compressor speed to suit the type of refrigerant under investigation. The refrigeration unit will allow for a preliminary evaluation of the performance (and hence suitability), of the proposed new refrigerant blends in refrigeration applications; and the identification of optimum operating ranges in different cycles.

In this study, it was necessary to first commission the test unit. This was achieved by ensuring that the unit was sealed and could maintain a vacuum level of 26.6 kPa abs. Refrigerant R134a was used to test the unit to deem it functional and suitable for refrigeration experimental work by obtaining repeatable and reproducible experimental results which were comparable to published data. Two commercial blends, R413a and R507a, were proposed for investigations so that their performance could be compared with that of R134a, and their suitability for replacing R134a in its refrigeration cycles. Laboratory synthesised mixtures of R134a/R125 in different weightings were then studied and their performance was compared to that of R134a, R507a, and R413a.

Vapour compression refrigeration cycle simulations were performed using the REFPROP program in Aspen Plus V8.6, an engineering software package, to compare the performance of the simulations (ideal) with experimental results.

1.3 Thesis Overview

In this study, the performance of two commercial refrigerant blends, R413a and R507 as well as a laboratory synthesised blend composed of R134a/R125 in the ratios 50/50 and 66/34 by wt.% were analysed in a vapour compression refrigeration cycle (VCRS). Refrigerant R134a was used as the benchmark in the study.

Chapter two briefly explains the principles of refrigeration. It describes the purpose of each component in the refrigeration cycle, different refrigeration cycles, and the energy as well exergy analysis of the vapour compression refrigeration cycles.

Chapter three presents a literature review on refrigerant blends and their environmental effects. It also describes the nature of different refrigerants and its properties. Literature data is presented from studies performed on R134a, R413a, R507 and various refrigerant blends. In the fourth Chapter, equipment reviews of the refrigerant test units previously employed for refrigeration studies is presented.

The description of the refrigeration unit used in this study is presented in Chapter five. Chapter six outlines the experimental procedure followed in operating the unit. The results obtained in this study are presented and discussed in Chapter seven. These include the chemical purity and physical properties of the refrigerants, uncertainty in measurements, commissioning results obtained, compatible analysis of the performance of the refrigerant blends in the test rig and the simulation results. Lastly, the conclusions and recommendations are provided in Chapter eight and nine respectively.

Chapter 2

2 Principles of Refrigeration

Refrigeration utilises a chemical substance to maintain a low-temperature environment by continuously rejecting heat to a higher temperature environment when the vapour produced is condensed for reuse. The absorption of heat is traditionally achieved by the evaporation of a liquid in a continuous flow process. In the refrigeration cycle, the direction of heat transfer is from a lower temperature point to an elevated temperature point. However, according to the second law of thermodynamics, this is not possible without an external supply of energy (Smith et al., 2005).

Vapour compression systems are widespread in refrigeration. In these systems, a vapour cycling process causes the working fluid, also known as the refrigerant to undergo phase changes. For the refrigeration process to occur a continuous removal of heat from the low-temperature point must occur. This cooling can be achieved by evaporating the liquid refrigerant in a steady-state flow process. The vapour can be returned to its original liquid state to be re-evaporated either one of two ways:

- it can simply be compressed and then condensed;
- it can be absorbed by a less volatile liquid, whence it can be evaporated at an elevated pressure (Smith et al., 2005).

To fully comprehend the refrigeration cycle, the Carnot vapour refrigeration cycle must be understood, as the operation of the refrigeration cycle is derived from that of the Carnot cycle (the most efficient cycle with the highest coefficient of performance (COP).

2.1 Refrigeration Cycles

2.1.1 Vapour Compression Refrigeration Cycle

The principle of operation of vapour refrigeration originated from a reversed Carnot power cycle. In the vapour compression cycle, the turbine in the Carnot cycle is replaced with a throttling device which can be an expansion valve, an expansion engine or capillary tube. It is cheaper to use an expansion valve or capillary tube than an expansion engine due to the high cost of the engine required to operate with two-phase flow. Components of an ideal vapour compression refrigeration cycle are illustrated in Figure 2.1. This cycle finds wide application

in refrigerators, heat pumps and air conditioning systems. Figure 2.1 shows work and energy transfer when the system is operating in a steady state. A brief description of the units in the cycle is given below.

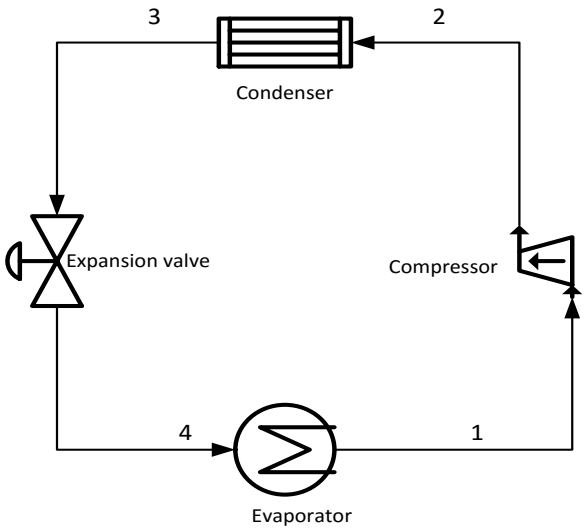

Figure 2-1: Components of Vapour-Compression Refrigeration Cycle.

Evaporator

The low pressure, cool liquid-vapour refrigerant passes through the evaporator where it interacts with the heat load or the medium to be maintained at a low temperature. The low-pressure refrigerant in the evaporator absorbs heat from the medium to be cooled and boils, producing low-pressure vapour at saturation conditions.

Compressor

The saturated vapour exits the evaporator and then passes into the compressor. The addition of shaft work to the saturated vapour raises its pressure. When the pressure of the refrigerant increases, the boiling and condensing temperatures of the refrigerant are elevated as well. Sufficiently compressing the gas raises its boiling point higher than the temperature of the heat sink (cooling medium), which is the higher temperature medium of the system.

Condenser

The compressed high-pressure gas carrying heat energy acquired at the evaporator as well as from the work done by the compressor (in gas-compression and due to friction) enters the condenser. The high-pressure refrigerant changes phase at constant temperature and pressure

to a saturated liquid as it rejects heat to the system's heat sink. The heat source (high-pressure vapour) is condensed as it transfers heat energy to the heat sink.

Expansion Valve

The pressurized saturated liquid refrigerant expands at the throttling valve to the evaporator pressure. An irreversible adiabatic expansion resulting in the decrease in refrigerant pressure, as well as an increase in entropy occurs. At the valve's outlet, a liquid-vapour mixture of the refrigerant is obtained.

The performance of the ideal vapour –compression cycle can be evaluated if the irreversibilities within the compressor, condenser and evaporator are neglected. Therefore, no pressure drops due to friction are experienced. This also means there are no pressure losses due to refrigerant's flows through the heat exchangers. If the compression of the refrigerant occurs without irreversibility and heat losses from the system, then the compression process is isentropic. Considering the above assumptions, the temperature-entropy diagram for a vapour-compression refrigeration cycle is shown in Figure 2.2.

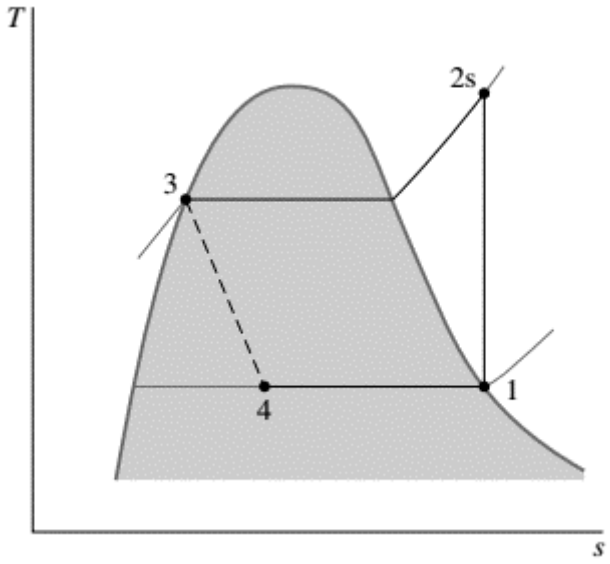

Figure 2-2 : T-S diagram of an ideal vapour- compression cycle.(Extracted from Moran and Shapiro, 2006).

The ideal cycle is made up of the following sequence of processes:

Process 1-2s: The refrigerant vapour is compressed isentropically from the evaporator pressure at state 1 to the condenser pressure at state 2s.

Process 2s-3: Isobaric cooling occurs from point 2s to the vapour saturation curve. Subsequently, the gaseous refrigerant loses heat as it transverses through the condenser at constant pressure. The refrigerant leaves the condenser as saturated liquid at state 3.

Process 3 -4: Isenthalpic expansion of the saturated liquid refrigerant from state 3 to a liquid – vapour mixture (two-phase mixture) at stage 4.

Process 4- 1: Evaporation of liquid refrigerant at a constant (low) pressure and temperature, as heat is absorbed from the surroundings/ heat transfer fluid.

The actual vapour –compression cycle is at variance from the ideal cycle because of the irreversibilities in some components in the refrigeration cycle. The pressure-entropy diagram of a real cycle is shown in Figure 2.3.

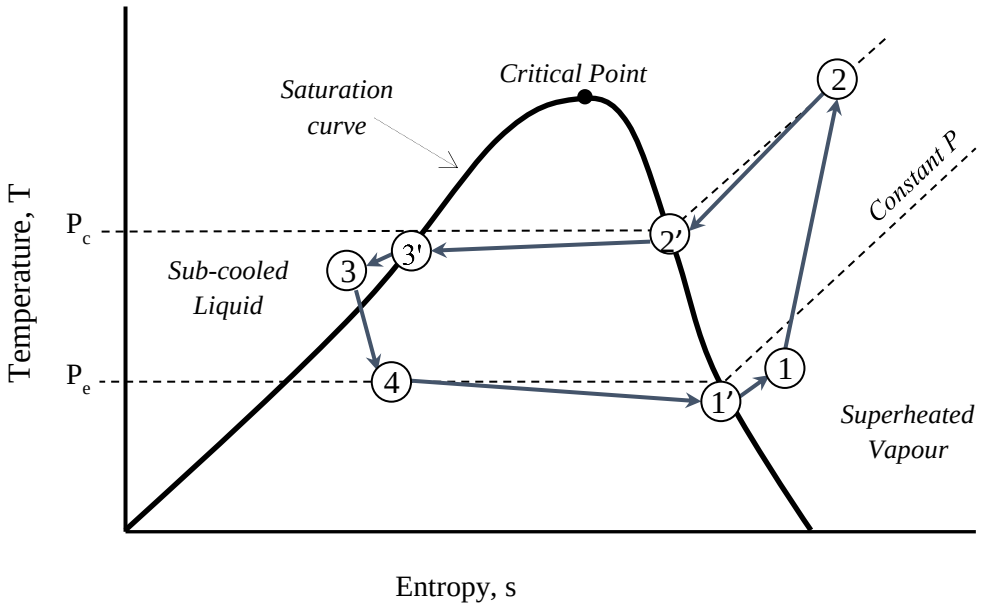

Figure 2-3: T-S diagram for a real simple vapour compression cycle.

The real cycle deviates from the ideal (theoretical) cycle in the following ways:

- In the actual cycle, at the compressor inlet at state 1, the refrigerant vapour is slightly superheated instead of a saturated vapour as in the ideal cycle.
- Heat losses to the surroundings and pressure drop can be substantial in the suction line (pipeline connecting the evaporator to the compressor) (process 1'-1) in Figure 2-3.

- Due to the internal irreversibility of the compressor, the entropy of the vapour is increased. However, a multi-stage compressor with inter-cooling results in a lower entropy at 2'.
- In practice, the refrigerant leaving the condenser is a subcooled liquid, hence it has a higher cooling capacity. Furthermore, sub cooling prevents vapour flashing at the expansion valve. This process is represented by 3'-3 in Figure 2-3.
- Addition and rejection of heat at the evaporator and condenser respectively do not occur at constant temperature and pressure.

2.1.2 Multistage Refrigeration Cycles

Vapour compression cycles are used for a broad range of applications. However, their performance is inadequate for the numerous and diverse industrial applications. The vapour compression cycles are modified to produce other refrigerant cycles which provide very low temperatures which are otherwise not possible with the simple vapour compression cycle. It provides a means where refrigeration is achievable for a system with a vast variance between the suction and discharge pressures without increasing the temperature of the compressor.

Multi-stage compression refrigeration is generated by combining two simple vapour compression cycles. A flash chamber with a small mixer takes the place of the condenser of low-pressure cycle and evaporator in the high-pressure cycle. The multistage compression refrigeration system illustrated in Figure 2.4, with compression accomplished by two compressors in a single refrigeration circuit using the same refrigerant.

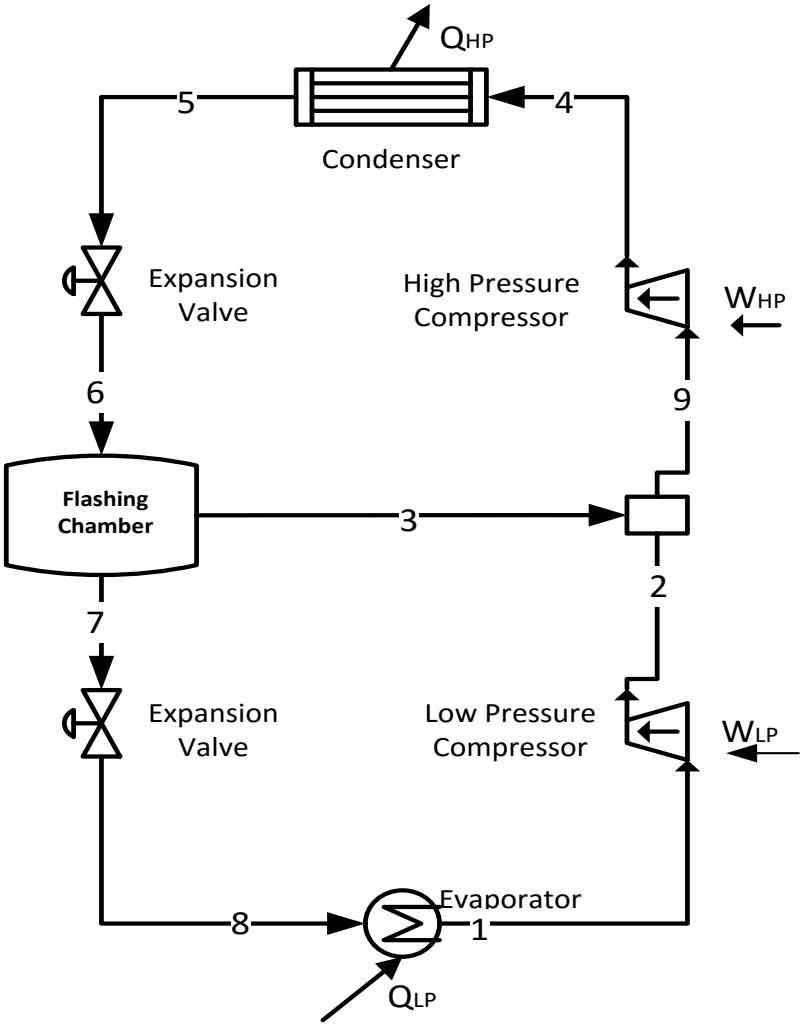

Figure 2-4 : Multistage Compression Refrigeration System with a Flashing Chamber.

Liquid refrigerant leaving the condenser expands as it passes through the throttling valve in the line 5-6 to the flash chamber. Partial vaporization of the liquid occurs, the saturated vapour then passes via line 3 then mixes with the superheated vapour from the low-pressure compressor coming via line 2. The mixture passes into the high-pressure compressor via line 9 for further compression, This is a regeneration process. The liquid coming from the flash chamber in state 7 is saturated, it is throttled at the second expansion valve then enters the evaporator where it draws heat from the environment to be cooled.

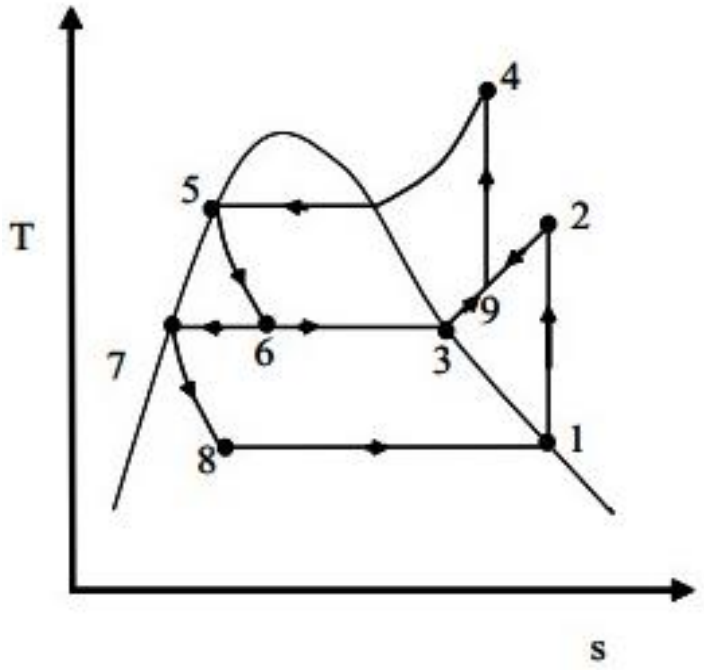

Figure 2-5 : Temperature-entropy diagram of a Multi-stage Compression System.(Extracted from Çengel and Boles, 2006).

The condenser and evaporator can have significantly large pressure and temperature differences in this system. The compression process in this cycle arrangement is executed in a two-stage compression process with intercooler, hence the compressor work decreases.

2.1.3 Cascade Refrigeration Systems

A cascade refrigeration system utilises two different refrigerants having different physical properties which run through two independent refrigeration cycles. These cycles are linked by a heat exchanger which operates as a condenser in the low-temperature cycle at the same time being an evaporator in the high-temperature cycle. This system is ideal for conditions where there is a substantial pressure difference between the evaporator and the condenser. A large temperature difference means a large pressure difference as well. To overcome this situation, the refrigerant systems are arrayed in a parallel connection resulting in a cascade system of vapour compression cycles.

A two-stage cascade refrigeration system, in Figure 2.6 shows the heat exchanger connecting the two cycles, it serves as an evaporator for cycle A (High-temperature circuit) and the condenser for cycle B (Low-temperature circuit).

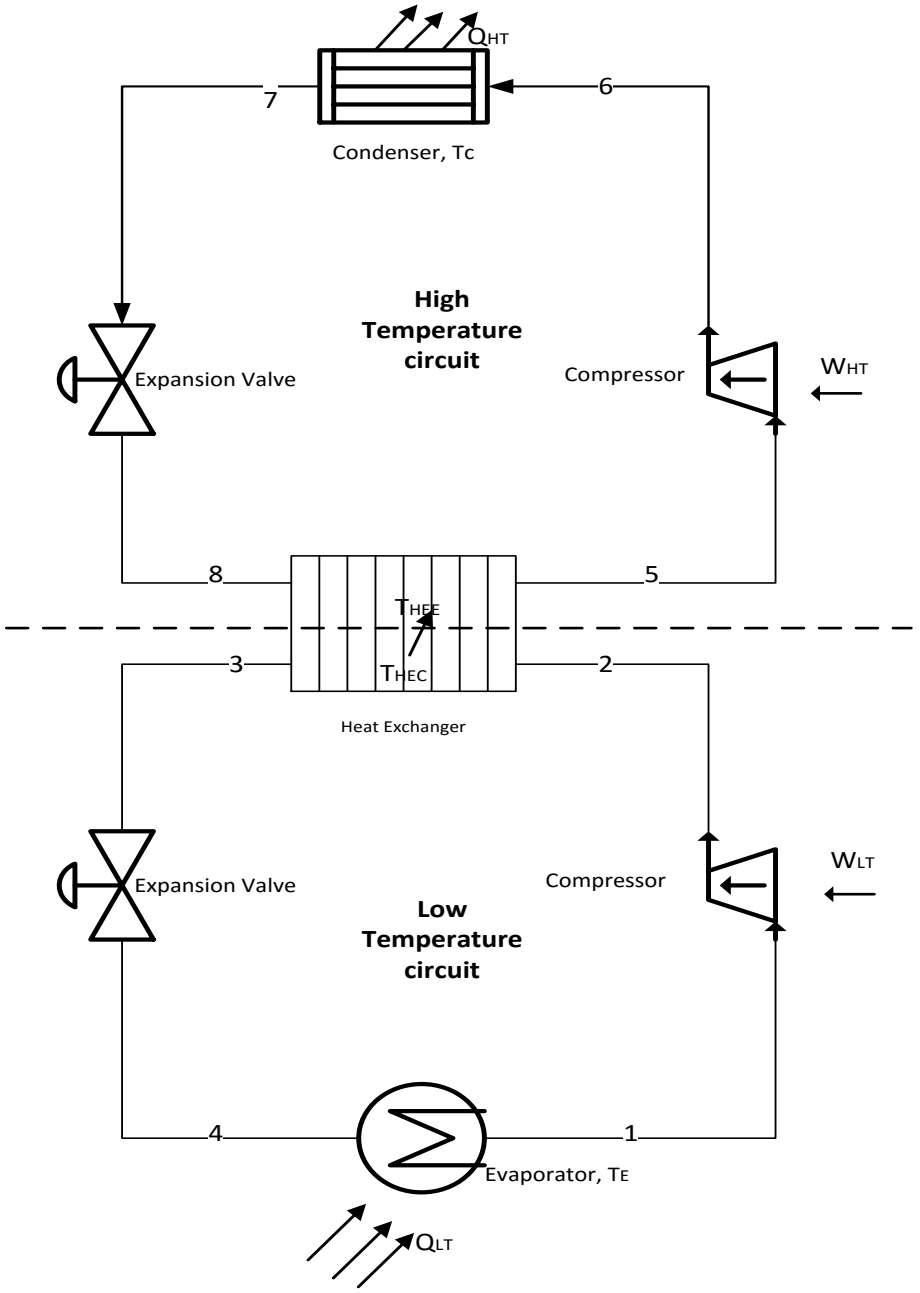

Figure 2-6 : Two-Stage Cascade Refrigeration Cycle.

The temperature-entropy diagram for a cascade system is shown in Figure 2.7. It can be noted that the cascade system increases the refrigeration effect and decreases the compressor power when compared to a simple VCC. These effects result in an overall increase of the refrigeration system's COP.

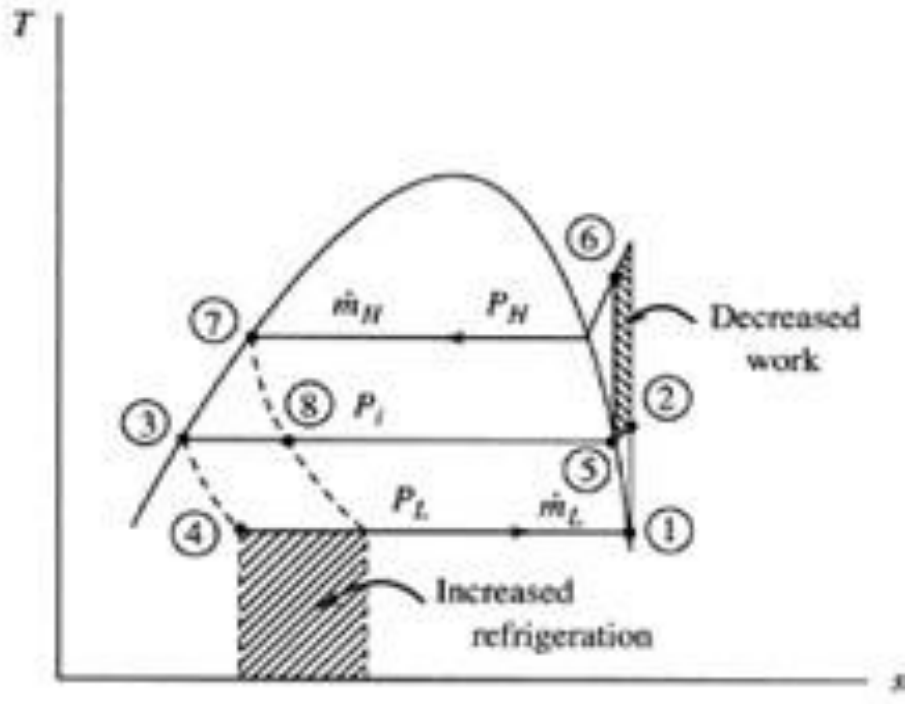

Figure 2-7 : Temperature-entropy diagram for Cascade Refrigeration system (Extracted from Çengel and Boles, 2006).

There are two thermodynamic methods used to gauge the performance of energy conversion systems, namely energy analysis and exergy analysis. Although energy analysis finds wide use and application, exergy analysis is more valuable as it not only measures the proximity of the system to the ideal operation but also identifies the system components subject to thermodynamic losses and irreversibilities. The results of exergy and energy analysis are expressed in the forms of energy and exergy efficiency indicators. These two are the key performance indicators in refrigeration.

2.2 Energy Analysis

All the major components in the vapour compression cycle shown in Figure 2.1 are internally reversible except for the throttling process. Since all the four components in the vapour-compression refrigeration cycle are steady-flow units, therefore, it is referred to as an ideal cycle. For this reason, the analyses of all the cycle components processes can be done under *steady-flow conditions* (Moran and Shapiro, 2006):

$$\dot{Q}_{CV} = \sum_{0}\left(h + \frac{u^2}{2} + gz\right)_{o} \dot{m}_o - \sum_{i}\left(h + \frac{u^2}{2} + gz\right)_{i} \dot{m}_\iota + \dot{W}_{CV} \qquad 2.1a$$

Where $\dot{Q}_{CV}$ is the rate of heat transfer between the control volume and its surroundings [J/s] , h is the specific enthalpy [J/kg] , $\dot{W}_{CV}$ is the energy crossing the boundary of a closed system [J/s], $\dot{m}_o$ and $\dot{m}_\iota$ are inlet and outlet mass flow rates, $\frac{u^2}{2}$ is the kinetic energy term, and gz the potential energy term.

The potential and kinetic energy changes of the refrigerant across the cycle's components are small and thus can be neglected. Considering only work and heat transfer terms;

$$\dot{Q}_{CV} = \dot{h}_o\dot{m}_o - \dot{h}_i\dot{m}_i + \dot{W}_{CV} \qquad 2.1b$$

Then the steady-state equation on a unit mass basis assuming constant mass flow rate in the system reduces to:

$$q - w = h_o - h_i \qquad 2.1c$$

where q is the heat transfer per unit mass [J/kg], Q̇ is the rate of heat transfer between the control volume and its surroundings [J/s], ṁ is the mass flow rate of the refrigerant [kg/s] and w is the work done per unit mass of the system.

Evaporator

Considering the refrigerant side of the evaporator as the control volume, denoted by 4-1 in Figures 2.1 and 2.7 the energy and mass rate balances (Equation 2.1b) gives the rate of heat transfer per unit mass of the refrigerant flowing as:

$$\frac{\dot{Q}in}{\dot{m}} = h_1 - h_4 \qquad 2.2$$

Compressor

Supposing no heat exchange occurs between the compressor and its surroundings, the energy and mass rate balances for a control volume encircling the compressor gives:

$$\frac{\dot{W}c}{\dot{m}} = h_2 - h_1 \qquad 2.3$$

Condenser

Considering the refrigerant side of the condenser as the control volume, the heat transfer rate from the refrigerant per unit mass flowing is:

$$\frac{\dot{Q}o}{\dot{m}} = h_2 - h_3 \qquad 2.4$$

Expansion Valve

A two-phase liquid-vapour refrigerant mixture exits the valve at the state 4 (Figure 2.2). The pressure decrease of the refrigerant is an adiabatic process which is not reversible, accompanied by an increment in specific entropy:

$$h_4 = h_3 \qquad 2.5$$

The coefficient of performance (COP) of the refrigeration system is given by:

$$\text{COP} = \frac{Refrigeration\ Effect}{Work\ Input} \qquad 2.6a$$

$$= \frac{\dot{Q}_{in}/\dot{m}}{\dot{w}_c/\dot{m}}$$

$$\text{COP} = \frac{h_1 - h_4}{h_2 - h_1} \qquad 2.6b$$

COP is higher for refrigerants with higher critical temperatures. Furthermore, it decreases as the temperature of the condenser reaches the refrigerant's critical temperature (Venkatarathnam and Murthy, 2012). In summary, to obtain a high COP, vapour density, liquid

thermal conductivity, and latent heat should have high values. Whereas molecular weight and liquid viscosity values should be low (Prapainop and Suen, 2012).

Multistage Refrigeration Cycle

The work done by the compressors in Figure 2.4 is given by:

$$W_{in} = w_{LP,in} + w_{HP,in} \quad 2.7$$

The coefficient of performance is given by:

$$COP_R = \frac{Q_{LP}}{W_{in}} \quad 2.8$$

The refrigeration efficiency is given by:

$$\eta = \frac{COP_R}{COP_{Carnot}} \quad 2.9$$

Gupta et al. (2017) obtained a maximum COP value of 3.087, in the study of a two stage VCRS using waste heat from the intercooler for heating up water using ammonia as a refrigerant. A mathematical model was also developed to perform exergy and energy analysis of the refrigeration system.

Cascade Refrigeration Cycle

If conservation of both energy and mass applies in the cascade system in Figure 2.6 and that mass and energy interaction between the two cycles. The ratio of mass flow rates around each cycle would be given by the following expression:

$$\dot{m}_A(h_5 - h_8) = \dot{m}_B(h_2 - h_3) \quad 2.10a$$

Therefore:

$$\frac{\dot{m}_A}{\dot{m}_B} = \frac{h_2 - h_3}{h_5 - h_8} \quad 2.10b$$

Also, the coefficient of performance is given by:

$$COP_{R,cascade} = \frac{\dot{Q}_{LT}}{\dot{W}_{net,in}} = \frac{\dot{m}_B(h_1 - h_4)}{\dot{m}_A(h_6 - h_5) + \dot{m}_B(h_2 - h_1)} \quad 2.11$$

Hoşöz (2005), in the analysis of a single stage and cascade system noted that the overall COP value for the cascade system was lower than the one for a single stage system. This scenario was caused by high power requirement of the higher unit compressor in the cascade system. In deriving the above expressions, the assumption made was that the refrigerants are the same in both cycles which would not necessarily be the case.

2.3 Exergy Analysis

Exergy is the highest possible work which a system can produce as it undertakes a reversible process from a defined original state to that of its environment, which is termed a dead state (Çengel and Boles, 2006). Practically it may be defined as a measure of the system's ability to bring about change because of not being in equilibrium with a reference (dead) state. A system is said to be in *dead* state when in thermodynamic equilibrium with its surroundings, i.e., it is the same temperature, pressure and is chemically unreactive with its environment. The exergy of a system at dead state is zero.

A flowing stream has exergy associated with it in addition to flow energy which is needed to sustain the flow. The stream specific exergy is denoted by the symbol, ***e*** (Yataganbaba et al., 2015):

$$e = (h - h_o) - T_o\,(s - s_o) + \frac{V^2}{2} + gz \quad 2.12$$

Where s_o and h_o are the entropy and enthalpy values of the dead state at temperature T_o, $\frac{V^2}{2}$ and gz are the kinetic and potential exergy terms, respectively.

Exergy transfer by heat:

$$X_{heat} = \left(1 - \frac{T_o}{T}\right) Q \qquad 2.13$$

Exergy transfer by mass:

$$X_{mass} = m\, e \qquad 2.14$$

Exergy transfer by work:

$$X_{work} = \begin{cases} W - W_{surr} & (for\ boundary\ work) \\ W & (for\ other\ forms\ of\ work) \end{cases} \qquad 2.15$$

All the equipment in the refrigeration unit operate under steady state condition; they do not undergo any changes in their energy, mass, entropy, and energy. Therefore, the rate of the generated exergy for steady flow is:

$$\sum \left(1 - \frac{T_o}{T_k}\right) \dot{Q}_k - \dot{W} + \sum_{in} \dot{m}\ e - \sum_{out} \dot{m}\ e - \dot{X}_{destroyed} - 0 \qquad 2.16$$

In the four main components of the refrigerant system exergy is destroyed or consumed due to entropy generated depending on the related processes. In the exergy analysis for components in the VCRS, the following assumptions were made:

i. All components remain in steady state conditions.
ii. Neglecting pressure losses in the pipelines.
iii. Heat exchange between the system and its surroundings are considered negligible.
iv. Potential and kinetic energy, as well as exergy losses, are ignored (Ahamed et al., 2011).

The mathematical formula for exergy destroyed in each unit in the cycle is given below for component (Stanciu et al., 2011; Yataganbaba et al., 2015):

- For the evaporator (*ev*):

$$I_{ev} = \dot{E}_4 - \dot{E}_1 + Q_v(1 - \frac{T_o}{T_v}) \quad \text{2.17a}$$

where I is the exergy destruction rate computed in watts and $\dot{E}$ is exergy

Replacing equation (2.12) into the above equation:

$$I_{ev} = \dot{m}[(h_4 - T_o s_4) - (h_1 - T_o s_1)] + Q_v(1 - \frac{T_0}{T_v}) \quad \text{2.17b}$$

Substituting equation (2.16) in the other components:

- For the condenser (*c*):

$$I_C = \dot{E}_2 - \dot{E}_3 \quad \text{2.18a}$$

$$I_c = \dot{m}[(h_2 - T_o s_2) - (h_3 - T_o s_3)] \quad \text{2.18b}$$

- For the compressor (*cp*):

$$I_{cp} = \dot{E}_1 - \dot{E}_2 + |\dot{W}_{cp}| \quad \text{2.19a}$$

$$I_{cp} = \dot{m}[(h_1 - T_o s_1) - (h_2 - T_o s_2)] + |\dot{W}_{cp}| \quad \text{2.19b}$$

- For the throttling valve (*tv*) :

$$I_{tv} = \dot{E}_3 - \dot{E}_4 \quad \text{2.20a}$$

$$I_{tv} = \dot{m}[(h_3 - T_o s_3) - (h_4 - T_o s_4)] \quad \text{2.20b}$$

$$= \dot{m}\, T_o(s_4 - s_3) \quad \text{2.20c}$$

The overall exergy distribution rate is:

$$I_{TOT} = I_{ev} + I_c + I_{cp} + I_{tv} \quad \text{2.21}$$

The exergy efficiency of the system is evaluated by the ratio of product exergy to fuel exergy:

$$\eta_E = \frac{\dot{E}_p}{\dot{E}_f} \tag{2.22}$$

Where the product exergy rate is:

$$\dot{E}_p = \dot{Q}_v \left(1 - \frac{T_o}{T_v}\right) \tag{2.23}$$

Moreover, the fuel exergy rate is:

$$\dot{E}_f = \left|\dot{W}_{cp}\right| \tag{2.24}$$

The system's exergy efficiency depends significantly on the state of the system and the environment, such that a decrease in environmental impact denotes an increase in exergy efficiency (Ahamed et al., 2011).

Yataganbaba et al. (2015), studied the exergy analysis of R1234yf (2,3,3,3- tetrafluoropropene) and R1234ze (1,3,3,3- tetrafluoropropene) as alternatives for R134a (1,1,1,2-tetrafluoroethane) in a two evaporator VCRS. An engineering tool, Engineering Equation Solver (EES-V9.172-3D) was used in the study. Figure 2.8 shows the flowchart of the procedure followed in the analysis. A thermodynamic property database in EES software package was utilised in the calculation. In this study, it was observed that as the evaporator temperature increased, exergy destruction declined, refrigerant R134a produced the least exergy destruction whereas R1234yf had the highest. Moreover, it was noted that exergy destruction increases to a certain value with an increase in the evaporator temperature then after it falls as the evaporator temperature is increasing. On the other hand, exergy efficiency reduces with the increase in the condenser temperature. The compressor had the highest portion of exergy destruction as compared to the other components in the refrigeration cycle.

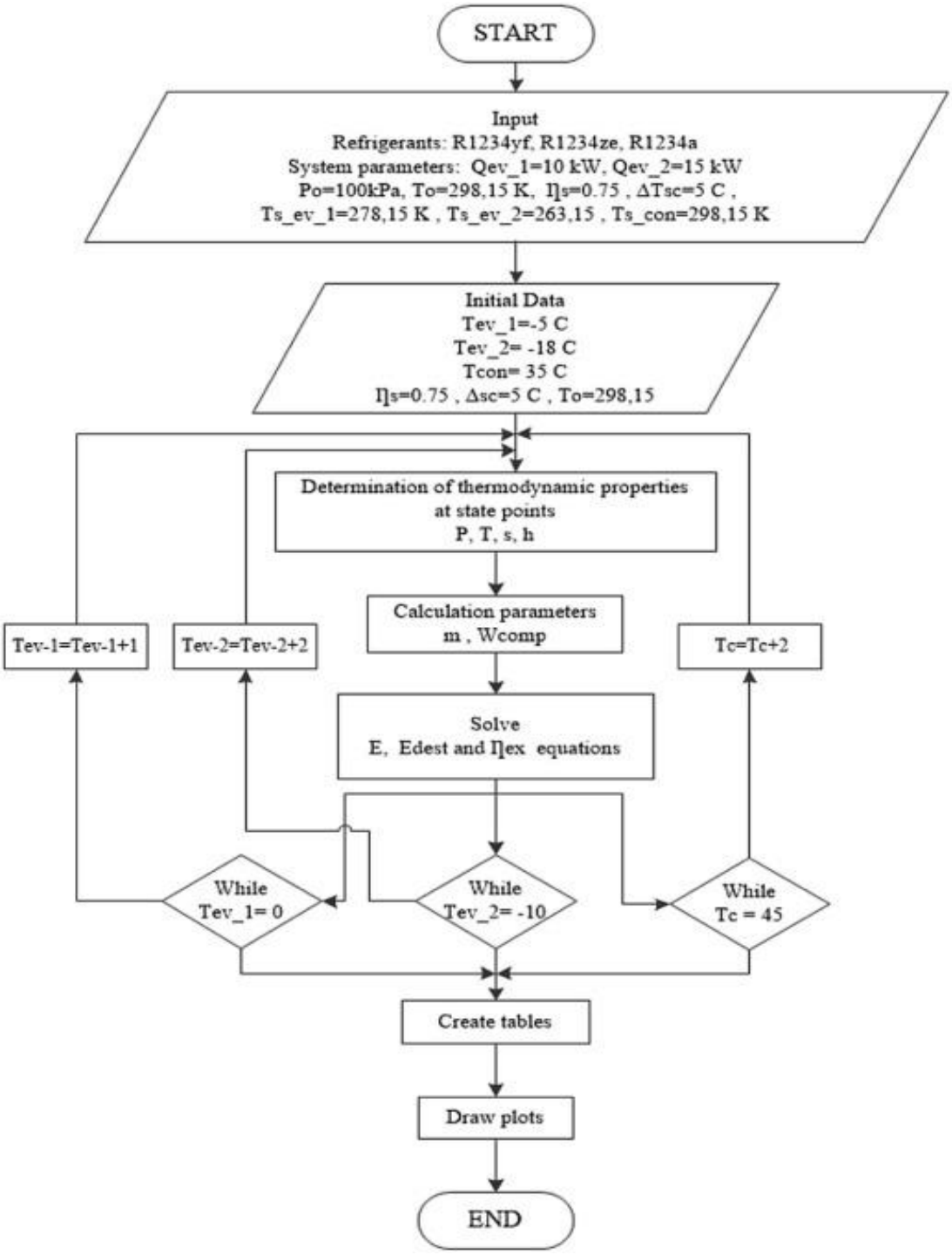

Figure 2-8 : Flowchart for the Exergy Analysis for a VCRS with two-Evaporators (Extracted from Yataganbaba et al., 2015).

Chapter 3

3 Refrigerant and Refrigerant Blends

Refrigerants have evolved from the 1800s with ethers being the first recorded refrigerants applied in hand operated vapour compression cycles in the year 1875 (Arora, 2009). In the period 1800-1900 (first generation of refrigerants) any substance that had refrigeration properties was utilised. Thus natural substances such as carbon dioxide, ethyl chloride ammonia and sulphur dioxide were used. The second generation of refrigerants (1930-1990) came into use because of the genius of three researchers: Thomas Midgley Jr, Robert R. McNary and Albert L. Henne (Calm, 2008). These refrigerants were neither toxic nor flammable, the focus being safety and durability. Substances applied during this period era were chlorofluorocarbons, hydrochlorofluorocarbons, ammonia, and water. Ozone protection characterised third generation refrigerants during the period 1990-2010 and refrigerants utilised were hydrofluorocarbons, ammonia, isobutene, propane and carbon dioxide (Calm, 2008).

From 2010 onwards the fourth-generation refrigerants came into the market. These focussed on low global warming, zero ozone depleting potential, high efficiency and short atmospheric life. Venkatarathnam and Murthy (2012) and Bhatkar et al. (2013) stated that due to their excellent refrigerant and environmental properties, hydrofluorooelifins, hydrofluorocarbons, hydrocarbons, carbon dioxide and water are proving to be refrigerant candidates for the future. Furthermore, Sekiya and Misaki (2000), investigated the feasibility of replacing CFCs, HCFCs, and PFCs with hydrofluoroether in refrigeration and other application. They also evaluated their GWP, TEWI, LCCP, and carried out life-cycle assessments (LCAs) for these refrigerants. Fluorinated ethers proved to have a short atmospheric lifetime, thus making them suitable candidates for refrigeration applications. The boiling points of the fluorinated ethers were found to be close to those of the compounds they were replacing. Density and surface tension were satisfactory, additionally, toxicity and flammability were satisfactorily low.

Currently, blending of different refrigerants is being investigated globally to formulate a viable refrigerant with excellent thermodynamic, physical and chemical refrigerant properties (Szymurski, 2005; Bitzter, 2014; Goetzler et al., 2014). Furthermore, it is very imperative for the refrigerants to be environmentally friendly in line with the drive towards sustainable development. Refrigerant R134a (1, 1, 1, 2-Tetrafluoroethane) is being used as a main component in producing refrigerant blends due to its zero ODP, non-flammability, chemical

stability and low vapour pressure. However, its GWP is a cause of concern (Mani and Selladurai, 2008).

Refrigerant blends have been utilised as drop-in replacements in diverse refrigeration systems and cycles. This replacement process is the substitution of the original refrigerant with a compatible or suitable refrigerant blend without altering the cycle components or compromising the performance of the system. Investigations on refrigerants drop–replacements with refrigerant blends have been successfully performed by the following researchers: Jung et al. (2000); Halimic et al. (2003); Hwang et al. (2007); Park et al. (2009); Dalkilic and Wongwises (2010) and Rasti et al. (2011). The details of their studies are discussed in the subsequent sections, highlighting the properties necessary for providing a suitable refrigeration effect as drop-in replacements.

3.1 Refrigerant Properties

A number of factors are crucial when selecting refrigerants for use in a refrigeration cycle. A refrigerant has to satisfy the desired properties which are classified as physical, chemical and thermodynamic (Arora, 2009). Selection of a refrigerant for a specific application depends on it satisfying the requirements for that particular application as there is no one substance ideal for all refrigeration applications (Hundy et al., 2008). Table 3.1 gives a summary of most important the desirable refrigerant properties.

Thermodynamic properties are imperative in the operation cycle of the refrigerant, the most important being its boiling point as other properties depend on it. The important thermodynamic properties of concern are the volume of the suction vapour per ton, condensing and evaporating pressures, critical pressure, and temperature, as well as COP among others. Figure 3.1 is a plot of $In\ p^{sat}$ against $\frac{1}{T^{sat}}$ derived from the Clausius - Clapeyron equation. It can be observed from the plot that, the higher the boiling point the steeper is the slope of $In\ p^{sat}$ against $\frac{1}{T^{sat}}$ line. Therefore, the high b.p refrigerants have higher latent heat of vaporisation than the lower boiling point refrigerants with a flatter slope.

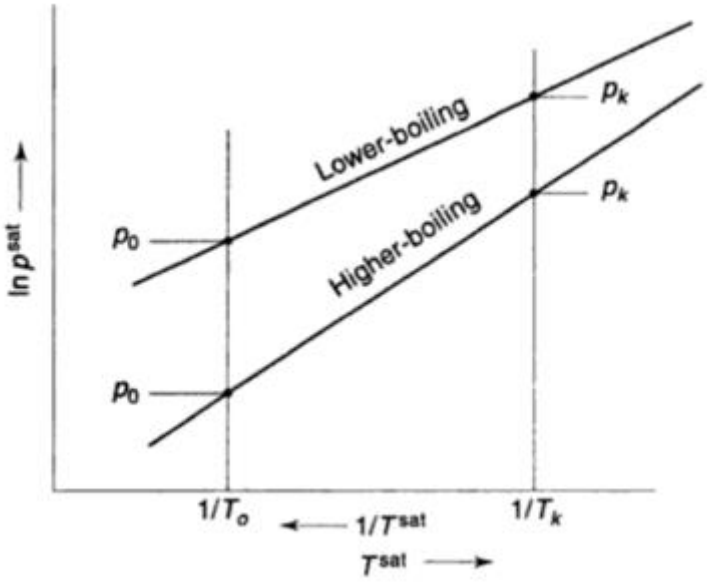

Figure 3-1 : Comparison of Pressures of Lower Boiling and Higher Boiling Refrigerants at given Evaporator and Condenser Temperature. (Extracted from Arora, 2009).

Moreover, at a fixed temperature, the condenser and evaporator pressure are lower for higher boiling temperature refrigerants. Conversely, higher-pressure refrigerants boil at a lower temperature. Furthermore, the high boiling refrigerants have a higher-pressure ratio while low boiling refrigerants have lower pressure ratios.

Table 3-1 : Summarised Properties of an ideal Refrigerant (Compiled from Arora, 2009; Sapali, 2009; Mohanraj et al., 2011).

Property	Description	Specification
Thermodynamic	Ozone Depleting Potential	Zero
	Global Warming Potential	Zero
	Latent heat of evaporation	High
	Critical pressure	High
	Critical temperature	High
	Condensing pressure	High
	Evaporating pressure	Relatively low
Chemical	Toxicity	Non-toxic
	Flammability	Non-flammable
	Corrosiveness	Non-corrosive
	Miscibility with oil	Low
	Miscibility with water/moisture	Low
Physical	Leak detection	Easy
	Cost and availability	Cheap and available
	Heat transfer coefficient	High
	Viscosity	Low
	Thermal conductivity	High
	Dielectric strength	Compatible with air, refrigerants, and motor windings

A special emphasis on chemical miscibility with the lubricating oil is that chlorine-based refrigerant blends mix perfectly with mineral oil. However, HFC refrigerant blends are not miscible with mineral oil and require synthetic lubricants (Mohanraj et al., 2011). The synthetic lubricates in use are Polyol ester oil (POE) and alkyl benzene (AB).

3.1.1 Evaporator thermodynamic features

The evaporator is a critical component in the refrigeration cycle as it is the point where the actual cooling occurs (heat absorption). It is essential for the evaporator pressure to be relatively low so that the condenser pressure is not very high leading to high cost of condenser equipment. Also, the evaporator pressure must be above atmospheric pressure, if extremely low it will result in a substantial volume of suction vapour. The compressor size can be determined by the volume of suction vapour required per unit of refrigeration. For high-pressure and small volumes of suction vapour refrigerants, reciprocating compressors can be applied while centrifugal compressors are used for low pressure as well as large volumes of suction vapour refrigerants. Additionally, the high latent heat of vaporisation is ideal for maximum heat absorption during the refrigeration (heat absorption at the evaporator). Likewise, the refrigerant must operate in the cycle above its freezing point to prevent condensation of the refrigerant at the expansion valve, hence starving the evaporator. Similarly,a low compression ratio is preferable as it leads to high volumetric efficiency and low compressor power consumption. This results in the increase of the cooling capability because of the increase in the specific refrigerating effect (Arora, 2009; Venkatarathnam and Murthy, 2012).

3.2 Refrigerant Blends

Synthesis of refrigerant blends is accomplished by mixing one or more refrigerants to produce a mixture which exhibits desired properties as shown in Table 3.1. The refrigerant mixtures behave differently from pure refrigerants because two or more molecules of the constituent substances are present in the liquid or vapour phase of the resultant refrigerant blend. The exploitation of refrigerant blends was motivated by the phasing out of current refrigerants (mostly pure fluids) due to their ODP and GWP (Montreal and Kyoto Protocols). Refrigerant blends are required to meet specific or certain criteria for their application to be economical. These include:

- compatibility with most materials of construction in today's systems
- compatibility with oils already in the market
- the need to have comparable capacity and efficiency when measured against CFCs and HCFCs

3.2.1 Types of Refrigerant Blends

Refrigerant blends classification focusses on their behavior. There are three types of refrigerant blends, these are azeotropic, near-azeotropic and zeotropic blends. Figure 3.2 shows the temperature – pressure of these blends.

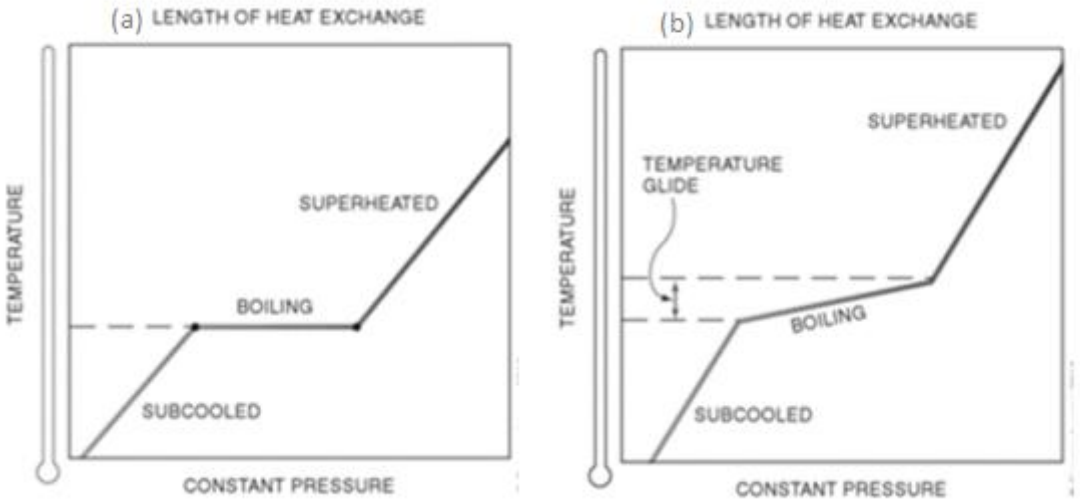

Figure 3-2 : An (a) azeotropic refrigerant and (b) near-azeotropic refrigerant blend at a given pressure as they boil (Extracted from Whitman et al., 2013).

Azeotropic Blends – are constant boiling mixtures and, they behave as a single substance. Their chemical proportions cannot be changed by the application of heat. An attractive force holds different constituting molecules therefore, the blend cannot be separated by distillation. Its properties are distinct from those of the constituent substances; it behaves as a single chemical compound (Whitman et al., 2013).

Near Azeotropic Blends – these mixtures exhibit characteristics that are comparable to those of azeotropic mixtures. Although these blends have properties similar to those of azeotropic mixtures, they are defined as zeotropic or non-azeotropic and exhibit temperature glide.

Zeotropic Mixture –do not behave as a single substance as there is no attraction between its different constituent molecules. They have a temperature glide when they boil (vaporize) and condense, which results from blend fractionation. That is, at equilibrium they have different vapour and liquid compositions. This composition difference results from the difference in

boiling point of the constituent substances in the mixture. When the mixture boils, due to the existence of substances with different boiling points there is composition change of the mixture changing in phase. The composition changes lead to changes in the bubble (T_{bub}) and the dew (T_{dew}) points of the residual mixture.

3.2.2 Behavior of Blends

Temperature glide – is the difference between the dew point temperature and the bubble point temperature ($TG= T_{dew} – T_{bub}$). It occurs when at a given pressure, the blends have a range of evaporating and condensing temperatures. A temperature glide occurs because the phase change takes place at a different pressure-temperature relationship for each component in the blend. Phase changes occur along the length of the vessel or heat exchanger; this gives rise to a range of boiling or condensing points for each pressure. Figure 3.2 illustrates the temperature glide for a near azeotropic blend. Refrigerant blends with a temperature glide (of approximately 5 ^{0}C or larger) have the potential of improving the performance and the energy efficiency of vapour compression system through a process known as temperature glide matching. A full discussion of temperature glide matching is included in Appendix A along with the effects of phase change of zeotropic blends on heat transfer coefficients (HTC).

Blend Fractionation – this is the change in the composition of the refrigerant blend due to preferential vapourisation of the more volatile component in the blend or preferential condensation of the less volatile component. Also, leakage of one component from the refrigeration cycle to the environment at a faster rate than the other components in the blend causes fractionation. The difference in leakage rate is caused by different partial pressures of each constituting substance in the blend (Lavelle, 2006).

3.3 Review of the Performances of Refrigerants and Refrigerant Blends

Table 3.2 provides a summary of the performance of different refrigerant blends relative to pure refrigerants as presented in various literature sources, as published over the years of study in air-conditioning and refrigeration. The comparative study also pays attention to studies which were both theoretically and experimentally executed.

Table 3-2: A Review of Studies published on Refrigerants and Refrigerant Blends.

Reference	*Refrigerant Studied*	*Application/Method for Study*	*Results and Conclusions*	*Comments*
(Rigola et al., 1996) and (Rigola et al., 1998)	R12, R290a, R600a, R404a, and R134a	An experimental unit was built to compare the results obtained from the numerical simulations with the experimental data. Working on a single-stage vapour compression refrigerant scheme, mass flow rate, and inlet temperature were independently fixed in the secondary condenser and evaporator circuits.	In the theoretical study the COP values for the refrigerants R134a, R12 and R290 were 1.69, 1.58 and 1.55 respectively. In the experimental runs refrigerants R134a, R600a, and R404a were studied, and their COP values were 1.57, 1.49 and 1.18.	Considering refrigerant R134a which was used both in the theoretical and experimental studies, it is observable that the COP values obtained in the investigation were comparable.
(Jung et al., 2000)	Refrigerant blends made from refrigerants, R22, R32, R125, R134a, R152a, R290, and R1270	Investigation of the performance of 14 refrigerant mixtures. The experimental set up consisted of a simple vapour compression cycle (VCC) composed of a suction line heat exchanger, a condenser, an evaporator and an expansion valve	COPs and refrigeration capacities of three refrigerants consisting of R125, R32, and R134a were 4-5% higher than those of R22. Blends with a greater mass fraction of R32 and R134a and a lower mass fraction of R125 proved to have better performance than R407C. COP increased to a maximum of 3.9% for mixtures with high quantities of R125. The COP values for the refrigerant blends investigated were in the range of 2.339 to 2.660, with (75%R125/5%R134a/20%R152a) blend having the lowest value and (26%R32/14%R125/60%R134a) had the highest value for COP and relatively a high discharge temperature.	The use of suction line heat exchanger (SLHX) increased the COPs of most refrigerants tested however it lowered their capacity. Furthermore, from the results published in this study, it can be established that increasing the percentage of R125 in the blend decreased the COP of the blend.

Table 3-2: *A Review of Studies published on Refrigerants and Refrigerant Blends. (Continued)*

Reference	*Refrigerant Studied*	*Application/Method for Study*	*Results and Conclusions*	*Comments*
(Halimic et al., 2003)	R12, R134a R401, and R290	Experimental work carried out in vapour compression refrigeration unit originally designed to operate with R12	R290 had the largest cooling capacity. COP of R12. R290 and R134a are shown to be comparable. With regards to environmental effect, R290 showed the best performance. R401 displayed a level of performance like that of R12 in both COP and capacity.	Satisfactory performance was shown by refrigerant blend R401 in the vapour system of refrigerant R12.
(Hwang et al., 2004)	R290, R410a, R404a	The environmental impact of the refrigerant blend is of paramount importance in selecting refrigerant for use. Lifecycle climate analysis performance on the given refrigerants for low and medium temperature applications.	The COP of R410a is almost the same as that of R290 within the measurement error range, while the COP of R404a is 5-10% lower than that of R290. Also, the LCCP of R290 is always lower than that of R410a and R404a if the annual emission is kept below 10%, therefore, it is conclusive that HCs have lower LCCP than HFCs.	As far as environmental aspects were concerned which are summarised by LCCP analysis, R404a and R410a exhibited better performance than R290.
(Wongwises et al., 2006)	Refrigerant blends made from, R134a, R290, R600, and R600a.	Investigated the performance of blends in an Automobile air conditioning, with a capacity of 3.5 kW driven by a diesel engine. Parameters evaluated were compressor power, refrigeration capacity and COP.	Every blend composition had a larger COP than R134a, lower discharge temperature, however the capacity was comparable. The blend R290/R600/R600a in the ratio (50%/40%/10%) had the highest COP in all the tested conditions. At compressor speed of 1500 rpm, evaporator temperature of 5 ℃, COP for R290/R600/R600a in the ratio (50%/40%/10%) was 1.55 while that for R134a was 1.33 Hence it is the best alternative to R134a.	The hydrocarbon blends exhibited excellent refrigeration capabilities in the study with regards to COP, compressor power, and the cooling capacity. The performance of the refrigerant blends was satisfactory in the automobile air conditioning designed for use with pure refrigerants.

Table 3-2: *A Review of Studies published on Refrigerants and Refrigerant Blends. (Continued)*

Reference	*Refrigerant Studied*	*Application/Method for Study*	*Results and Conclusions*	*Comments*
(Mani and Selladurai, 2008)	R12, R134a, and R290/R600a	Experimental performance of the refrigerants was investigated in a vapour compression refrigeration system originally designed to operate with R12. Investigations were carried out at various evaporating temperatures between -2 and 18 ℃.	Refrigerant mixture R290/R600a in the ratio (68/32 by wt %) showed the best performance with regards to major environmental impacts (ODP) and GWP). The blend had comparable discharge temperature and pressure with R134a and R12.	In this study, the hydrocarbon blend showed better performance than pure refrigerants used in the study. It can also be drawn from the study that different refrigerant mixture compositions behave differently in different proportions.
(Dalkilic and Wongwises, 2010)	R12, R134a, R134a, R152a, R32, R290, R1270, R600 and R600a.	A theoretical study of a VCRC was carried out with various refrigerant blends at different ratios, the parameters of interest were the COP, degree of superheating and sub-cooling, the refrigeration effect, the environmental impacts of ozone layer depletion and global warming.	Refrigerant blends R290/R600a (40/60 by wt %) and R290/R1270 (20/80 by wt %) with COP values of 2.893 and 3.180, were found to be most suitable replacements for R12 and R22 respectively. The COP value obtained for R134a was 3.097 while for R12 it was 3.233, with the condenser temperature set at 50 ℃ and the evaporator temperature at -10 ℃.	Satisfactory performance of the refrigerant blends in the theoretical analyses carried out in this study.
(Padilla et al., 2010)	R12 and R413a	Investigation of Exergy performance of the two refrigerants in the domestic refrigeration system.	Refrigerant R413 showed better performance than R12, the COP value for R413 was 3.72 while that of R12 was 3.53.	R413a exhibited excellent refrigeration performance, exergy efficiency and ozone friendly therefore a safe, viable alternative to R12. R413a can be used to replace R12 with little or no system's modification.

Table 3-2: *A Review of Studies published on Refrigerants and Refrigerant Blends. (Continued)*

Reference	*Refrigerant Studied*	*Application/Method for Study*	*Results and Conclusions*	*Comments*
(Jain et al., 2011)	R22, R134a, R410A, R407C, and M20	COP computation by a simulation program (RERPROF) based on the following input data: evaporator coolant inlet temperature, condenser coolant inlet temperature, the rate of heat absorbed by the evaporator, the efficiency of the compressor, and product evaporator (and condenser) effectiveness and capacitance rate of the external fluid.	The COP value obtained for R134a was 2.31, while the compressor work was 28.92 kW with the refrigerant flow rate of 0.535 kg/s. The COP value of R22, R410a, R407C and M20 was 2.35, 2.06, 2.33 and 2.18 respectively. Their compressor work (kW) was 28.25, 32.34, 28.63 and 30.54 respectively.	From the comparisons made, it was conclusive that R407C was the potential HFC refrigerant for new and existing systems using R22 with minimum costs and human efforts.
(Bolaji, 2011)	R22, R507, and R404A	Window air-conditioner application. R22 was used as a benchmark to assess the performance of the two refrigerant blends. COP, pressure ratios, compressor power. Refrigeration capacity and discharge temperature were the parameters investigated.	R507 had a high COP value compared to that for the other refrigerants studied. The COP of the refrigerants R22, R507 and R404a were 2.07, 2.19 and 2.93 respectively and the compressor work (kW) was 1.86, 1.83 and 1.90 respectively. While the discharge temperatures (℃) 47.5, 49.4 and 54.6 respectively.	The study proved the excellent refrigeration performance of the refrigerant blends as their performance was better than that of the pure refrigerant used in the study.

Table 3-2: *A Review of Studies published on Refrigerants and Refrigerant Blends. (Continued)*

Reference	Refrigerant Studied	Application/Method for Study	Results and Conclusions	Comments
(Baskaran and Mathews, 2012)	R152a, R32, R290, R1270, R600, and RE170 (a laboratory synthesised blend).	Simulating tool **(**CYCLE_D 4.0) was used in the performance analysis of a vapour compression refrigeration system. Compressor and electric motor efficiency, condenser and evaporator temperature, sub cooling and superheat were specified and then other parameters were computed from these fixed values.	R134a was selected as a reference fluid in the study, and its COP was 3.315, and the COP value of R600 was 3.421, COP value of R600 was 3.258. RE170 showed best performance with a COP value of 3.523 and R32 had the lowest COP value of 3.141.	Considering performance comparison of (COP), environmental impacts of ODP and GWP and pressure ratio, the synthesised blend RE170 showed the best performance. The composition of RE170 was not specified in the publication.
(Jerald and Kumaran, 2014)	R12 and R404a	R12 vapour compression refrigeration cycle retrofitted with R404a a zeotropic refrigerant blend. The experimental set up was made up of a reciprocating compressor, an air-cooled condenser, a capillary device for throttling purposes, and a coiled evaporator. The five different configurations of capillaries were 0.030”, 0.036”, 0.044”, 0.050” and two 0.33”.	From the experimental results, it was found that the zeotropic refrigerant R404a was compatible with the diameter 0.030” (double) on the evaporator load, work of compression, mass flow rate and coefficient of performance. Moreover, R404a showed better cooling capacity, better oil miscibility than R134a hence better system efficiency. R404a used a smaller mass of refrigerant for the same cooling capacity as compared to R134a.	The performance of the commercial blend proved to be comparable to that of a pure refrigerant R12. Moreover, with the appropriate throttling action, the performance of the blend was better than that of R134a.

Table 3-2: *A Review of Studies published on Refrigerants and Refrigerant Blends. (Continued)*

Reference	Refrigerant Studied	Application/Method for Study	Results and Conclusions	Comments
(Mishra, 2014)	R507a, R125, R134a, R290, R600, R600a, R1234ze, R1234yf, R410a, R407c, R707, R404a and R152a.	Investigation of methods for improving the exergetic efficiency of multi-evaporators with a compressor and an expansion valve, in VCRS. The evaluation was done in a 4.75 kW window air conditioner with a condenser temperature range of 303 to 333 K and an evaporator with a temperature range of 253 to 278 K.	The COP values of R134a, R507a, and R125 obtained were 3.022, 2.678 and 2.473 respectively. The value of COP increased to 3.104, 2.80 and 2,628 with an inline heat exchanger incorporation into the cycle.	The study proved that the performance of refrigerant blend R507 was comparable to the performance of R134a. The difference in performance was due to the fact that R507 is a high-pressure refrigerant while R134a is a medium temperature refrigerant.
(Gomaa, 2015)	R134a	Automotive air conditioning system.	Observations made were that keeping the compressor speed and evaporator conditions constant, a higher COP value was achieved at the minimum condensing temperature for R134a refrigerant.	In the systems investigated, the COP was directly proportional to the evaporating temperature due to the increase in the cooling effect and the decrease in the compressor power.
(Brijendra et al., 2017)	Refrigerant blends M1, M2, M3 composed of R134a, R32, R152a in the ratio 2.3/0.3/0.4, M1, 0.1/0.4/0.5 M2 and 0.4/0.3/0.3 M3	Experimental work was carried out on ice-candy plant working on vapour compression refrigeration cycle which uses R22 as a refrigerant. Enthalpy charts were used in the calculations of enthalpy.	The performance of the refrigerant mixtures is compared to R22 a non-zero ODP. It was noted that the higher the latent heat of vaporization, the lower is the molecular weight. The COP of the refrigerants R22, M1, M2, and M3 was 5.28, 5.2, 5.47 and 5.1 respectively, while the GWP were 1700, 633,450 and 751 respectively. The ODP of all the blends was zero, except for R22.	The mixtures investigated proved to be suitable for use as replacements for refrigerant R22 due to their comparable performance and their satisfactory environmental impact.

Chapter 4

4 Equipment Review

Laboratory scale refrigerant units are designed and assembled for investigating and analysing the performance of refrigerants and refrigerant blends. Refrigerant test units are designed and assembled differently to meet specific and unique experimental requirements. Modifications are sometimes necessary when refrigerant blends are investigated in a unit originally intended for pure refrigerants. Additionally, laboratory scale refrigeration units are not novel, but available pre-constructed, in parts or designed for specific research purposes. The capabilities of these units are as vast as the interests of the industry today. A literature review of the equipment used in the laboratory scale refrigeration experimental research is provided in this chapter.

4.1 Equipment Setups presented in literature

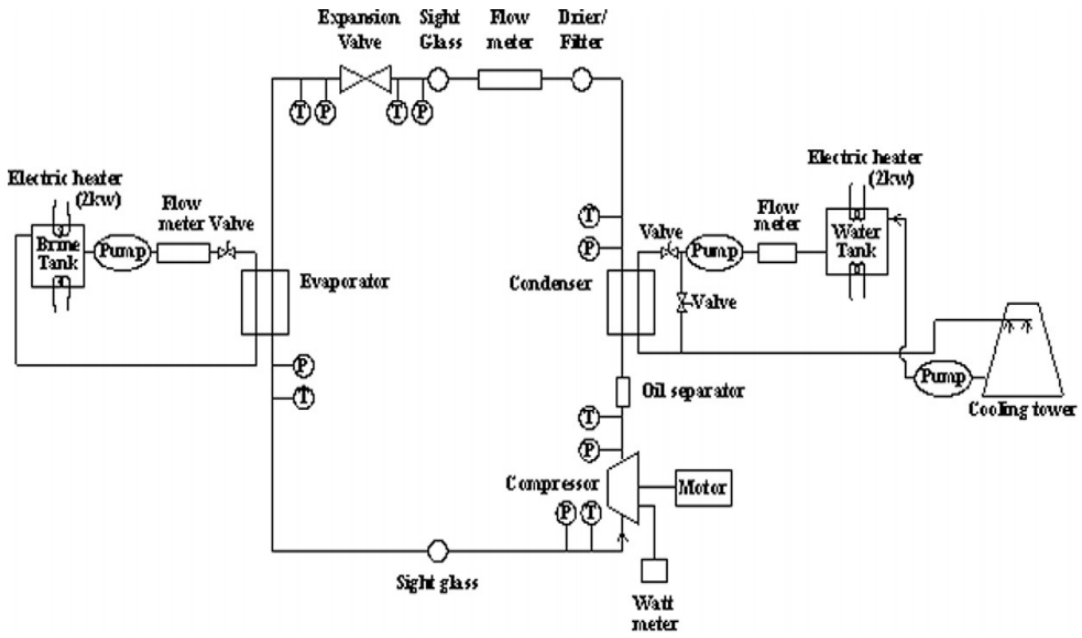

Figure 4-1 : Experimental set-up for R12, R134a, and R290/600a investigation (Extracted from Mani and Selladurai, 2008).

Mani and Selladurai (2008) performed an experimental study on a vapour compression cycle on the equipment setup shown in Figure 4.1 constructed for the study. The refrigerants studied

were R12, R134a and R290/R600a. Two loops are evident in the setup, the main loop, and the secondary loop. The compressor, the evaporator, a filter drier, the condenser, sight glass, flow-meter and expansion valve make up the main refrigeration loop.

The evaporator and the condenser were of double tubes made from copper. In the condenser, the refrigerant flows in the inside tube whereas the cooling water flows through the annular space between the interior and exterior tubes. In the evaporator, a calcium chloride solution was used as a heat transfer fluid, and it flows through the interior tube while the refrigerant flows in the annular space.

A reciprocating compressor selected for the study had a rotating speed of 855 rpm which could be adjusted by an electrical motor. The tube and refrigerant lines were insulated to reduce heat loss. Two sight glasses were included in the unit, one on the liquid line and the other on the suction line. Cooling water from one tank was circulated through the condenser whereas brine solution in another tank was circulated through the evaporator. Cooling water from the condenser was cooled in a cooling tower. Highly sensitive rotameters were utilised to meter the flow rates of the brine solution and the cooling water, their accuracy was $\pm$ 0.05 L/min. RTD thermocouples were employed to measure the temperature, with an accuracy of $\pm$ 0.1 ℃ and the pressure gauges used to measure pressure were calibrated with an accuracy of $\pm$ 6.89 kPa.

Jung et al. (2000) in their investigation of potential substitutes for R22 in household air-conditioners used the breadboard heat pump set-up shown in Figure 4.2. The refrigerant mixtures tested in the unit were: R32, R125, R290, R1270, R134a and R152a.

The condenser and evaporator were of the double line heat exchanger type designed to have counter- current flow. The refrigerant fluid flows through the annulus, while the secondary heat transfer which was water in both the evaporator and condenser flowed in the inner tube. The temperature of the water was controlled by a chiller and a heater at the condenser and evaporator respectively. This unit was also used by Park et al. (2009) to prove the suitability of R413a as a drop-in substitute for R22 in residential air-conditioners and heat pumps.

For pressure changers, a hermetic compressor, designed for use with R22, was installed. A fine metering valve was used as the expansion valve. To increase the efficiency of the system, an SLHX was connected. The vapour exiting the evaporator was channelled into the innermost tube while the liquid from the condenser flowed through the annulus of the SLHX. The unit

was insulated by polyurethane and fibreglass to reduce heat loss. Charging ports were at the evaporator inlet for liquids and the other at the condenser inlet for gases.

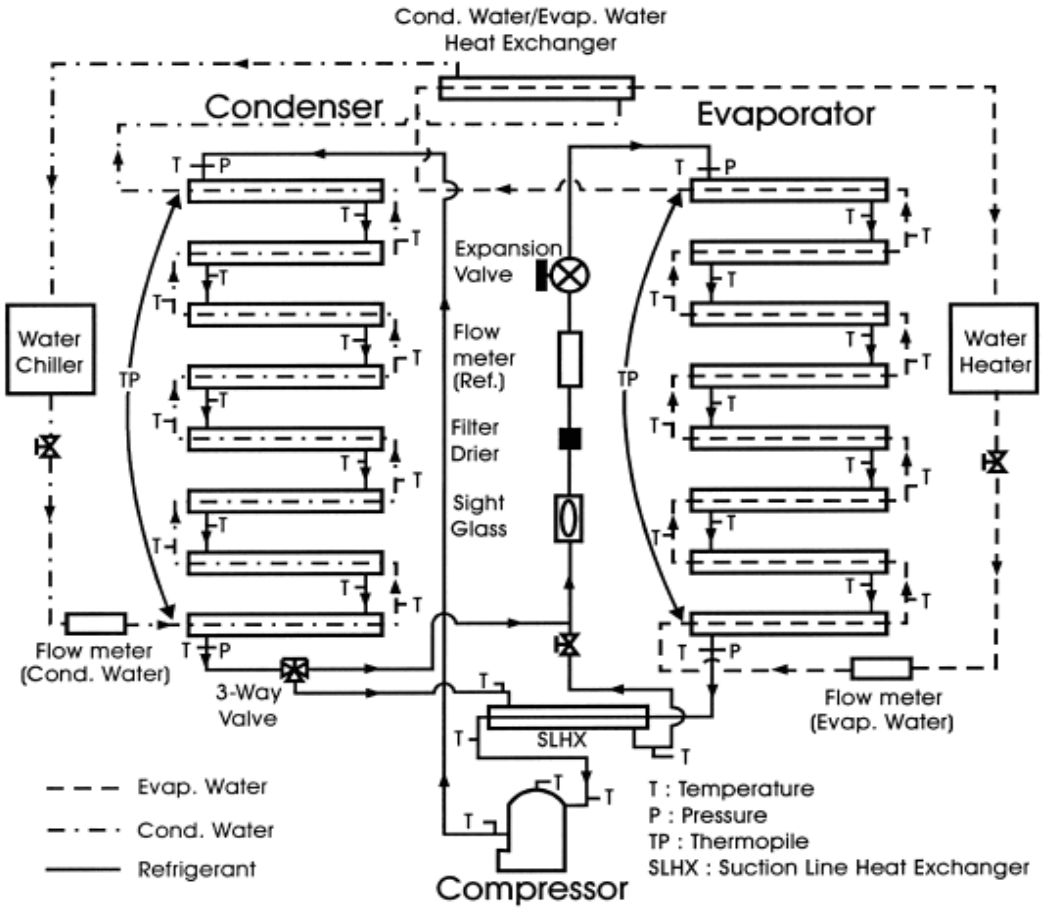

Figure 4-2 : The breadboard heat pump (Extracted from Jung et al., 2000).

Halimic et al. (2003) compared the performances of R410, R290, and R134a with R12 in a vapour compression refrigeration cycle in a test rig designed for R12 refrigerant, using the equipment set up shown in Figure 4.3. To facilitate the examination of alternative refrigerants, it was necessary to dismount the temperature sensor at the expansion valve which was originally intended to optimise system performance with R12 refrigerant. A sight glass positioned, between the expansion valve and the condenser, in the Halimic et al (2003) unit it is used to detect the refrigerant phase as it enters the expansion valve. In the test procedure, the evaporator temperature value was fixed. Other parameters, i.e. the condenser temperature, cooling water temperature, refrigerant flow rate, condenser and evaporator pressures, were adjusted to meet the operational conditions. In every experimental run, once stable conditions were achieved, readings were taken and recorded after an hour of operation. The observations

were; the COP of R290 was similar to that of R12 and R290 had the largest cooling capability of the refrigerants tested.

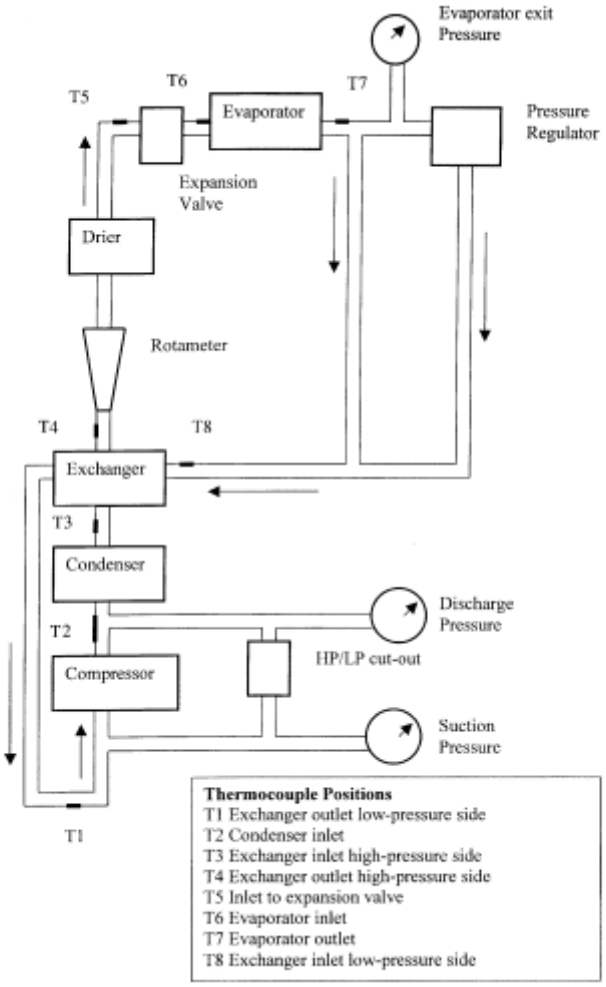

Figure 4-3 : Schematic of the refrigeration unit (Extracted from Halimic et al., 2003).

Sami and Desjardins (2000) in evaluating the performance of R407B, R507, R408a, and R404a as new refrigerant alternatives for R502, used an air-source heat pump with improved surface tubing under standard ARI conditions. The diagram of the experimental setup is presented in Figure 4.4. The unit was made up of a compressor with a power rating of 3 kW, an air-source heat pump, oil separator, pre-evaporator, an evaporator pre-condenser, condenser, an expansion device, and capillary tubes. Temperature, flowrate and pressure measuring positions are indicated in Figure 4.4. Pressures readings were measured using pressure transducers calibrated in the range of 0-800 kPa, with an accuracy of ± 2.5 %. RTD sensors measured temperatures with an accuracy of ± 0.5 %.

The flowrate of the refrigerant was gauged by a calibrated orifice installed in the liquid line. Data were collected with a P100 data acquisition system. Thus, pressure, temperatures, flow rates and power logging occurred simultaneously.

The testing was carried out under steady–state conditions with the adherence ARI Standard-240 stipulations and to ANSI/ASHRAE Standard 37-1978. Performance characteristics of R502 were used as a refrigerant of reference in the investigation and the refrigerant charge was not varied at each single test (Air-Conditioning Heating and Refrigeration Institute, 2007).

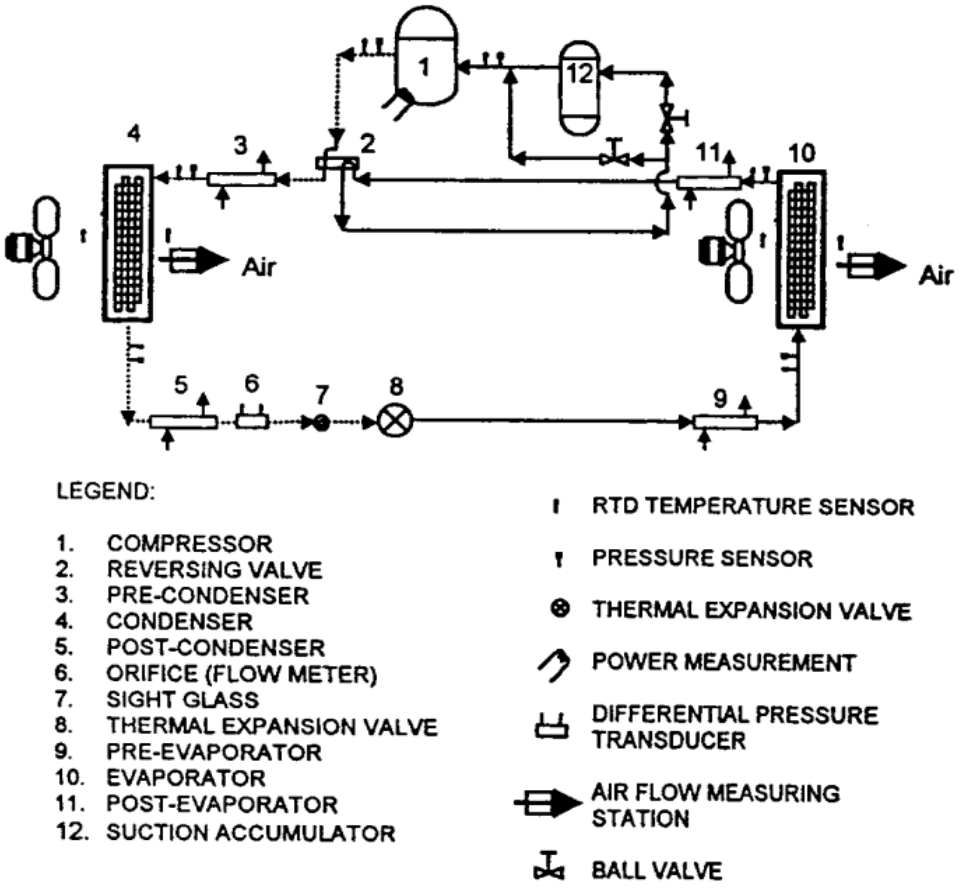

Figure 4-4 : Schematic representation of the air/air heat pump test unit (Extracted from Sami and Desjardins, 2000).

Kim et al. (2007) in investigating circulation concentration of CO_2/propane mixtures and the effects of their charge on the cooling performance in the air conditioners, developed the air-conditioning unit shown in Figure 4.5. The positioning of the charging point for the liquid feed was near the evaporator inlet, as per standard requirements. The heat exchangers employed in the unit are counter-flow types with concentric tubes for high-pressure operations.

The inclusion of the oil separator in the unit was prompted by the fact that the thermodynamic interactions of the oil and refrigerant were not known. The unit was equipped with instruments to gauge pressure, temperature, circulation concentration, mass flow rate, and compressor power. To measure the concentration of propane/carbon dioxide in the circulation, refrigerant mixture samples were taken in liquid and gas form from the liquid receiver and evaporator outlet respectively. Gas chromatography analysed samples in adherence to the standards of ANSI/ASME, (Air-Conditioning Heating and Refrigeration Institute, 2007).

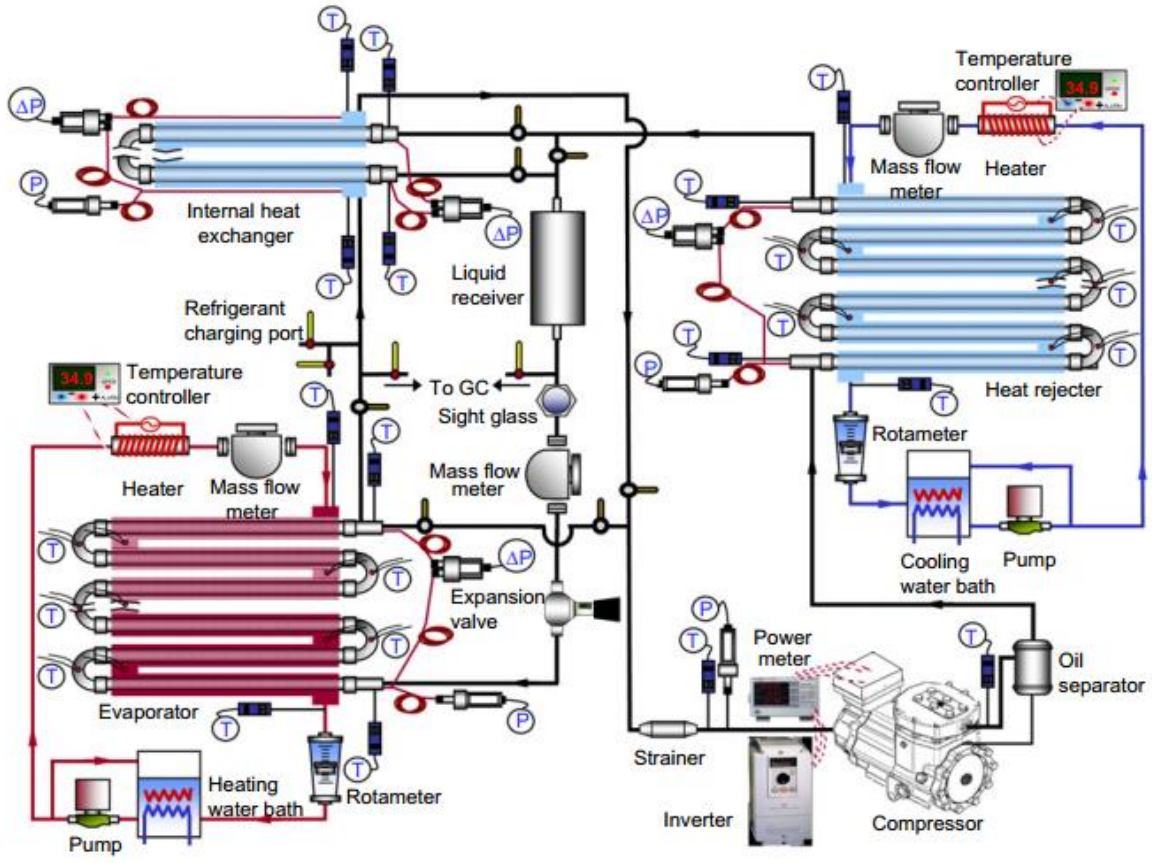

Figure 4-5 : Schematic of the experimental setup for the performance test of CO_2/propane mixture (Extracted from Kim et al., 2007).

Chesi et al. (2012) designed and assembled a refrigeration test rig to investigate the performance of R744 in several cycle layouts. The unit comprised a complete vapour compression cycle with the addition of inter-coolers, economizers and an internal heat exchanger (Figure 4.6) rated up to 14 MPa. The piping and valve network allows for the individual system components to be bypassed and incorporate external components, thus increasing system versatility. Data acquisition software records the following measurements temperature, power, pressure, and mass flow rate.

With the aid of flexible connections and movable basements up to two double-stage compressors can be used, with individual inverters for rotational speed control. Strategically installed oil separators minimize oil circulation through the system on the suction and discharge lines.

Four identical multi-tube-in-tube heat exchangers make up the gas cooler. They are arranged (as seen in Figure 4.6) to partially adjust the flow to the change in density incurred during cooling.

The expansion is facilitated by a needle electronic expansion valve (EEV) and controlled by a bipolar stepper that is set to maintain evaporator superheat. A throttling device is mounted parallel to the EEV for direct control of the expansion process if/when necessary. An additional differential expansion valve (bypass able) was mounted on the gas cooler outlet for adjustment of gas cooler pressure.

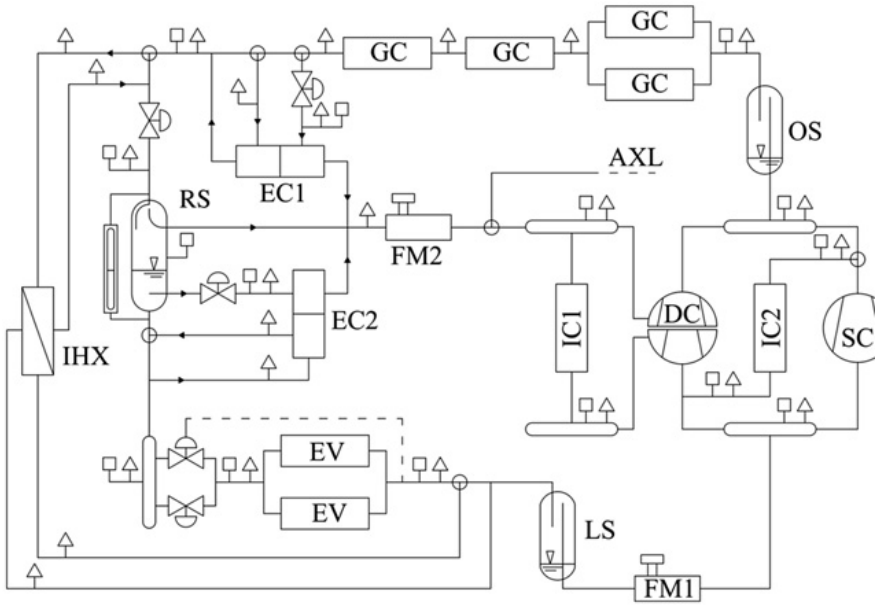

Symbol	Equipment
AXL	Auxiliary line
D/SC	Compressor
EC	Economizer
EV	Evaporator
FM	Flow meter
GC	Gas cooler
IC	Intercooler
IHX	Internal heat exchanger
L/OS	Oil separators
RS	Intermediate pressure receiver

Figure 4-6 : Schematic of the multi-cycle R744 test rig (Extracted from Chesi et al., 2012).

A passive thermal load management system (TLMS) was designed to eliminate the need for additional heaters/ coolers and consequently reduce plant and operation cost. It consisted of three thermally interconnected loops as seen in Figure 4.6. A 5 m^3 water tank (WT) served as the heat sink to the entire TLMS.

The temperature of the (50/50) water/ ethylene glycol stream that provides the heat duty to the evaporator was maintained by heat transfer (HX2) with the water circulating through the gas cooler. To balance the heat duties for this process, a portion of the gas cooler water is first pre-cooled in HX1. The set of valves denoted by circles in Figure 4.7 allowed for two different TLMS configurations that facilitate different temperature ranges for the evaporator and gas cooler. Both heat exchangers were fitted with bypass lines and mixing valves for varying temperatures. These temperatures were maintained by thermostatic PI control of the respective mixing valves. A numerical model was developed to approximate the limitations and performance of the TLMS.

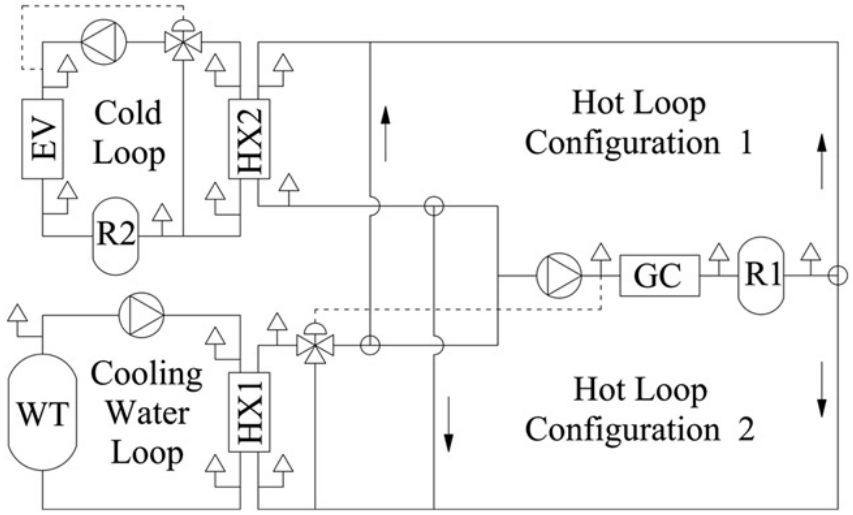

Symbol	Equipment
EV	Evaporator
GC	Gas cooler
HX	Heat exchanger
R1/ R2	Receivers
WT	Water tank

Figure 4-7 : Layout of the thermal load management system (Extracted from Chesi et al., 2012).

The effect of adding an inner heat exchanger (IHX) to a single stage system was also reperted in the study. Experiments were carried out at suction pressures of 2.6 and 3.3 MPa and gas cooler pressures in the range of 6 to 12 MPa (for water outlet temperatures corresponding to 20, 30 and 40 ℃). Evaporator pressure and suction superheat were controlled by adjustment of the expansion valve and variation of evaporator HTF temperature respectively. Gas cooling pressure and outlet R744 temperature were controlled by adjustment of the differential expansion valve and variation of the HTF temperature.

Presented in this chapter are published refrigerant equipment which were used in various laboratory experimental investigations of refrigeration applications. In designing the refrigerant unit utilised for this study, essential technical details stated in the publications were

incorporated and some improvements were crucial due to a number of cycles which were to be operated on the unit. As previously discussed, the properties of different refrigerants are such that they place many restrictions on the units for which they are designed, the majority of which are only economically operable with the design refrigerant.

In the test rig developed for this study, the positioning of critical components such as sight glasses and filter dryers in this study was in line with specifications outlined in this preview.

The refrigerant unit was designed to operate in a number of cycles which are simple vapour - compression cycle, two-stage vapour compression cycle, cascade system, vapour compression cycle with a suction-line heat exchange. Also, the test rig can be used for the investigation of the following refrigerants and refrigerant blends, R134a, R22, R404a, R407C, R407F, R410a or R507a as per filter dryer specifications and refrigerants R134a, R404a, R407A/C/F, and R507a as these are compatible with the compressor oil. Moreover, there are limitations due to temperature and pressure pertaining to the unit's operation range, these being 100 ℃ and 1.9 MPa respectively.

Chapter 5

5 Equipment Description

This chapter presents the original design of the test unit, the description, and specifics of each component in the unit and the modifications carried out.

The refrigeration test rig used in this study was designed and built in the Thermodynamics Research Unit by a MSc. Eng. student, Ms. Alisha Kate Shadrach, under the supervision of Professors J.D Raal, P Naidoo, and D Ramjugernath. The unit was designed in the year 2012. Although the unit was assembled during 2014, it was not commissioned. Calibration of sensors and pressure tests were carried out soon after the construction phase however, Shadrach did not overcome the issues of sealing in achieving very low pressures/desired level of vacuum required in the refrigeration unit.

During the initial part of this study, the need for major modifications were identified and as such changes had to be made to the equipment design and construction. These modifications are discussed in section 5.7 which included overcoming the sealing problems encountered in the unit which were mainly due to leaks in the condenser seals, vibration eliminators and in a number of loose joints in the unit. Furthermore, to achieve the throttling effect the metering valves were removed due to their small orifice which was a hindrance to the passage of the liquid refrigerant to the expansion valve. There was also a need to replace water baths at the condenser and evaporator with larger ones to meet the duties of these two heat exchangers.

5.1 Original Design

The refrigeration unit was intended to be utilised in evaluating the performance of the existing, potential and alternative refrigerants and refrigerant blends for refrigeration application. In this study, the experimental measurements were carried out in a simple vapour -compression cycle. Additionally, the test rig can also be configured into the following different cycles:

- Two stage Vapour – Compression Cycle
- Cascade System
- Vapour –Compression Cycle with a Suction-line Heat Exchanger

The presentation of the schematic design of the original refrigeration unit is shown in Figure 5.1. The unit has three main parts: the low-pressure (LP) section: the data acquisition section and the high pressure (HP) section. The LP section contains an evaporator (EV-01); the HP

section houses a condenser (CN-01) and; the data acquisition system has a cRIO (Compact Reconfigurable Input and Output unit). The unit has two compressors for use in the cascade cycle and two-stage vapour compression cycle. The components of the units and their specifications are listed below:

- a suction line heat exchanger: 3.5 kW capacity B3-012-28-H brazed plate heat exchangers
- an evaporator: 2.5 kW capacity B3-012-14-H brazed plate heat exchangers
- a condenser: 3.82 kW capacity B3-027-16-H brazed-plate heat exchangers
- two semi-hermetic reciprocating Bitzer 2KES-05(Y) compressors (each with a compressor control panel),
- two Danfoss VLT Microdrive for motor frequency control,
- two Afcon Industrial Equipment Heldon oil separators,
- two Afcon Industrial Equipment Heldon suction accumulators,
- two Afcon Industrial Equipment liquid receivers,
- two water baths (10 litres and 34 litres),
- two Elepon-seal-less SL-10S 0.1 kW, 220 V (centrifugal) liquid pumps,
- two 1-10 L/min Ximatrix water rotameters, bottom/top entry brass,
- two SAD-163 solid core liquid line filter driers,
- two ¼ flares KSG2MF liquid line sight glass moisture indicators,
- two Swagelok SS-4MG-BU-MH, 0.0056inch/1.42mm metering valves,
- two Swagelok SS-4L-BU-MH, 0.128inch/3.25mm orifice expansion valves,
- two variable frequency drives (VLTs) (one for each compressor), and
- multiple two ports and three port Swagelok valves,
- nine WIKA A-10 pressure transmitters
- eleven WIKA T1TEBTSS15 temperature thermocouples,
- A network of copper and stainless pipes that connect the components in the unit.
- two Grant TX150 digital temperature controller
- two PolyScience flow through chillers model KR-80A

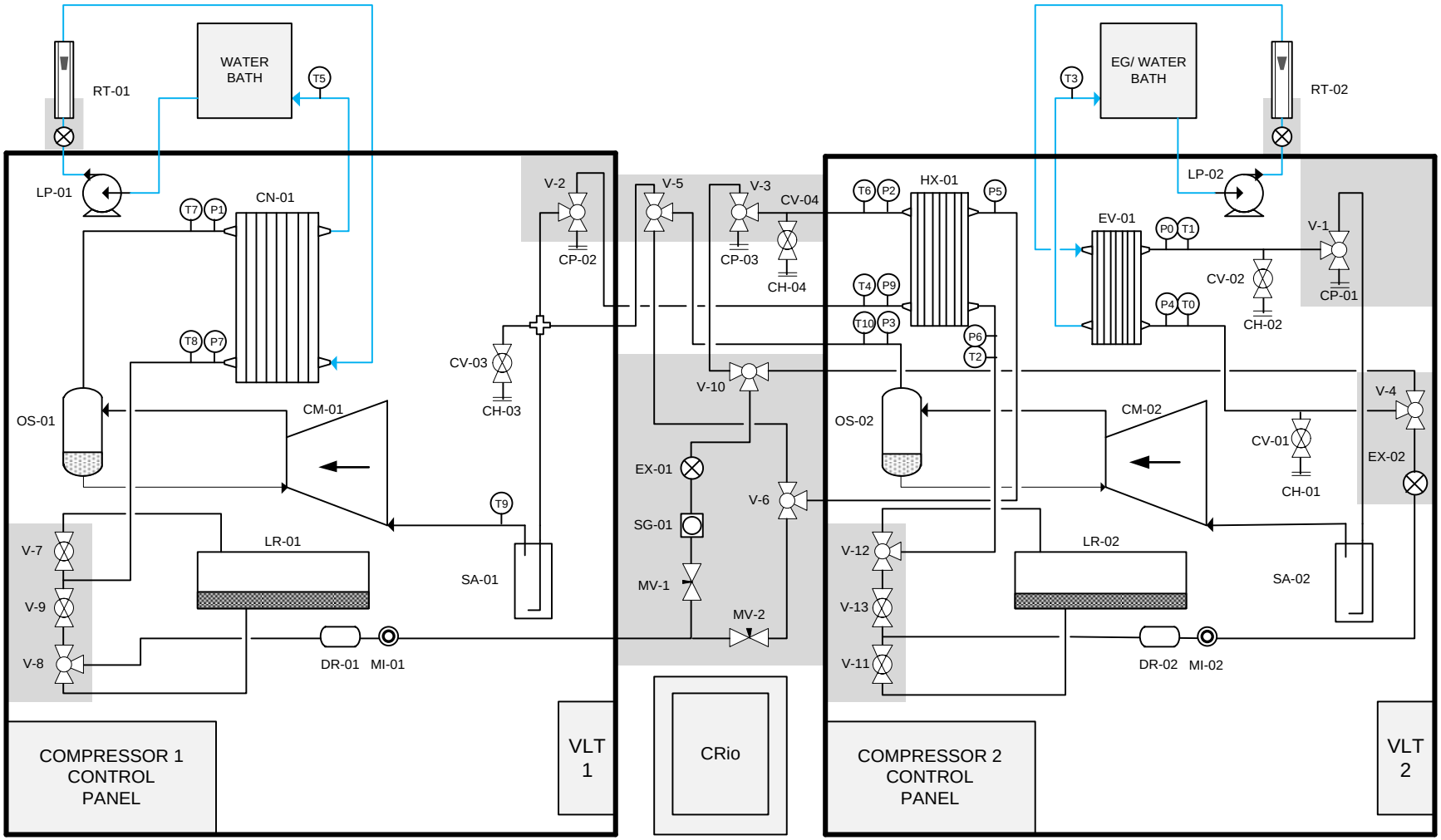

Figure 5-1 : Original schematic of the test unit (Produced by Shadrach, 2014).

CH-Charging point, **CM**-Compressor, **CN**-Condenser, **CP**-Connection point, **CRio**-Data acquisition unit, **CV**-Charging valve, **DR**-Filter drier, **EV**-Evaporator, **EX**-Expansion valve, **HX**-Inter-heat exchanger, **LP**-Liquid pump, **LR**-Liquid receiver, **MI**-Moisture indicator, **MV**-Metering valve, **OS**-Oil separator, **P**-Pressure transducer, **RT**-Rotameter, **SA**-Suction accumulator, **SG**-Sight glass, **T**-Thermocouple, **V**-Valve, **VLT**-Variable frequency drive.

5.2 Refrigerant Cycles in the Test rig

Schematic representations and descriptions of each refrigeration cycle configuration possible in the unit are detailed in Appendix C.

5.3 General Unit Description

The refrigeration unit comprises of four charging points, labeled CH (charging point) as shown in Figure 5.1. These ports were used to introduce the refrigerant into the unit. CH-01 and CH-04 were liquid refrigerant inlets located in the liquid line, while gaseous refrigerant charging ports CH-02 and CH-03 were located on the suction line.

5.3.1 Piping

Copper and stainless-steel pipes commonly used in air-conditioning and refrigeration systems, were used as refrigerant pipelines in the unit. Metal pipes are named after their internal pipe diameters. In this unit, ⅝" (⅝ inch), ⅜" (⅜ inch), ⅛" (⅛ inch), ¼" (¼ inch), ½" (½ inch) pipes were used for refrigerant pipeline in the test rig. These pipes were insulated with nitrile rubber insulation, of Armaflex class O type, to exclude the environmental influence on the system.

The ½" copper pipe was used as the compressor suction lines and in linking the oil separators and the compressor. In these sections, the refrigerant was in the vapour phase.

The ⅛" stainless steel pipes are the smallest in diameter when compared to the other pipes fixed in the unit. These pipes were fitted in between the pressure tap-off points and the pressure transducers.

The use of ⅜" copper pipe was extensive in the unit. It was mainly utilised in the transportation of the liquid-vapour refrigerant mixtures. Primarily, the ⅜" line was used to convey the compressed gas from the compressor to the condenser; and to carry the refrigerant from the oil separator, i.e., OS-02 to valve 6 (refer to Figure 5.1). Also, it was installed at the heat exchanger outlet, via P2 and T6 through V-3, and then to V-10, where the pipe branched: one end led to EX-01 and the

other to V-4. Emanating from V-4 were two lines of ⅜" pipe lines, one led to the evaporator through P4 and T0 the other one terminates at EX-02.

The ¼" copper pipe was utilised mainly in the transportation of the liquid refrigerant. It was fitted at the condenser outlet, where it channelled the refrigerant through the liquid receiver. It conveyed the refrigerant through the filter drier and sight glass, then branched to EX-01 and MV-2, through V-6, towards the heat exchanger inlet, through P5. Also, the ¼" pipe was fitted at the suction line heat exchanger outlet, through P6 towards V-12, through the liquid receiver, the filter drier (DR-02) and moisture indicator, towards EX-02.

The ⅝" was used as the inlet and outlet pipes for the two suction accumulators, the oil separator outlet and for the liquid receiver outlet pipe.

A steel hose constructed from deep pitch corrugated hose covered with a stainless-steel braid, was used as a connection hose between points CP-01 and CP-02 in the vapour compression cycle (the suction line).

The suction and discharge lines of the compressors had flexible hose pipe inserted along their length. These act as vibration eliminators that absorbs compressor vibrations, thus reducing the risk of pipework and equipment damage. Each vibration eliminator was made up of stainless steel braids which cover deep pitch corrugated hose with ferrules to reinforce the hose. At the end of each hose, steel braids were joined to the copper tube ends by means of a high-temperature braze alloy. A typical vibration eliminator is shown in Figure 5.2.

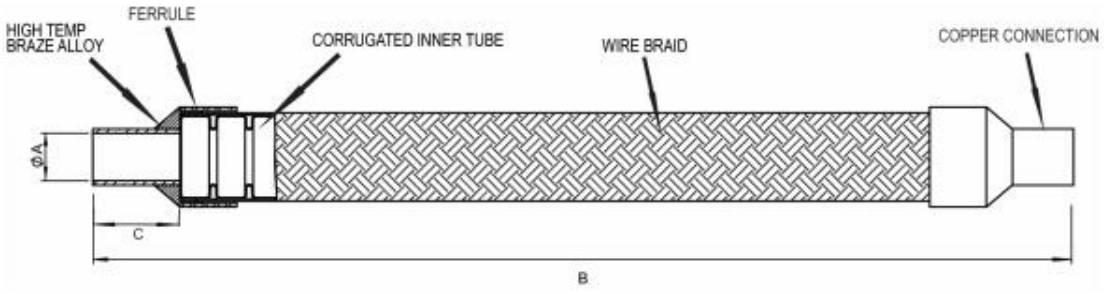

Figure 5-2 : Stainless Steel vibration eliminator (Extracted from Heldon, 2009b).

5.4 Component Specification

5.4.1 Expansion Valve

The throttling devices used in the test rig were Swagelok fine metering valves. These pressure changers were manually operated valves, i.e., they were hand adjusted depending on the system's load. The valve was a screw down, needle valve, designed to provide fine adjustments (McGeorge, 1998). The properties of the valves are given in Table B.2 in Appendix B.

In the hand-operated valve, the change in diameter in the flow pipe gives resistance to the liquid, which provides the needed pressure drop in the refrigerant flow. In this case, the maximum orifice of the throttling valve was 0,128 inches (3.25 mm).

In the original design of the unit, a metering valve was placed before the throttling valve with the purpose of metering the refrigerant flow and regulating the amount of refrigerant passing through to the expansion valve. The metering valve was hand-operated, with the same specifications as the expansion valve: its maximum orifice was 0.0056 inch/1.42 mm. It was placed at the high-pressure section of the flow. In the experimental runs, the expansion valve was set at either a fully open position or the half open position.

5.4.2 Heat Exchangers

Three brazed-plate heat exchangers acquired from MIT Smart solution perfect systems (in Turkey) were used as the condenser, the evaporator, and the suction line heat exchanger in the unit. The specifications of these units are provided in Table 5.1. This type of heat exchanger was selected because of its compactness and efficient performance in refrigeration applications (Hesselgreaves, 2011).

Plate Heat Exchanger

The plate heat exchangers (PHE), consist of a stack of corrugated or pressed metal plates in mutual contact for effective heat exchange by fluid spreading evenly over the plates. Inlet and outlet ports are positioned at the four corners and their seals designed to direct the fluids in other flow passages. The fluids flow in spaces between the adjacent plates which enables the two flowing streams in

adjoining plates to exchange heat as shown in Figure 5.3. The flow pattern shown is referred to as a single pass counter-current of the U-arrangement type.

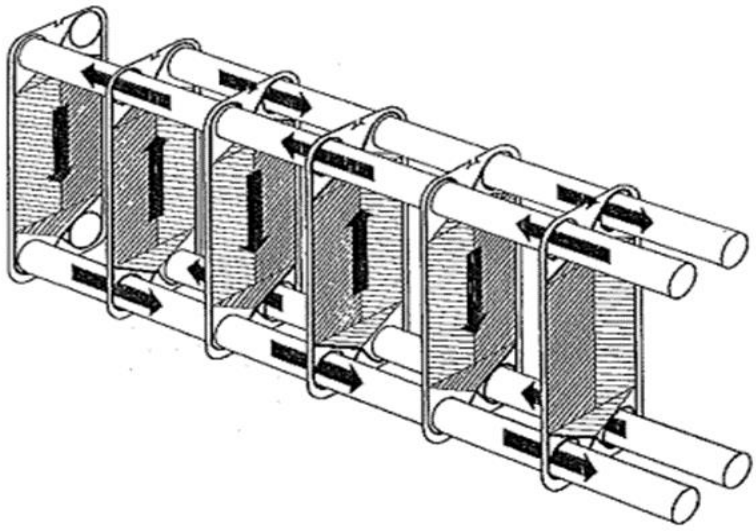

Figure 5-3: Flow diagram of a single-pass counter flow arrangement (Extracted from Kakac et al., 2012).

5.4.3 Evaporator

Water and the refrigerant were the two fluids which flowed counter-current through the evaporator. The liquid-gas mixture, which entered the evaporator, existed in the gaseous form after it gained heat energy from water at a higher temperature, in alternate plates. The evaporator was insulated from the surroundings with nitrile rubber of armaflex class O type.

5.4.4 Condenser

Water and the refrigerant were the two fluids which flowed counter-current through the condenser. The refrigerant entered in a gaseous state and existed in the liquid state. The heat discarded by the refrigerant was evident in the temperature increment of water as it exited the condenser. To eliminate heat exchange with the atmosphere, fiberglass cloth was wrapped around the condenser.

5.4.5 Suction Line Heat Exchanger

In the heat exchanger, two refrigerants interacted as they flowed in different refrigeration cycles. These are combined in refrigeration cycles to increase the performance of the system, and to ensure full evaporation of the liquid that may still be in the suction line (Klein et al., 2000). The specifications of the heat exchangers in the unit are given in Table 5.1.

Table 5-1 : Geometric Specifications of the Heat Exchangers.

Geometric character	***Evaporator***	***Condenser***	***SL Heat Exchanger***
Design capacity (kW)	2.5	3.82	3.5
Fluid flow plate length L (mm)	154	250	154
Plate width W (mm)	72	111	72
Area per plate A (m^2)	0.001	0.021	0.001
Number of Plates	14	16	28
Channels of refrigerant side	6	7	13
Channels on water side	7	8	14

5.4.6 Compressor

Two identical Bitzer, semi-hermetic, reciprocating compressors were installed in the unit. The compressor specifications are given in Table B.1 in Appendix B. These were two-stage compressors capable of two delivery strokes per revolution of the crankshaft (Yadav, 2007). A piston-cylinder arrangement allowed the displacement of the piston in the cylinder to cause a rise in pressure. Each compressor, with little mass handling capacity, could cause large pressure increments.

A single compressor had a power rating of 1.5 kW and could operate between 1.9 to 2.8 MPa gauge pressures. Each was equipped with a Danfoss VLT Microdrive for motor frequency control. This allowed capacity adjustments for different refrigerants and test conditions.

5.4.7 Suction Accumulator

A suction accumulator, also known as the surge drum, was positioned between the evaporator and compressor. It consisted of a U-shaped pipe enclosed in a large cylindrical vessel. One end of this pipe was connected to the suction line leading to the compressor, and the other end was open to the vessel, as shown in Figure 5.4.

The pipeline from the evaporator was fixed to the top of the suction accumulator tank. Any liquid refrigerant entering the tank was exposed to a large volume of this vessel, causing it to evaporate. Consequently, only the gaseous refrigerant was permitted to pass through to the compressor.

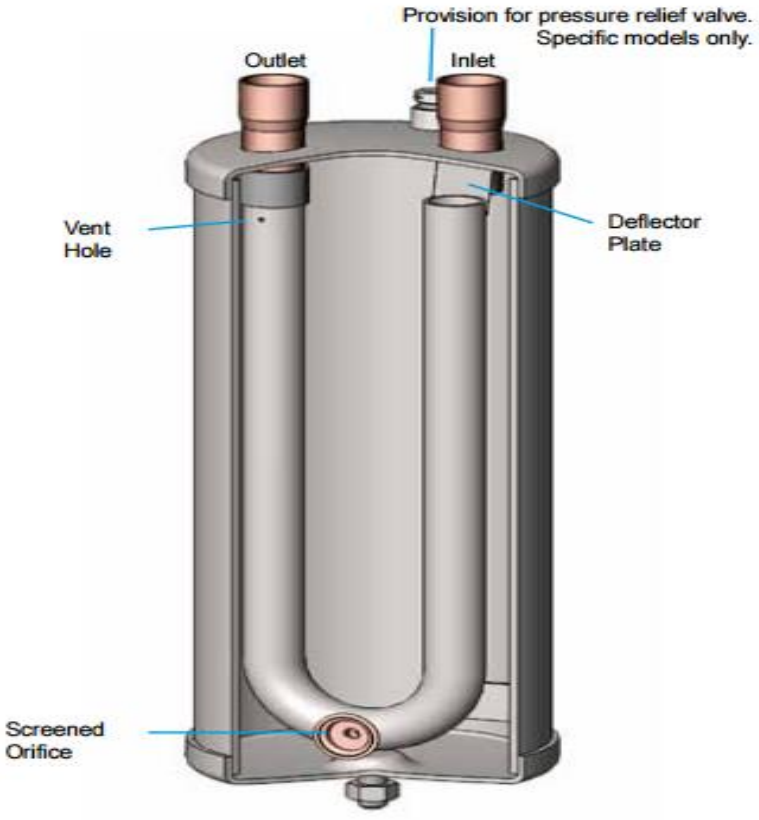

Figure 5-4 : A Cross-sectional view of a Suction Accumulator (Extracted from Heldon, 2009a).

There were two tiny holes drilled into the U-shaped pipe, one was at the bottom where this pipe bends and the other was at the top towards the exit to the compressor. The bottom hole was meant

to allow oil and some liquid refrigerant collected at the bottom of the tank to be channeled back to the compressor. The apex hole was a pressure equalisation orifice. It was for equalising pressure on both sides of the liquid in the pipe to prevent liquid refrigerant, which collected at the bottom of the tank during the off-cycle, from being sucked into the compressor on start-up. Further technical information on the suction accumulators can be found in Appendix B.

5.4.8 Moisture Indicator

As shown in Figure 5.1, moisture indicators were located immediately after the filter driers. There were two moisture indicators in the unit used located in each section (MI-01 and MI-02). The ¼" flare KSG2MF liquid line sight glass was utilised in the unit. The sight-glass had a dual purpose: to confirm that sufficient refrigerant has been charged into the unit, and for indicating the presence of moisture in the flowing refrigerant stream.

In assessing the amount of refrigerant in the system, the sight glass was positioned away from valves and was fixed in a vertical position. In this position, the appearance of bubbles indicated insufficient charge in the refrigeration system.

The colours on the sight glass were used to indicate the moisture content of the refrigerant flowing in the refrigeration system. The signalling material was a porous filter paper saturated with a chemical salt that is sensitive to moisture. As the refrigerant flowed past the indicator, a colour change was observed relative to the moisture content of the refrigerant. A dark green colour indicated that the refrigerant was dry and a yellow colour indicated a wet condition (presence of moisture).

5.4.9 Filter Dryer

The SAD-163 solid core liquid line filter drier was selected for use in the test unit. It had small spherical particles of high strength sintered desiccant in its core, combined with high-density filter cloth which made an effective filter system. The drier was certified by the manufacturer to be effective for use with different refrigerants such as R12, R134a, R410a, R404a, R22, R407C, R500

and R507. The pressure limit of the filter drier was specified as 4.7 MPa and insignificant pressure loss was experienced when the liquid was flowing (Parker Hannifin Corporation, 2015).

The main purpose of the filter drier was to trap and eliminate moisture in the system, for satisfactory operation and longevity of the equipment (Dennis et al., 2010). It could also act as a physical filter for small particles suspendered in the refrigerant.

Possible sources of moisture in the refrigerant unit included the residue of wet lubricant, refrigerant, and desiccant, leakage of water in the water-cooled heat exchanger, admission of moisture-laden air via leaks, admission of moisture into the non-hermitic refrigerant system through hoses and seals.

It was therefore essential to have a drier in the liquid line to remove the moisture/water present in the refrigerant line. To enable a drier to collect and hold moisture it needed to contain a desiccant. Substances usually used in the driers as dessicants are activated alumina, silica gel, and molecular sieves. In this unit (shown in Figure 5.1), the filter dryer was positioned in the liquid line prior to the expansion valve, to prevent moisture from freezing in the expansion valve.

5.4.10 Liquid Receivers

Liquid receivers labelled (LR-01 and LR-02) in Figure 5.1 were located downstream from the condenser and heat exchanger respectively. These receivers maintained a constant liquid (only) flow to the expansion valve and store excess refrigerant during operation at partial load. The valve, installed at the outlet of the receiver, when shut, impeded refrigerant flow to the expansion valve. By shutting this valve, the low-pressure side could be isolated and opened for service, and easily restarted afterward. The bypass lines installed over the liquid receivers were used to gauge the effect of the presence of the liquid receiver on the circulating flowrate and composition.

5.5 Instrumentation

5.5.1 Compact reconfigurable input and output (CRio)

The CRio is a data acquisition system that imports data from the pressure transducers and temperature thermocouples situated at different points in the refrigerant unit and linked to a

computer, through a line flow system of data acquisition. The thermocouples were positioned on the surface of the pipes and held in place using insulating tape while the pressure transducers were tapped from the interior of the pipes.

Pressure and temperature signals from the refrigerant unit were detected by pressure transducers and thermocouples respectively, then fed to the LabVIEW data acquisition software package, using a National Instruments' Field Point DAQ module, for encryption. A total of 9 pressure transducer and 13 thermocouple channels were connected to the unit to measure pressure and temperature changes at their fixed points. The user interface of the data acquisition system is shown in photograph 5-1.

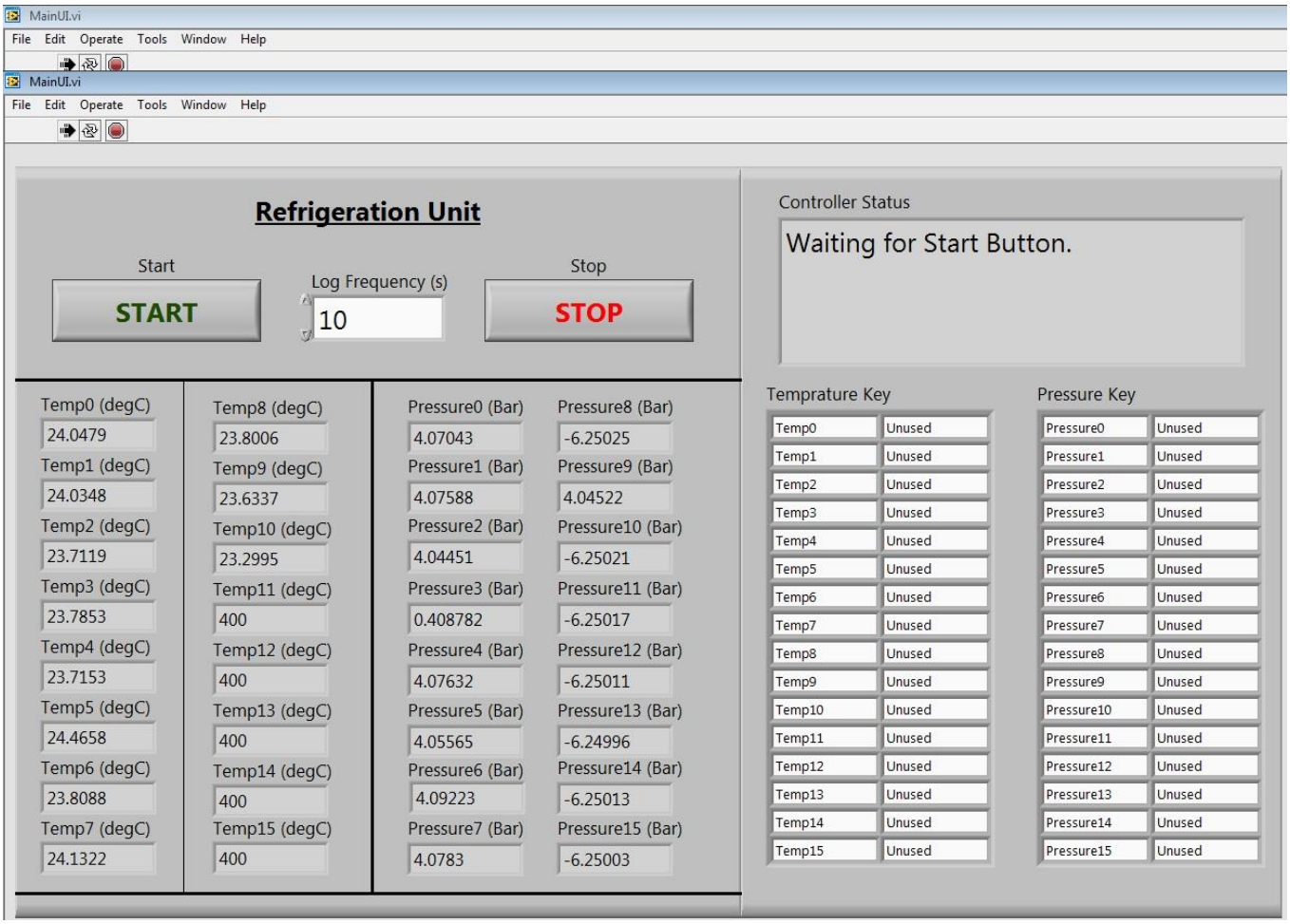

Photograph 5-1: Screenshot of the LabVIEW data acquisition software for the refrigerant unit.

Specifics of the temperature probe and pressure transducers are given in Table 5.2. All channels of data were sent to the computer for screen visualisation of the system operating parameters. This data acquisition system allowed the user to access data from the unit as it operates.

Table 5-2 : Specifications of Instruments

Measured Variable	***Instrument***	***Measurement Range***	***Standard Instrument Uncertainty***
Pressure	Pressure Transducers	0-2.5 MPa	± 0.005 %
Temperature	Thermocouples	-20 to 100 ℃	±0.03 ℃

5.5.2 Variable Frequency Drive (VLT)

The variable frequency drive was used to adjust the speed of the compressor motor and to control the capacity of the compressor. The VLT drive enables the user to vary the speed of the compressor, thereby operating more efficiently at partial load. By closely matching the load, variations in evaporating pressure and fluctuations in load temperature are minimised.

The VLT converts alternating current to direct current, and from this, it generates a simulated alternating current signal at varying frequencies. The compressor was driven by the motor, which operated at a speed proportional to the frequency input to the drive (Emerson Climate Technologies AE4-1299 R9, 2010).

5.6 Water Circuits

The thermal load on the system received water that was electrically-heated in a hot water bath and circulated through the evaporator. The heat transfer fluid (HTF) was selected due to its high heat transfer coefficient, lower freezing point and the ease with which the bath maintained its temperature in comparison to the air temperature of a room/container. Similarly, cold water circulated through the condenser from an electrically-cooled water bath.

In both cases, elepon-seal-less 0.1 kW, centrifugal liquid pumps propelled the water circulation from the water bath through PVC plastic pipes to the evaporator or condenser respectively and back to the water bath. Both the evaporator and condenser bath temperatures were controlled by a

Grant TX150 digital temperature controller. Also, the water flow rate in both water baths was measured by 1-10 L/min bottom/top entry water rotameter supplied by Ximatrix.

To maintain the low temperature of the cold sink, a PolyScience Flow through Chiller, Model KR-80A was used. The return temperatures of liquid water to the water bath was measured by K-type thermocouples inserted into the rubber hose. Calibrated rotameters controlled and measured water flowrates through the heat exchangers.

To maintain a constant water temperature at the condenser inlet, two water baths were utilised, one as a condenser water supply and the other as the hot water sink. The Polyscience temperature Controllers (Model KR-80A) were used in the water baths.

5.7 Design Modifications carried out in this work.

On acquiring the unit and performing initial tests, some leaks were identified during pressure testing. The major leaks were identified on the condensers outlet fittings and along the flexible hose on the vibration eliminators. After the unit had been sealed, it was deemed necessary that modifications were essential to ensure that the unit met the required operating standards.

The modified refrigeration unit used for the study is shown in Figure 5.5, with the red marking indicating the changes made to the original design. These changes are described and explained in the sections below:

5.7.1 Valves

The metering valve, SS-4MG-BU-MH, with a small orifice (ID= 0.00056 inch/1.42 mm) was removed from the liquid line, as it could not facilitate the flow of refrigerant to the low-pressure side. In its place, a stainless-steel Swagelok tube fitting Union Tee (ID=¼ inch/ 6.35 mm) was installed with its branch-off end sealed by welding a piece of metal onto its orifice.

5.7.2 Evaporator water bath

A small (10 litres) water bath for the evaporator, was selected in the original design. It was replaced with a larger (35 litres) water bath. This was motivated by the need to maintain the evaporator load inlet temperature at 25 ℃. Using the 10-litre water bath, the chilled water from the evaporator would reduce the temperature of the evaporator water bath. Thus water at a lower temperature than the set value was pumped into the evaporator.

The continuous chilling of the heat transfer fluid, at the evaporator by the refrigerant, led to a continuous decrease in the evaporator water bath temperature. Therefore, a larger bath (35litre) replaced the smaller one (10litre) to enable the larger water volume to be maintained at an unvarying temperature in the bath.

5.7.3 Evaporator Rotameter

Originally a rotameter measuring in the range of 1-10 litres per minute was selected to measure the heat transfer fluid flowrate through the evaporator. However, at this flowrate the refrigeration effect was not significant. This rotameter was replaced with a Swagelok plastic ball valve. This was done to enable manual manipulation of the valve's aperture to achieve lower flowrates, so that a maximum refrigeration effect could be obtained at minimum evaporator load (Jerald and Kumaran, 2014). The flow rate through the valve was determined using a calibrated orifice.

5.7.4 Condenser Chiller Bath

The 34 litres chiller bath in the original design proved inadequate to chill the warm water coming from the condenser. The water had to be returned, at a lower set temperature, to cool the refrigerant passing through the condenser. Thus a 50-litre water bath was placed alongside the smaller bath (34-litre). The 50-litre bath was used as a cold sink, receiving warm water from the condenser outlet to chill, before it flowed into the 34-litre bath. The smaller water bath was maintained at a constant temperature to supply the condenser with water at a fixed temperature. This was done to keep the heat sink at a constant temperature hence maintained a constant temperature in the system. The baths were positioned in such a manner that the 50-litre bath was placed directly above the

34-litre bath, using a support structure. Water was pumped from the 34-litre bath (feed bath) to the condenser, then high-temperature water emerging from the condenser was directed to the 50-litre bath where it was cooled. To replenish the 34-litre bath, a small diameter pipe siphoned water from the 50 litre. The temperature of the feeder water bath to the condenser was controlled by a Grant TX150 digital temperature controller. The modified condenser water bath is shown in Photograph 5.2.

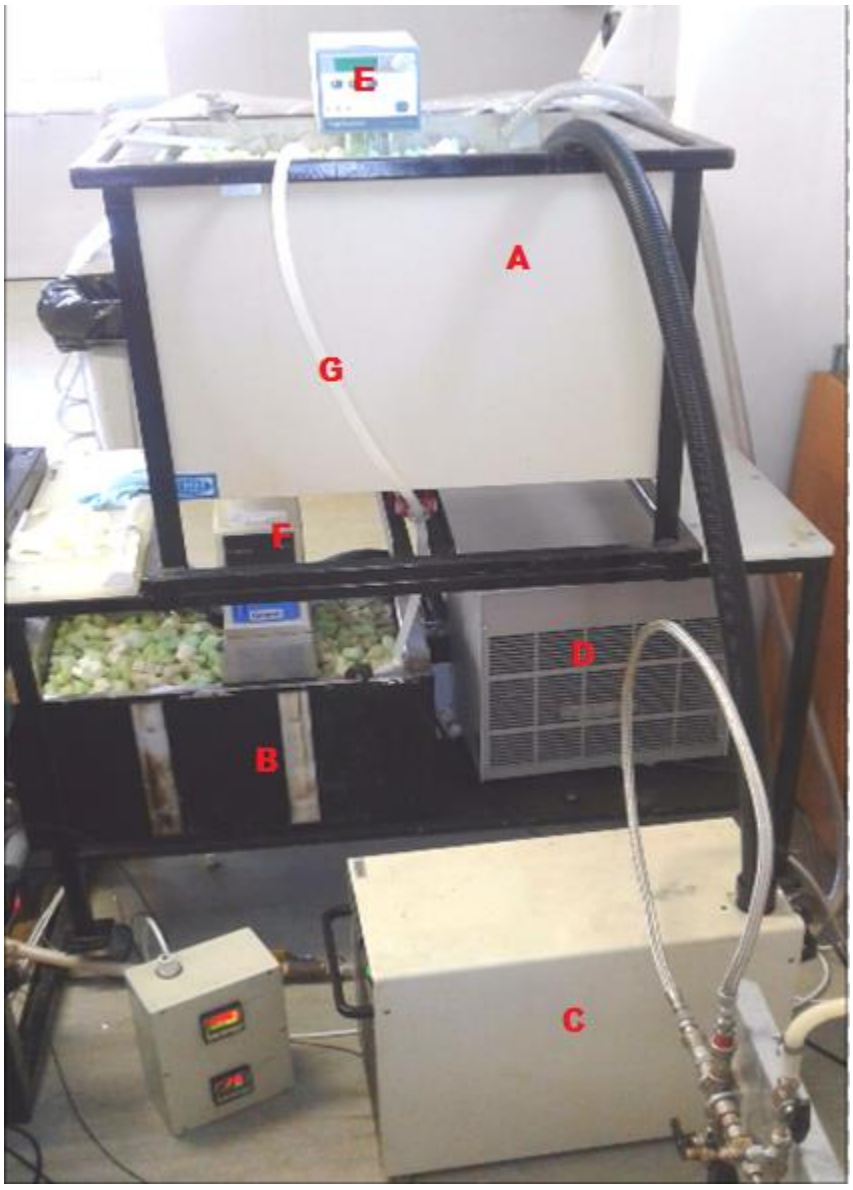

Photograph 5-2 : Modified Condenser water bath set-up. **A**: 50 litre water bath, **B**: 34 litre water bath, **C** and **D**: Cold fingers for the water baths, **E** : Polyscienc temperature controller, **F**: Grant TXF200 programmable temperature controller, **G**: Siphon pipe.

5.7.5 Addition of Temperature Probes

Two Pt 100 temperature probes were added to the unit; one at the expansion valve outlet and the other at the compressor outlet of the refrigerant line. This was motivated by the need to meter the compressor discharge and the expansion valve exit temperature which was not catered for in the original design. However, these could not be added to the LabVIEW data logging system as the type of probes used were not compatible with the system's hardware. Therefore, their readings were manually recorded at regular intervals during system operation.

5.7.6 Charging Gauge

A 5.5/3.8 MPa VMG-2-R410A anti-collision series charging gauge was acquired to meter the pressure difference between low and high pressure during the charging process. It was connected to the suction and discharge valves on the compressor. It was used to monitor the pressure variations in the suction and discharge line of the system during operation.

5.7.7 Insulation

The two heat exchangers were insulated to minimise the heat loss to the environment. The evaporator was encapsulated with armflex rubber foam pipe insulation a low-temperature insulating material, while the condenser was insulated with a high-temperature fiberglass insulating material. A ½ inch/12.7 mm armflex rubber foam pipe insulating material was added to the pipeline connecting the expansion valve exit and the evaporator inlet, the suction line and the suction accumulator, to conserve energy in the system.

5.7.8 Mass Balance

A DE150K2DL Kern floor standing scale (non-automatic balance) was acquired to meter the mass of the refrigerant charged into the unit. The scale had a maximum weight limit of 150 kg, a minimum weight limit of 4 g, readability, and reproducibility of 5 g. Its uncertainty as specified by the supplier was ± 2 g with a stabilisation time of 2.5 s. The measuring platform dimensions in

the format (B×D×M) mm were: (522×406×100) mm. The refrigerant tank was placed manually at the centre of the weighing plate. When a stable weighing value was observed on the balance reader the refrigerant tank weighing value could be read. Its operating temperature was between 5 and 35 ^{o}C, it could tolerate the air humidity of upto 80%. The following were observed in locating the balance for use;

- was placed in a flat surface, away from open windows and doors to protect it against direct droughts.
- was not be exposed direclty to sunlight to prevent temperature fluctuations and it was not be exposed to extreme heat.
- was not to be exposed to extreme damp conditions for long periods of time.

Photographs 5-3 and 5-4 show the top view of the low pressure and the high-pressure sections of the refrigerant test unit respectively.

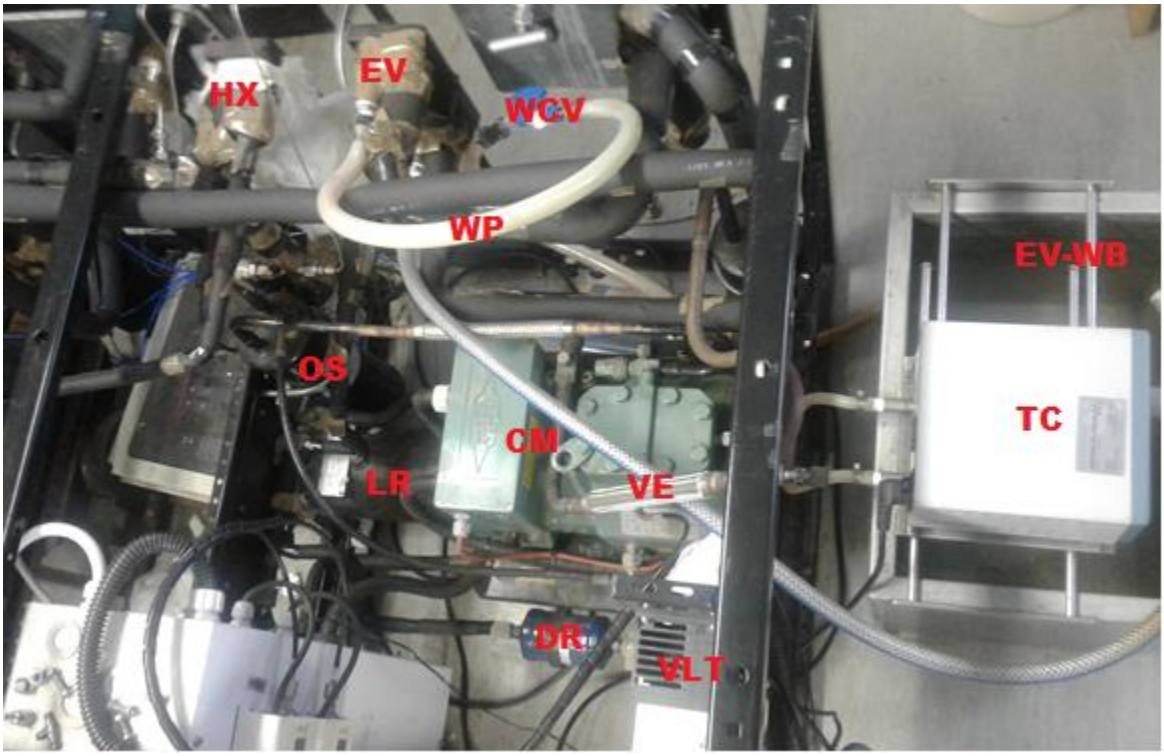

Photograph 5-3: Top view of the low-pressure section of the refrigerant unit. **HX**-Inter-heat exchanger, **VLT**-Variable frequency drive, **CM**-Compressor, **LR**-Liquid receiver, **EV**-Evaporator, **DR**-Filter drier, **TC**-Temperature controller, **WP**-Water pipe, **EV-WB**-Evaporator water bath, **WCV**-Evaporator water control valve.

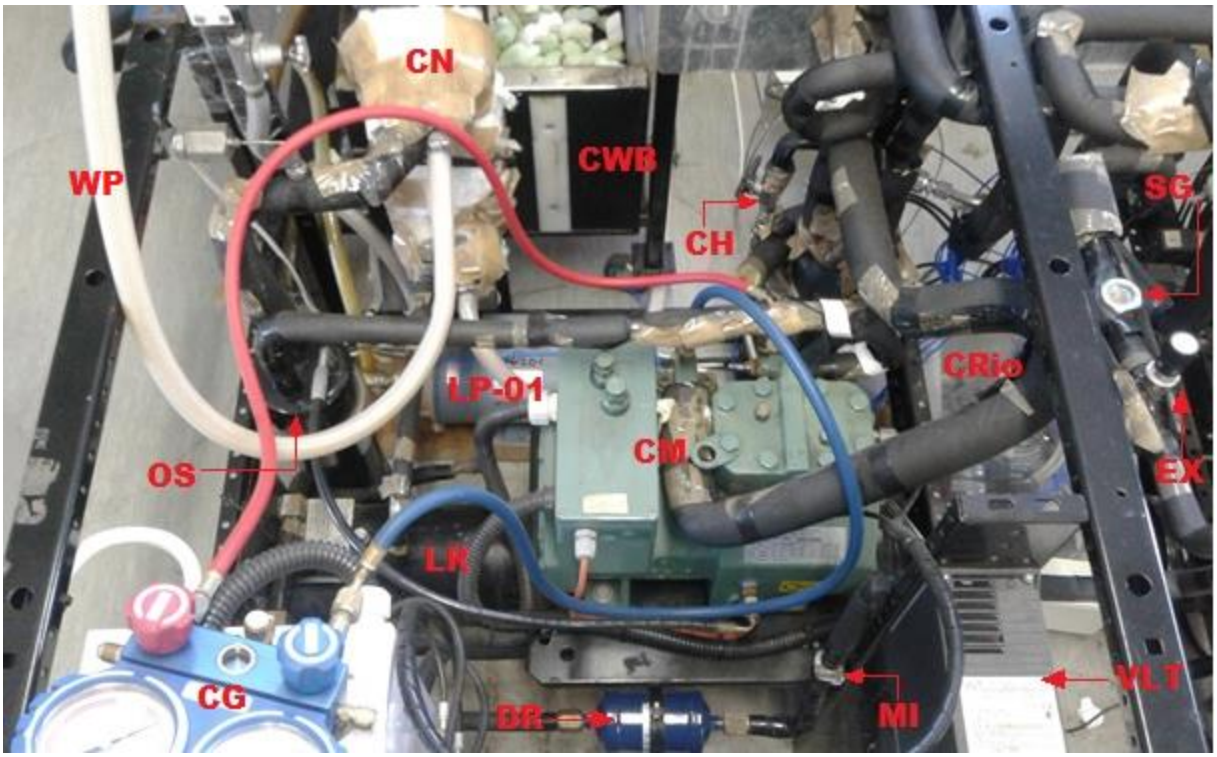

Photograph 5-4: Top view of the high-pressure section of the refrigerant test unit. **CH**-Charging point, **CM**-Compressor, **CN**-Condenser, **CRio**-Data acquisition unit, **DR**-Filter drier, **EV**-Evaporator, **EX**-Expansion valve, **LP**-Liquid pump, **LR**-Liquid receiver, **MI**-Moisture indicator, **OS**-Oil separator, **SG**-Sight glass, **VLT**-Variable frequency drive, **CG**-Charging Gauge, **WP**-Water pipe, **CWB**- Condenser water bath.

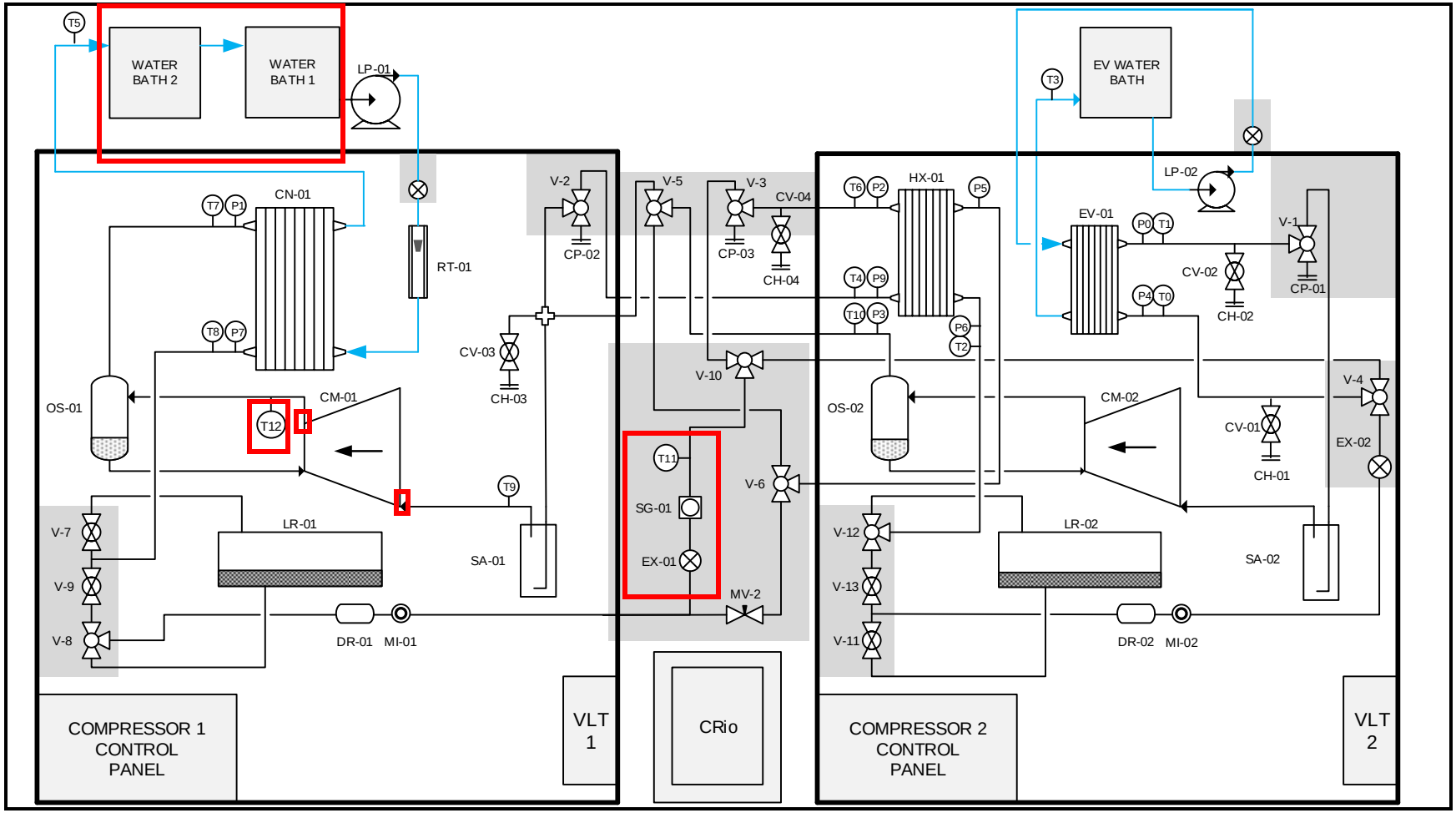

Figure 5-5 : Schematic Design of Modified test unit

CH-Charging point, **CM**-Compressor, **CN**-Condenser, **CP**-Connection point, **CRio**-Data acquisition unit, **CV**-Charging valve, **DR**-Filter drier, **EV**-Evaporator, **EX**-Expansion valve, **HX**-Inter-heat exchanger, **LP**-Liquid pump, **LR**-Liquid receiver, **MI**-Moisture indicator, **OS**-Oil separator, **P**-Pressure transducer, **RT**-Rotameter, **SA**-Suction accumulator, **SG**-Sight glass, **T**-Thermocouple, **V**-Valve, **VLT**-Variable frequency drive**.**

Chapter 6

6 Experimental Procedure

This chapter outlines the equipment preparation procedure prior to use as well as the operation procedure for carrying out experimental measurements. Special emphasis is on the simple vapour compression cycle which is the focus of this study.

6.1 Preparation

It important to ensure that there are no leaks in the system; this is checked by carrying out the leak testing procedure. This system is purged of air and moisture by filling it with nitrogen gas. This is then vented and the system is evacuated using a vacuum pump. The desired operating cycle is achieved by correct configuration of system lines via the use of flexible hoses and manipulation of valves.

6.2 Leak Testing and Detection

It is imperative to ensure that there are no leaks in the system, prior to its use as the leaks would not only affect the performance and control aspects of operation but may also pose a health hazard. The different leak detection procedures for vacant and charged systems are described below. Since all pathways and fittings could not be tested simultaneously the following procedure should be repeated when necessary for the different cycle configurations so that no possible leaks are overlooked. The leak testing procedure is outlined below:

i. Leak testing is effective on a vacant system.
ii. Set the valves such that the whole unit can be pressurised at once through a single charging point.
iii. Use oxygen-free nitrogen (OFN) to pressurise the system via any of the four charging points. Do not use oxygen or other industrial gases. When using dry air isolate the compressor (i.e. keep shut-off valves closed) to avoid compressor oil oxidation.
iv. Test pressure should not exceed the maximum operating pressure indicated on the compressor nameplate (i.e. 1.9 MPa low-pressure limit).
v. Pressurize the unit to a constant pressure value in all sections and shut off the charging port.

vi. Isolate different components and monitor the pressure readings from various transducers overnight or over an extended period. Pressure drop is indicative of a leak/s in that section.

vii. To pinpoint the source of the leak, apply a soapy solution or SNOOP® to joints and other places susceptible to leaks. Formation of bubbles in an area where the soapy solution is applied is an indication of a leak.

viii. Alternatively, an electronic leak detector can be used. With this method, Helium gas must be used to get the desired outcome.

6.3 Start-Up

6.3.1 Vacant System

i. Wear goggles and gloves.

ii. Check the oil level in the compressor: It should be between ½ and ¾ full in the compressor sight glass.

iii. Connect hoses for the desired cycle and set the valve to direct flow in desired directions.

iv. Evacuate the system to a vacuum level of between 53.2 - 26.6 kPa abs, then isolate the vacuum pump. N.B.: Do not evacuate to below 26.6 kPa abs as it will degas particles of the refrigerant oil.

v. Set the heat transfer fluid bath temperatures and leave them to stabilise.

vi. Circulate respective HTFs through the evaporator and the condenser at desired flow rates.

vii. Charge the charging cell with slightly larger volume of refrigerant than is necessary to cater for any unforeseen hiccups.

viii. Connect the charging hosepipe from the valve at the bottom of charging cylinder to the valve on the refrigerant cylinder. The refrigerant cylinder is kept upright so that only gas leaves the refrigeration tank. When the liquid refrigerant is required the tank must be inverted so that the valve is down, with this arrangement, only liquid refrigerant will flow out of the tank.

ix. Connect the charging hose to charging point CH-01 which is at the evaporator inlet when charging a liquid refrigerant or to CH-02 at the suction line when charging vapour refrigerant.

x. To quantify the amount of refrigerant charged into the unit the charging cylinder should be weighed on a digital balance.

xi. The refrigerant is admitted into the system until the pressure of the cylinder is reached, that is, the pressure of the unit is equal to that of the charging cylinder.

xii. At this point operate the refrigerant unit by turning on the compressor (Coggins, 2007).

xiii. With the compressor running continue charging the unit, adjusting the expansion valve in the processing unit until a superheat of between 5-12 ^{0}C and a sub-cooling in the range of 5-15 ^{0}C is achieved.

xiv. The sight glass can also be used to gauge when enough refrigerant has been loaded into the cell; this is shown by the absence of bubbles in the glass.

xv. The system is given about 30 - 40 minutes to reach steady state before results are logged at one-minute intervals for a minimum period of 30 minutes.

xvi. N.B.: Compressor should not be started more than eight times per hour, so as to protect the start capacitors and avoid compressor overheating due to locked up rotor current.

xvii. N.B.: **Charging Vapour Refrigerant**: CH-02 situated at the inlet to the second compressor and CH-03 at the inlet to the first compressor are used for the admission of pure fluid, vapour refrigerants. Following the necessary connections, the refrigerant is then admitted into the system until it has reached the cylinder pressure. The compressor is then started, and the expansion valve reduces pressure in the charging line to a level below that of the cylinder so that the refrigerant will continue to flow into the system. Alternatively, the charging cell pressure may be gradually raised in the hot bath at less than 40 ^{0}C (Hundy et al., 2008) such that the required charge may be admitted before switching the compressor on without the use of the expansion valve. This method of charging is less time-consuming.

Charging Liquid Refrigerant: CH-04 upstream from the inter-heat exchanger and CH-01 at the inlet to the evaporator are used for the admission of (pre-mixed) liquid refrigerant blends. For new mixtures, charge a lower vapour pressure refrigerant at the compressor inlet first, followed by a higher vapour pressure fluid (Jung et al., 2000).

6.3.2 Charged System

i. Set the HTF bath temperatures and leave to stabilize.

ii. Ensure that all valves are configured to the desired cycle.

iii. Circulate the HTFs, at the desired flowrate, through the condenser and evaporator.

iv. Start the compressor.

v. Keep check of the oil level several times within the first hour of operation.
vi. Condenser and evaporator pressures are set by adjusting the respective flowrates.
vii. The expansion valve orifice size is simultaneously adjusted to provide superheat and sub-cooling.
viii. Do not leave the unit unattended until normal operating conditions are achieved.
ix. The system is given about 30 - 40 minutes to reach steady state before results are logged at one-minute intervals for a minimum time of 30 minutes.

6.4 Recovery of refrigerant Blends

The recovery of the refrigerant is the process of obtaining the refrigerant from the equipment and storing it in a separate container.

It is imperative to recover the refrigerant procedurally so as to reduce emission to the atmosphere. When recovering the refrigerant:

i. The container should not be filled over 80 % of capacity because the liquid refrigerant can vaporize and rupture the container.
ii. High and medium pressure refrigerant is recovered with the use of the compressor which pumps the refrigerant to the external container, as shown in Figure 6.1.
iii. Refrigerant must be collected in a liquid form to speed up the process. The receiving container must be at a low temperature to cause a pressure difference between the unit and the container of receipt.
iv. A pump down of the unit is essential to remove all the vaporized refrigerant remaining in the unit.
v. Parts of the unit such as the accumulator can trap the liquid form of the refrigerant which can be reclaimed by gently heating the container using a heating jacket.
vi. Pressure must be monitored when recovery is completed to ascertain whether the evacuation was effective. An increase in the pressure of the system indicates the presence of gas in the system.

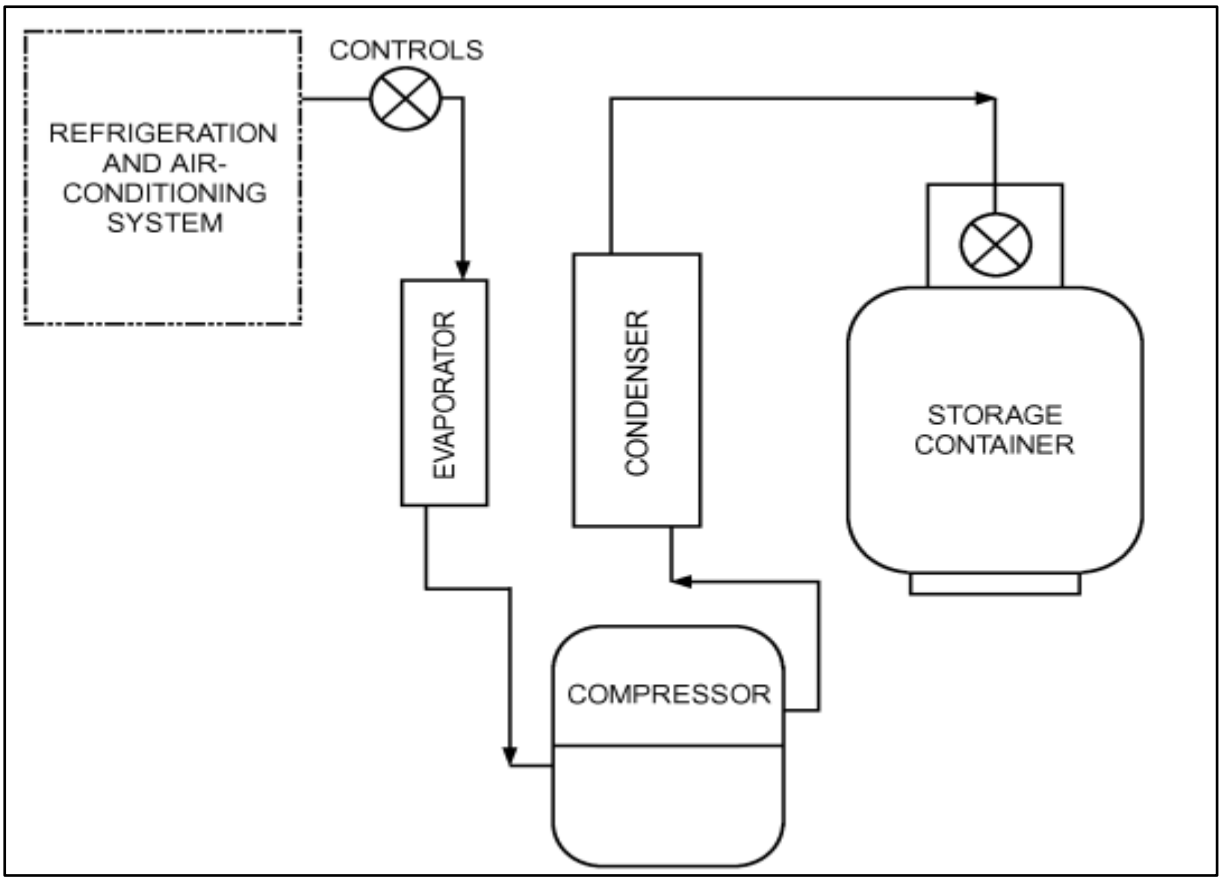

Figure 6-1 : Recovery Unit and the refrigeration system (Extracted from Dennis et al., 2010).

6.5 Calibrations

Prior to use of the refrigerant unit in experimental work, it was imperative to calibrate the temperature and pressure sensors to ensure that accurate readings were obtained.

6.5.1 Temperature

The temperature measurement was accomplished by a total of 13 WIKA T1TEBTSS15 thermocouples placed at different point in the refrigerant unit. These were calibrated against a Pt-100 CTB 9100 standard temperature probe with an uncertainty of 0.03 ^{o}C. The temperature sensor and the standard probe was dipped into the silicon oil bath. The temperature of the bath increment was from -20 to 100 ^{o}C. The temperature of the probes was logged by the LabVIEW data logging system while that of the standard was recorded manually from the monitor on the unit. The uncertainty of the K-type thermocouples was found to be ± 0.1 ^{o}C which is acceptable in temperature measurements for the type of devices used.

6.5.2 Pressure

Nine WIKA A-10 pressure transducers (0-25 MPa rating) were used for pressure measurements in the refrigerant unit. The pressure transducers were calibrated against a standard CPT 600 pressure transducer with an operating range of 0-25 MPa, with an accuracy of 0.005% of the full scale, calibrated by WIKA South Africa. The data collected in the calibration process was fitted into a first order polynomial, and the accuracy of each transducer was ± 0.026 MPa.

6.5.3 Flowrate

A liquid ½" bottom/top entry brass rotameter was used to meter the water flow rate through the condenser. Water was pumped through the rotameter, which had a needle valve at the bottom inlet to control the amount of incoming fluid. The rotameter was graduated to meter flow in the range of 0.5-10 L/min, with an increment of 0.5 L, while a float was used to set the flowrate at to the desired value.

In the calibration of the rotameter, water was pumped into a measuring cylinder for a minute; the flow rate was then increased. The process was timed using a stopwatch, and repeated runs were performed with the average value being used. The data obtained was then fitted to a first order polynomial. A ball valve controlled the water flow through the evaporator. The flow rate was determined by repeatedly timing water flow into a 5000-ml measuring cylinder. By changing the orifice opening, markings were made on the orifice, with each marking denoting a specific flowrate.

6.5.4 Experimental Uncertainty Measurements

In computing the uncertainty in the temperature and pressure measurements in this study a full description of formulaes and methods used are given in Appendix E. The combined uncertainty $u_c(x)$ is calculated from the uncertainty which arises from any of the two categories of uncertainty type A or type B. The type A uncertainty is evaluated by statistical methods in which the mean is taken to represent the true value (Taylor and Kuyatt, 1994). It is calculated by the flowing formula:

$$u_i(x) = \frac{\sigma}{\sqrt{N}} \qquad 6.1$$

where σ the standard deviation of the data and N is the number of data points. Type B uncertainty is evaluated by several methods and information related to the measurements. The uncertainty can lie anywhere between the distribution and such distributions are known as rectangular. They are represented by:

$$u_i(x) = \frac{b}{\sqrt{3}} \qquad 6.2$$

where b is the half the width of the interval. The rectangular distribution model is always the default model in the absence of any other information (Taylor and Kuyatt, 1994).The combined uncertainty of temperature is given by:

$$u_c(T) = \pm\sqrt{u_{calib}(T)^2 + u_{rep}(T)^2 + u_{instr}(T)^2} \qquad 6.3$$

where $u_{rep}(T)$ denotes the standard uncertainty because of repeatability of a measurement, $u_{instr}(T)$ is the uncertainty of the Pt-100 standard temperature probe and $u_{calib}(T)$ denotes the standard uncertainty as a result of temperature calibration and is determined by:

$$u_{calib}(T) = \pm\sqrt{u_{std}(T)^2 + u_{corr}(T)^2} \qquad 6.4$$

where $u_{corr}(T)$ denotes the standard uncertainty because of the temperature calibration correlation and $u_{std}(T)$ denotes the standard uncertainty inherent in the standard temperature probe. The value used for the calibration uncertainty in this study (in Table 7.5) was the largest

value obtained in the calibration of all the seven temperature sensors. Likewise, the combined standard uncertainty in pressure is calculated by:

$$u_c(P) = \pm\sqrt{u_{corr}(P)^2 + u_{rep}(P)^2 + u_{std}(P)^2 + u_{atm}(P)^2} \qquad 6.5$$

where $u_{corr}(P)$ is the standard uncertainty due to the pressure calibration correlation (Type B), $u_{std}(P)$ is the standard uncertainty of the pressure transducer, and $u_{rep}(P)$ is the standard uncertainty due to the repeatability of the pressure measurement. Likewise, the value used in the study for the calibration uncertainty in pressure was the largest values of all the values obtained from four pressure transmitters.

Rotameters measure the water flowrates through the condenser and evaporator. The combined uncertainty of flowrate is given by:

$$u_c(F) = \pm\sqrt{u_{corr}(F)^2 + u_{rep}(F)^2} \qquad 6.4$$

where $u_{rep}(F)$ is the standard uncertainty due to the repeatability of the flowrate measurement and $u_{corr}(P)$ is the standard uncertainty due to flowrate calibration correlation.

Chapter 7

7 Results and Discussions

The results obtained in the experiments and simulations carried out in this study are presented, analysed and discussed in this chapter. This chapter consists of three main sections. In the first section results obtained in the commissioning stage are presented and analysed, the second section is a comparative study of the performance of the three refrigerants studied. The third section is a comparison of the experimental performance of the refrigerants with the theoretical performance obtained from Aspen Plus ® simulations. In the final section, the refrigerant blends investigated are discussed with the aid of the simulated results. Firstly, the chemical purity, physical properties of refrigerants and uncertainty in measurements are discussed.

7.1 Chemical Purity and Physical Properties of Refrigerants

The chemical purity and supplier details are presented in Table 7.1.

Table 7-1 : Details of the chemicals used in this study.

Refrigerant	*CAS Number*	*Supplier*	*Purity (*wt %)*
R134a (1,1,1,2-Tetrafluoroethane)	811-97-2	Afrox	> 99.7
R507a (Pentafluoroethane/1,1,1-Trifluoroethane (50/50))	354-33-6/420-46-2	Afrox	> 99.7
R125 (Pentafluoroethane)	354-33-6	Kovco	> 99.5
R413a (Octafluoropropane/1,1,1,2-Tetrafluoroethane/Isobutane (9/88/3))	811-97-2/76-19-7/ 75-28-5	Kovco	> 99.7

*Purity stated by the supplier.

The chemicals were of high purity as per supplier specifications. It is imperative to use chemicals of high purity in refrigeration operations to avoid the clogging of the expansion valve orifice and the contamination of the compressor oil. Water used in the water baths, was acquired from the municipality water supply line.

Table 7.2 presents the physical properties of the refrigerants used in this study. As discussed by Venkatarathnam and Murthy (2012), the critical temperature and normal boiling point are fundamental thermodynamic properties of a refrigerant which influence the vapour pressure

and the latent heat of vaporisation. The refrigerants selected in this study have comparable critical pressures and temperatures, boiling points and molecular weights. Furthermore, their selection was influenced by their availability and zero ODP rating. However, while their GWP is in an acceptable range, the new European Union Fluorinated greenhouse gases (EU F-Gas) regulation states that from 2020, refrigerants with GWP value less than 2500 will be acceptable in refrigeration applications (Bitzter, 2014).

Table 7-2 : Thermodynamic Properties of Refrigerants

Refrigerant	***R134a[a]***	***R125[b]***	***R507a[c]***	***R413a[d]***
Molecular weight (g mol^{-1})	102	120	98.86	103.96
Critical Temperature (℃)	101.1	66.2	70.9	101.3
Critical Pressure (MPa)	4.06	3.63	3.79	4.11
Bubble point (℃)	-26.1	-54.6	-46.7	-35
Dew point (℃)	-101	-	-	-28.1
Temperature Glide (℃)	0	0	0	0
ODP	0	0	0	0
GWP	1300	3400	3900	1900

[a] (Karagoz et al., 2004) , [b] (Mohanraj et al., 2011) , [c] (Arora and Kaushik, 2008), [d] (ISCEON Refrigerants, 1998). (–) not determined.

7.2 Uncertainty in Measurements

In experimental work, it is imperative to maintain high accuracy and precision to ensure credibility of the results obtained. To ensure this, clinical adherence to the experimental procedure, careful equipment handling, and calibration of the sensors is crucial. The calibration is done to ensure that the measuring device is reporting a true measurand.

The result of a measurement is an estimate of the value of the specific quantity subject to a measurement called the measurand. Consequently, for the result to be complete, a numerical value of its uncertainty is supposed to be accompanying it.

In computing the uncertainty of a measurement, the instrumental error, calibration uncertainty, and repeatability uncertainty were incorporated. Appendix D gives the methods and formulas for calculating the uncertainty of temperature, pressure and flow rate measurements. The calibration procedures followed were discussed in Section 6.5 of this study. Tables 7.3 and 7.4 present the calibration information for the temperature sensors and pressure transducers respectively. The trend line equations in Table 7.3 were generated using an Excel worksheet by plotting the standard temperature obtained from the WIKA standard probe against the

temperature measured by each temperature sensor. The same method was used to derive the trend line equations for pressure transducers and the results are displayed in Table 7.4, however in this case, the pressure values from the standard pressure gauge were plotted against the pressure readings obtained from the pressure transducers. The details for the sensors and the transducers is given in section 5.5 and their location in the test rig are shown in Figure 5.5. The calibration uncertainty reported in Table 7.3 and Table 7.4 was determined by Equation 6.2.

Table 7-3 : Temperature Sensors Calibration Details.

Temperature Sensor	***Trend line Equation***	***R^2***	***Calibration Uncertainty/^oC***
T0	y = 1.0069x – 0.2009	1.000	±0.04
T1	y = 1.007x – 0.1219	1.000	±0.04
T3	y = 1.0073x – 0.003	1.000	±0.04
T5	y = 1.0065x + 0.1052	1.000	±0.04
T7	y = 1.0063x + 0.1875	1.000	±0.04
T8	y = 1.0056x + 0.2522	1.000	±0.03
T9	y = 1.0063x + 0.3016	1.000	±0.04
T11	y = 1.0074x – 0.0963	1.000	±0.04
T12	y = 1.0057x + 0.2475	1.000	±0.04

Table 7-4 : Pressure Transducers Calibration Details.

Pressure Transducer	***Trend line Equation***	***R^2***	***Calibration Uncertainty/kPa***
P0	y = 1.0029x – 0.0612	1.000	±2.24
P1	y = 0.9988x – 0.0009	1.000	±2.58
P4	y = 1.0042x – 0.0494	1.000	±2.46
P7	y = 1.0029x – 0.0427	1.000	±2.39

Table 7.5 presents the contributing uncertainties considered in computing combined expanded uncertainty for temperature and pressure measurements in this study. For the temperature calibration, the uncertainty due to repeatability had no effect on the measurements thus it was not considered. The formulas used to calculate the combined standard uncertainty are presented in Appendix D.

Table 7-5 : Uncertainties in measurements related to this study.

Uncertainty source (x)	*Temperature (°C)*	*Pressure (kPa)*
Instrument error, $u_{instr}(T)$	± 0.03	± 5.00
Standard instrument error, $u_{std}(T)$	± 0.02	± 3.00
Calibration, $u_{calib}(T)$	± 0.04	±2.58
Repeatability, $u_{rep}(T)$	± 0.00	± 1.50
Combined standard uncertainty, $u_c(x)$	± 0.05	± 13.16
Combined expanded uncertainty, $U(x)$	± 0.1	± 26.0

In Table 7.5, the value of the instrumental error for the standard temperature probe was 0.03 °C and 0.050% of the full scale for the pressure transducer as specified by WIKA the supplier of standard instruments. Using Equation 6.2 with maximum deviation value or quantity *b* as specified by the manufacturer, the standard instrument error values obtained were ± 0.02 °C and ± 3.00 kPa for temperature and pressure respectively. The calibration uncertainty value reported in Table 7.5 was the maximum value of the uncertainty values stated for temperature and pressure in Table 7.3 and Table 7.4 respectively.

The combined standard uncertainties (*U*) are both multiplied by a coverage factor of 2 to obtain the combined expanded uncertainty. The combined expanded uncertainty shown in the Table 7.5 provides the level of accuracy for all the pressure and temperature measurements undertaken in this study.

The uncertainty of the rotameter used to measure the volumetric flow rate was ± 0.094 L/min. For this calculation the calibration uncertainty only was taken into consideration. The refrigerant mass was determined by a DE150K2DL Kern floor standing scale with an uncertainty of ±0.002 kg as specified by the supplier.

7.2.1 Uncertainty Analysis for Refrigeration Systems

For refrigeration systems, the uncertainty analysis function *R* as computed by Moffat (1988) was assumed to be calculated from a set of totally *N* measurement (independent variables) represented by,

$$R = R(X_1, X_2, X_3, \ldots, X_N) \qquad 7.1$$

Therefore the uncertainty of the result *R* can be computed by summing up the uncertainties of singular terms using a root-sum-square method (Hoşöz, 2005), i.e.

$$\delta R = \left\{ \sum_{i=1}^{N} \left(\frac{\partial R}{\partial X_i} \partial x_i \right)^2 \right\}^{1/2} \qquad 7.2$$

The uncertainty of the following parameters $Q_{evap}, \dot{W}_{comp}$ and COP can be determined by Equation 7.2. Hoşöz (2005) using Moffat's method in the study to investigate the performance of refrigerant R134 in a single-stage and cascade refrigeration systems. The uncertainty values of $Q_{evap}, \dot{W}_{comp}$ and COP obtained were 4.4%, 16.5%, and 16.8% respectively. Likewise, Datta et al. (2014) employed Moffat's methods of computing uncertainties in the study of the performance of automotive air conditioning system. The uncertainties of $Q_{evap}, \dot{W}_{comp}$ and COP were reported to be 1.75%, 1.76% and 4.72% respectively at the highest charge level.

7.3 Commissioning of unit using R134a

Refrigerant R134a was selected for use in the commissioning stage due to its widespread usage in refrigeration systems and the availability of vast amount of data published on it. Mollier charts were used to analyse the experimental data to obtain the derived results such as COP, compressor work, cooling effect and compressor efficiency.

Test runs were undertaken to confirm that the unit was fit for use on a simple VC cycle. To accomplish this objective, three test runs were carried out at set conditions to assess the functionality of the unit and to produce repeatable and consistent readings within experimental uncertainty. In achieving this, the critical operating parameters were kept constant. These parameters were as follows: mass of the refrigerant, compressor power setting, expansion valve setting, evaporator water flow rate, condenser cooling water temperature, and condenser water flow rate.

The operating parameters selected to conduct the experiments were a refrigerant mass (charge) of 3.115 kg, condenser water flow rate of 2.75 L/min and a bath temperature of 20 ℃. The evaporator flow rate was 0.58 L/min and a bath temperature of 25 ℃ and the 0.128-inch/3.25

mm orifice Swagelok expansion valve was set in the half open position to achieve the desired level of superheating at the evaporator outlet. The compressor was set to 2.20 kW, the voltage to 400 V, current to 3 Amps and an operational speed of 1420 rpm.

Whilst conducting the experiments, the room temperature was maintained at approximately 22 ^{o}C at all times, with the aid of an air-conditioning unit. This temperature control was implemented to eliminate the effects of external temperature variations to ensure a fair test environment. However, ambient temperature fluctuations were experienced during the experiments due to the malfunctioning of the air-conditioning system. The system was assumed to have reached steady-state when temperature and pressure fluctuations had ceased at the condenser and evaporator refrigerant entry and exit points. The system took approximately 40 minutes to stabilise. Once the system had stabilised, the temperature and pressure readings were logged every minute, for more than 30 minutes on the LabVIEW data logging system connected to the computer. The experimental period was limited by the temperature increase in the condenser water bath, i.e., the heat sink.

The reproducibility of the measured results as illustrated in Table 7.6. These results validated the functionality of the unit as the pressure was maintained at a fixed value for each cycle run, indicating no pressure loss or loss of refrigerant to other compartments of the unit or the environment.

Table 7-6 : Results during commissioning of unit using R134a.

Variable	***Run 1***	***Run 2***	***Run 3***	***Run 4***
Evaporator Refrigerant Inlet temp (℃)	-3.2	-3.0	-2.4	-3.4
Evaporator Refrigerant Outlet temp (℃)	-2.3	-1.3	-1.3	-2.5
Compressor Refrigerant Inlet temp (℃)	5.3	6.7	7.1	4.6
Condenser Refrigerant Inlet temp (℃)	56.8	52.9	55.7	54.6
Condenser Refrigerant Outlet temp (℃)	24.7	24.2	24.6	24.2
Evaporator Inlet press (kPa)	233	234	238	228
Evaporator Outlet press (kPa)	226	226	231	220
Condenser inlet press (kPa)	692	673	679	674
Condenser Outlet press (kPa)	687	668	674	669

The variance in the temperature readings presented in Table 7.6 is acceptable relative to the experimental uncertainty with the largest temperature difference between runs being 3.9 ℃ obtained from condenser refrigerant inlet temperatures from run 1 and run 2. Likewise, the

largest pressure difference obtained was 19 kPa for the condenser pressures for run 1 and 2 which was within the acceptable pressure uncertainty. As portrayed in Table 7.6, reasonable repeatability in the reported temperature and pressure readings across the evaporator and condenser units can be observed from the four test runs carried out, thus confirming the reproducibility of the experimental results. However, to ensure that the unit was functioning correctly and providing accurate and reliable results, the variables were investigated at different operating conditions and are discussed in section 7.3.1. The results obtained are discussed in the sections which follow and are compared to the results published in literature.

7.3.1 Variables Investigated

The mass of the refrigerant, compressor power setting, expansion valve setting, evaporator water flow rate, condenser cooling water temperature, and condenser water flow rate were the operating parameters that were varied. The effects of varying these parameters on the pressure and temperature of the refrigerant at the compressor, evaporator, and condenser are presented and discussed in the subsequent sections. Derived parameters, such as system COP, cooling effect, compression work and efficiency were computed from the measured variables.

More than twenty experimental runs were conducted at varying refrigerant mass loadings of 1.437 kg, 2.667 kg, 3.000 kg and 3.115 kg. For each charge, the compressor power was set at either 1.50 kW or 2.2 kW, while the other compressor settings were kept constant. These settings were a voltage of 400 V, current of 3 Amps and an operational speed of 1420 rpm. The condenser water flow rate was varied between 2-3 L/min and its bath temperature set between 15- 20 ℃. The 0.128-inch/3.25 mm orifice Swagelok expansion valve was either fully open or half open. The water inlet temperature to the evaporator was kept at 25 ^{o}C, and its flow rate varied between 0.21-0.78 L/min.

7.3.1.1 Effects of Condenser Flowrate at Constant Mass

In investigating the effect of condenser flow rate at constant mass the following operational parameters were used, the refrigerant mass of 3.0 kg, the compressor power set to 1.5 kW, the condenser inlet water temperature set to 20 ^{o}C, the expansion valve was fully open, and the evaporator water inlet temperature fixed at 25 ^{o}C. The results obtained are tabulated in Table 7.7.

Table 7-7 : Effects of the Condenser Flowrate on system.

Variable	*Run 1*	*Run 2*	*Run 3*
Condenser Water flowrate (L/min)	2.0	2.5	3.0
Evaporator Refrigerant Inlet Temp (^oC)	-2.7	-2.5	-1.7
Evaporator refrigerant Outlet Temp (^oC)	12.9	11.4	-1.5
Compressor inlet Temp (^oC)	14.1	11.8	5.2
Cooling Effect (kJ/kg)	178	177	164
Expansion Valve Orifice/Inch	0.128[a]	0.128[a]	0.128[a]
COP	4.68	5.36	3.64
% Compressor Efficiency	73.7	71.1	55.6
Compression Ratio	3.30	3.17	3.11

[a] Fully open position

When the condenser flow rate was increased it can be observed from Table 7.7 that the evaporator inlet temperature of the refrigerant increased as well, whereas, the evaporator outlet temperature, compression ratio, and compressor efficiency decreased. The decrease in the cooling effect as the condenser flow rate increased was as a result of the reduction in the level of superheating at the evaporator outlet (as observed from the evaporator outlet temperature readings of 12.9, 11.4, and -1.5 ℃ in each of the runs). From the results obtained, the refrigerant exhibited the best performance at a condenser flowrate of 2.5 L/min, with the highest COP of 5.36. The level of superheating at the evaporator outlet is more evident in run 3 than in runs 1 and 2. This was due to the gradual increase of the condenser flow rate by 0.5 L/m from run 1 to run 3. Thus, the heat sink in run 3 had sufficient capacity to cool the refrigerant to cause controlled superheating at the evaporator exit.

7.3.1.2 Effects of Varying Refrigerant Mass

In investigating the effects of varying refrigerant mass, the temperature of the condenser water bath, which cools the condenser, was maintained at 20 ^oC, and the water flowrate through the condenser maintained at 2 L/min. The temperature of the evaporator water bath was kept at 25 ^oC, and the compressor power was set to 1.50 kW.

Table 7.8 presents the results obtained from investigating the effect of varying the refrigerant mass. It can be observed that the suction temperatures increased as the refrigerant charge was increased.

Table 7-8 : Effects of Refrigerant Mass on the system.

Variable	*Run 1*	*Run 2*	*Run 3*
Refrigerant Mass (kg)	3.115	3.000	2.667
Evaporator Water Flowrate (L/min)	0.78	0.76	0.60
Condenser Water flowrate (L/min)	2.0	2.0	2.0
Evaporator Refrigerant inlet temp (^oC)	-1.7	-2.7	-2.9
Evaporator refrigerant outlet temp (^oC)	-1.2	12.9	23.6
COP	3.93	4.68	4.92
Compressor inlet temp (^oC)	6.2	14.1	23.8
Compressor outlet temp (^oC)	61.3	64.6	70.2
% Compressor Efficiency	61.9	73.7	69.4
Gas fraction at Evaporator inlet	0.218	0.197	0.213
Compression Ratio	3.01	3.30	3.12

It can also be observed that the evaporator inlet temperature decreased as the refrigerant mass was increased. Furthermore, the change in the refrigerant charge affected the level of superheat at the evaporator outlet. From table 7.8 it is evident that there is no linear relationship between the vapour fraction at the evaporator inlet and the level of superheating at the evaporator exit. Therefore, it was conclusive that in this case, the level of superheat was influenced more by the amount of refrigerant charge in the system than by the fraction of liquid refrigerant in a refrigerant stream, as the level of superheat increases with a decrease in refrigerant mass. This occurrence might have been caused by insufficient refrigerant charge in the system. The compressor discharge temperature increased with the reduction in refrigerant mass. Low compressor discharge temperatures are desirable for long compressor life thus insufficient refrigerant charge in the unit is detrimental to the compressor. The high degree of superheat at the evaporator exit inflated the evaporator duty resulting in high COP value in run 3.

7.3.1.3 Effects of Compressor Power Settings

The effects of compressor power on the refrigerant performance was investigated and the results obtained are tabulated in Table 7.9.

Table 7-9 : Comparison of Effects of Power Settings on the system.

Variable	*Run 1*	*Run 2*	*Run 3*	*Run 4*	*Run 5*	*Run 6*
Refrigerant Mass (kg)	1.437	1.437	2.677	2.677	3.115	3.115
Compressor Power (kW)	1.50	2.20	1.50	2.20	1.50	2.20
Evap water Flow rate (L/min)	0.26	0.26	0.60	0.60	0.58	0.58
Cond water flow rate (L/min)	2.00	2.00	2.00	2.00	2.75	2.75
Evap refrigerant inlet temp (^oC)	-2.7	-4.2	-2.9	-2.1	-3.0	-2.5
Evap refrigerant outlet temp (^oC)	24.7	24.8	23.6	24.1	-1.3	-1.3
Compressor inlet temp (^oC)	24.8	25.5	23.9	24.4	6.7	7.1
Cooling Effect ($kJ.kg^{-1}$)	192	189	182	186	164	168
Expansion Valve Orifice (Inch)	0.128[a]	0.128[a]	0.128[a]	0.128[a]	0.064[b]	0.064[b]
COP	5.19	4.85	5.06	5.47	4.21	4.20
% Compressor Efficiency	78.4	76.9	69.4	82.4	64.1	62.5
Compression Ratio	3.45	3.48	3.12	3.20	3.03	3.17
Gas fraction at Evap inlet	0.217	0.218	0.213	0.222	0.223	0.204

[a] fully open position, [b] Half open position

Different refrigerant masses were used to investigate this effect. For each setting, the water bath temperatures and flow rates of the condenser and evaporator were kept constant. The ambient conditions were also kept constant to maintain the external variables at a constant state.

As shown in Table 7.9, an increase in the compressor power resulted in a small temperature reduction at the evaporator inlet. Moreover, there were negligible effects on superheating at the evaporator outlet for runs 1-4 but for runs 5 and 6, the throttling degree increased by reducing the expansion valve orifice thus lowering the level of superheating at the evaporator outlet. A decrease in the compressor inlet temperature was observed as well.

The compressor power step up had negligible effects on COP, compression ratio and efficiency, vapour fraction at the evaporator inlet, and on the cooling effect at the evaporator.

7.3.1.4 Effects of the degree of Throttling

A manual Swagelok metering valve was selected for use as a throttling device in the unit. The valve was actuated to render an optimum orifice diameter. This setting enabled sufficient

refrigerant to pass, resulting in the desired cooling effect at the evaporator. Consequently, maintaining a low inlet temperature at the respective unit.

In an endeavor to investigate the effects of the throttling degree on the system performance; three test system conditions were used. For each test system condition, the expansion valve was either fully or half open. Table 7.10 reports the results obtained for this set of experiments. The fixed experimental conditions in each experimental run were as follows:

Run 1 - 3.000 kg Refrigerant charge, 1.50 kW compressor power, 2.5 L/min condenser water flow rate, 0.78 L/min evaporator water flow rate.

Run 2 - 2.677 kg refrigerant charge, 1.50 kW compressor power, 2.0 L/min condenser flow rate, 0.60 L/min evaporator water flow rate.

Run 3 - 1.437 kg refrigerant charge, 2.20 kW compressor power, 2.0 L/min condenser flow rate, 0.26 L/min evaporator water flow rate.

Table 7-10 : Comparison of Refrigerant Properties at different degrees of throttling.

	Expansion Valve Orifice	***Evap Refrigerant In temp (°C)***	***Evaporator Refrigerant out temp (°C)***	***COP***	***Compression Ratio***	***% Compression Efficiency***	***Gas fraction at Evap inlet***
Run 1	0.128[a]	-2.5	11.4	5.36	3.17	71.1	0.217
	0.064[b]	-3.6	12.4	4.59	3.48	74.4	0.213
Run 2	0.128[a]	-2.9	23.6	5.06	3.12	69.4	0.213
	0.064[b]	-4.1	23.7	4.87	3.51	73.7	0.213
Run 3	0.128[a]	-4.2	24.8	4.80	3.48	77.5	0.181
	0.064[b]	-6.6	24.4	4.63	3.48	75.6	0.208

[a] fully open position, [b] Half open position

Run 1 - 3.000 kg Refrigerant charge, 1.50 kW compressor power, 2.5 L/min condenser water flow rate, 0.78 L/min evaporator water flow rate.

Run 2 - 2.677 kg refrigerant charge, 1.50 kW compressor power, 2.0 L/min condenser flow rate, 0.60 L/min evaporator water flow rate.

Run 3 - 1.437 kg refrigerant charge, 2.20 kW compressor power, 2.0 L/min condenser flow rate, 0.26 L/min evaporator water flow rate.

As illustrated in table 7.10, runs 1 and 2, had a comparable temperature decrease of about 1.2 ℃ while in run 3 a temperature decrease of 2.4 ℃ was obtained. These temperature changes resulted from changing the throttling effect. A higher temperature was observed in run 3 due to a higher power setting of the compressor and the low evaporator flow rate in comparison to runs 1 and 2. For each refrigerant charge, the compressor power setting, the water bath temperature and the flow rates of the condenser and evaporator were both kept constant.

7.3.2 Comparison of experimental results to literature.

The results obtained from the test rig were compared with data obtained from published articles found in open literature. The articles from literature utilised in this comparative study were selected based on the evaporator and condenser temperatures of the investigations in their respective publications. The operating conditions of the selected articles are discussed briefly below:

Domanski (2006) conducted an analytical investigation of R134a, R600a, R410a, R290, R22, and R32 in VCS used for air-conditioning applications. The assessment method was based on a system simulation model complemented with a module optimising the refrigerant circuitries in the condenser and evaporator. In this study, the R22 system was selected as the reference system with a compressor isentropic efficiency of 0.70, evaporator exit saturation temperature of 7.0 ^{0}C and a condenser inlet saturation temperature of 45.0 ^{o}C.

Mani and Selladurai (2008) conducted an experimental investigation on a vapour compression cycle with R290/R600 refrigerant mixture as a drop-in replacement for R12 and compared it to R134a. The equipment used in this study was described in Chapter 5. The compressor energy consumption varied between 0.656 kW to 0.793 kW for the range of interest.

Jain et al. (2011) conducted a simulation study using a refrigerant property dependent thermodynamic model of a simple reciprocating system, which could simulate the performance system as closely as possible. R22, R134a, R407C and R410a and M20 (a synthesised refrigerant blend) were analysed in the study. The design conditions specifications were as follows: a compressor efficiency of 0.65, an evaporator coolant inlet temperature of 3.85 ^{o}C, and condenser coolant inlet temperature of 39.85 ^{o}C. The product of condenser and evaporator effectiveness and capacitance rate of the external fluid were 9.39 kW/K and 8.20 kW/K respectively.

Baskaran and Mathews (2012) compared the performance of various eco-friendly refrigerants of low global warming potential in a vapour compression refrigeration system using a CYCLE_D 4 simulation software. The results obtained were compared to R134a. CYCLE_D 4 software was used to design the vapour compression cycle, with a compressor isentropic and volumetric efficiency of one. The compressor power was set to 0.302 kW.

In conducting the experiment on the refrigeration unit in this present study the compressor settings were: a voltage of 400 V, power of 1.50 kW, current 3.8 Amps and an operational speed of 1420 rpm. The water flow rate through the condenser was set at 2 L/min while its inlet

temperature was varied while the water inlet to the evaporator was maintained at 25 ^{o}C, its flowrate was adjusted to give the desired level of superheating of the refrigerant at the evaporator outlet. The refrigerant inlet temperature to the evaporator was controlled by adjusting the throttling effect at the expansion valves.

Table 7.11 shows a comparison of the data taken from literature sources and the results obtained from the measurements performed on the refrigerant test rig in this study. The reference conditions are the evaporator and condenser temperatures, and the resultant values at specific points are compared.

Table 7-11 : Comparison of Experimental results to literature for R134a with Evaporator (4-5 ^{o}C) and Condenser (40 ^{o}C).

Variable	***(Mani and Selladurai, 2008)***	***(Donald et al., 1997)***	***(Domanski, 2006)***	***(Jain et al., 2011)***	***(Baskaran and Mathews, 2012)***	***Run 1 from the test rig in this study***
Evap/Cond Temp (^{o}C)	2/40	3.85/36.85	7/45.6	3.85/39.85	-10/50	4.75/41.4
Evap Press (kPa)	345	336	365	250	200	320
Cond Press (kPa)	1003	934	1160	1314	1317	1113
Compression Ratio	2.91	2.78	3.14	5.26	6.57	3.65
Refrigeration Effect ($kJ.kg^{-1}$)	145	149	*****	124	137	152
W_{comp} ($kJ.kg^{-1}$)	*	*	*****	54	41.	45
Isentropic Efficiency	*****	*****	0.701	0.65	*	0.60
COP	2.34	*****	*	2.31	3.32	3.38

Data for the empty spaces was not documented in the respective publications.

From the results tabulated in Table 7.11, it can be observed that the condenser and evaporator pressures in literature are comparable to the data obtained from the test rig designed for this study. Furthermore, the compression ratio from the test rig falls within the range of the values reported in literature. The COP value from the test rig was higher than the literature values due to the uncontrolled level of superheating at the evaporator outlet in the test rig. However it was within the uncertainty of 16.8% as reported by Hoşöz (2005) using the uncertainty function *R* computed by Moffat.

Overall, from Table 7.11, it is evident that the results obtained from the experiments conducted on the unit were comparable to literature data. This outcome validates the design, equipment

assembly and experimental technique as accurate and reliable, and confirms the suitability of the equipment for use in conducting the experimental work in this study.

The compressor, which is the driving force in the vapour compression system, operated within the range of allowable temperatures that are safe for its components and lubricating oil. The degree of throttling produced at the expansion valve was adequate to influence the refrigeration effect at the evaporator. However, it was inconclusive that the same throttling effect would be reproduced with all refrigerants, as they require different degrees of throttling to produce the same refrigeration effect (Emerson, 1969).

The evaporator-compressor-condenser balance was satisfactory in the test rig using R134a. That is, the refrigerant vapour generated in the evaporator, was sufficiently compressed and displaced at the compressor, in the vapour phase. It condensed in the condenser to the required level of sub-cooling. If this balance was not satisfied, the refrigeration effect would limited, and as a result the compressor life will be shortened, making the cycle difficult to operate.

7.4 Performance analysis of refrigerants R413a, R507a and R134a.

The experimental performance of two commercial blends R413a and R507a was analysed and compared to that of R134a (a pure refrigerant). Moreover, the performance of the test rig was critically assessed in the investigation. However, the presence of auxiliary components and connecting pipes made it difficult to represent any practical refrigeration cycle purely based on a single parameter without the effects of the other parameters. Additionally, there was a limited number of measurement points with conventional sensors for pressure and temperature; this was due to the physical constraints on the system. (Datta et al., 2014). Hence, in this unit due to the lack of pressure sensors at the expansion valve, the pressure readings at its outlet were assumed to be equal to that of the evaporator inlet. This assumption was made so that a simplified representation of the thermodynamic cycle depicted by the system was a possibility. The investigation on refrigerant R507 on the test unit was limited since it is a high- pressure refrigerant and the unit utilised in this study had an upper pressure limit of 1.9 MPa. Parameters of interest in this analysis were the amount of refrigerant charge, condenser and evaporator water flow rates, evaporator temperatures, and condenser temperatures, compressor discharge temperature, cooling effect, COP compressor work and efficiency.

7.4.1 Variation of Compressor Work with COP

The Coefficient of Performance (COP) is defined as the ratio of cooling effect to compressor work. Consequently, an inverse proportionality relationship was expected when COP was plotted against compressor work. The expected trend was obtained and is shown below in Figure 7.1.

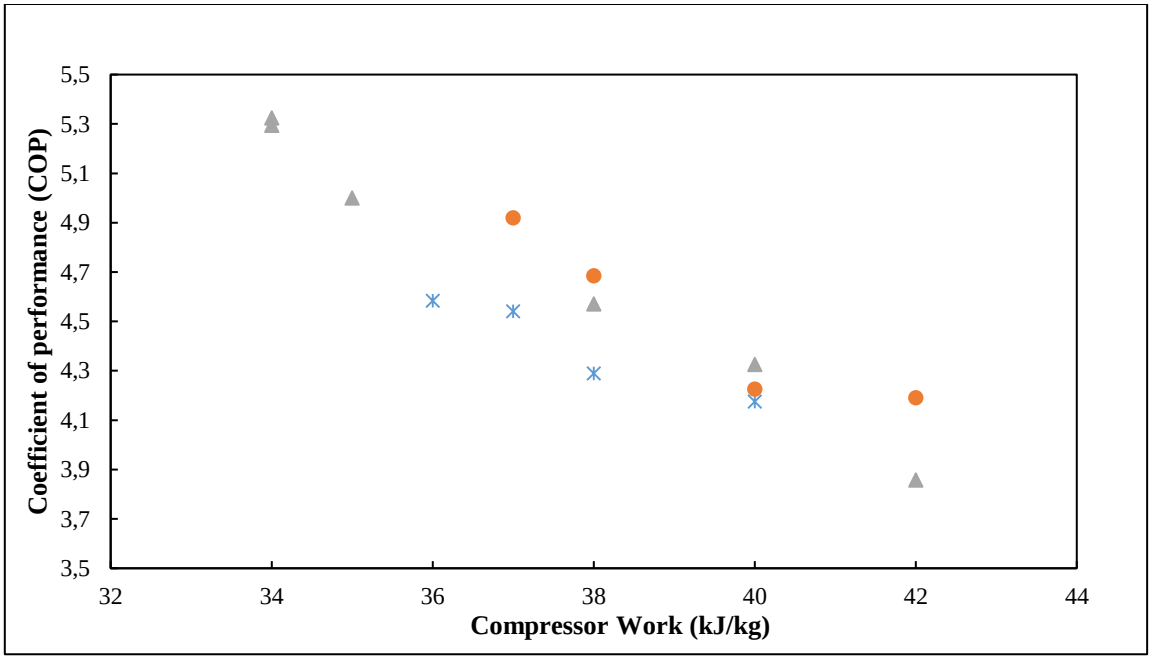

Figure 7-1 : Compressor Work vs. Coefficient of performance (COP). (*) R507, (▲) R413a, (●) R134a.

For the pure refrigerant R134a and refrigerant blend R507a (R125/R143a, 50/50 wt %) the COP decreased as the compressor work increased. The departure from linearity of the plot was because of the influence of the surroundings on the system. R404 a ternary blend showed the same behavior (Jerald and Kumaran, 2014). In this case, the departure from linearity was due to the influence of the other parameters such as oil circulation, temperature fluctuations in the condenser bath and influence of the environment on the system (heat loss to the environment).

7.4.2 Variation of Evaporator Temperature with COP

Extensive studies have been done and published on the variation of COP with evaporator temperature for various refrigerants investigated. The variation of evaporator temperature with COP for this study is shown below in Figure 7.2. It is evident from Figure 7.2 that the increase in evaporator temperature leads to an increase in COP.

The trend is not explicit in the graph in Figure 7.2 as other factors were changing during the experimental runs hence affecting the results obtained. The increase in the COP with evaporator temperature was due to the decrease in the compressor work and because of the reduction in the pressure ratio across the compressor.

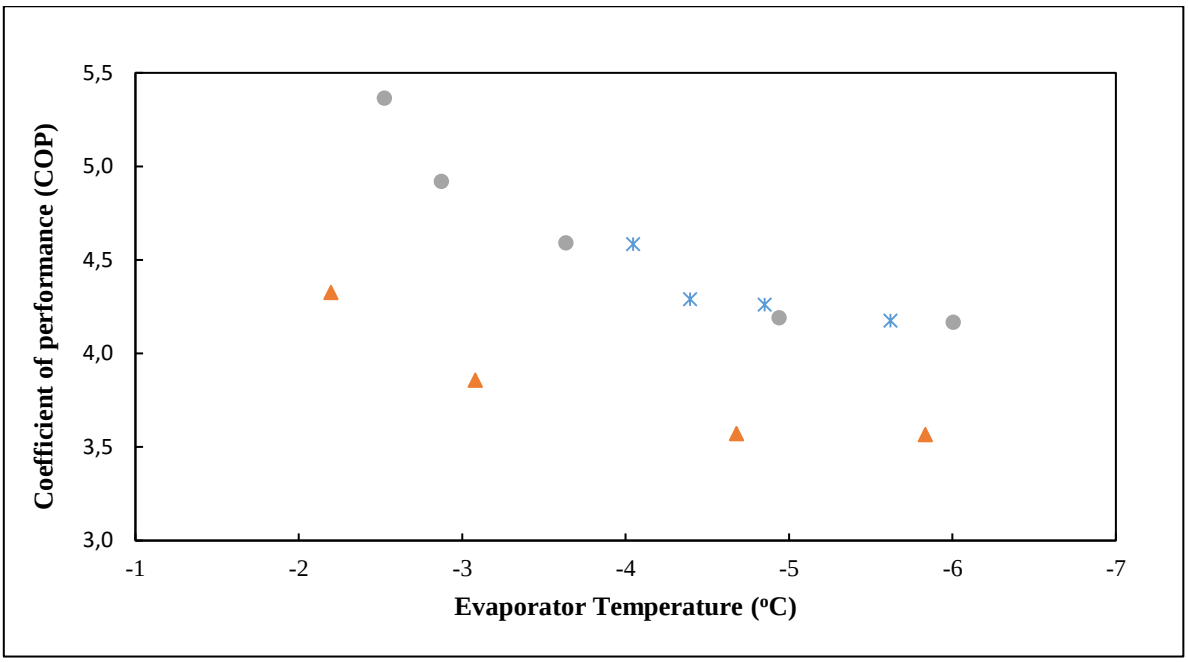

Figure 7-2 : Evaporating Temperature vs. Coefficient of performance (COP), (*) R507, (▲) R413a, (●) R134a

This change in the compressor results in the increase of the cooling capacity because of the increase in the specific refrigerating effect. These effects enhance the COP of the system (Arora and Kaushik, 2008). A similar trend was observed by Mani et al. (2013) with refrigerants R134a, R12, and R290/R600. The trend was attributed to the higher rate of increase of the refrigeration capacity than to the decrease of compressor work. Wongwises et al. (2006) observed a similar trend in his work with R134a in an automobile air conditioning system with the condenser flow kept constant and the engine speed varied. Narayan et al. (2013) investigated the retrofit of R12 with R134a, R413a, and R423a in the vapour compression refrigeration system and observed similar trends at different condensing temperatures. In their study, the trend line of COP with evaporator temperature for R134a was higher than that of R413a which is similar to the results obtained in this study. Likewise, Gomaa (2015) in his study on automotive air condition systems performance with R134a and its alternatives observed a similar trend. Dalkilic and Wongwises (2010) compared the performance of various refrigerants and refrigerant mixtures in a vapour compression cycle and observed a sharp

increase in COP as the evaporator temperature increased. Additionally, Halimic et al. (2003), presented a similar nonlinear trend in his comparison of the operating performance of alternative refrigerants and attributed it to the difference between equipment design and the experimental construction of the unit.

7.4.3 Variation of Condenser Temperature with Compressor Work

The compressor work varies directly with the condensing temperature of the refrigerants. This variation was due to the fact that the high condensing temperature led to a higher pressure ratio which resulted in high compressor work (Hwang et al., 2004). Hence more work was done in the compressor as it compressed the low-pressure gas to a high-pressure state. This variation is shown in Figure 7.3 with two refrigerants R134a and R413a.

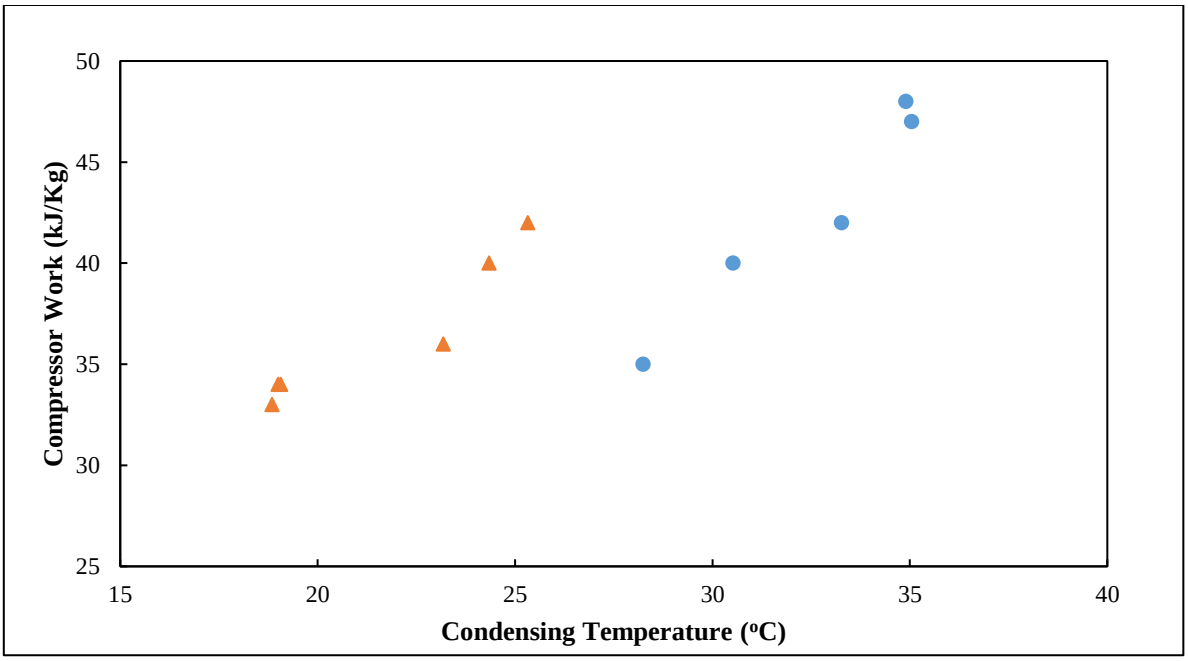

Figure 7-3 : Condensing Temperature vs. Compressor Work, (▲) R413a, (●) R134a

The trends obtained with these two refrigerants were the same, with refrigerant R413a operating at a lower condenser temperature than refrigerant R134a due to lower compressor work in the R413a system. This observation might have been due to good miscibility between R413a and the lubrication oil which led to less frictional work in the compressor hence low compressor discharge temperatures. Therefore, R413a performs better than R134a in the unit with regards to compressor operation and compressor life.

7.4.4 Variation of Condenser Temperature with COP

Figure 7.4 shows the variation of COP with condensing temperature. From the figure, it is apparent that COP was inversely proportional to the refrigerants' condensing temperature.

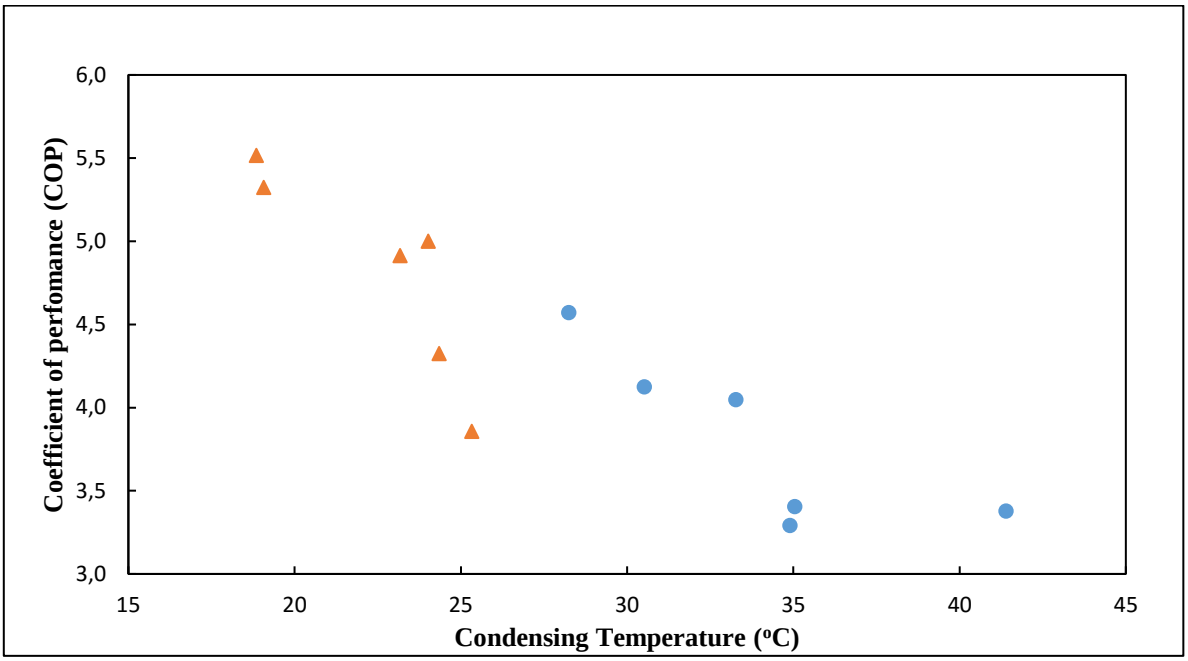

Figure 7-4 : Condensing Temperature vs. Coefficient of performance (COP), (▲) R413a, (●) R134a.

This observed trend was due to the decrease in refrigerating capacity and increase in the compressor work (Mani et al., 2013). Additionally, high condensing temperature leads to high-pressure ratio, which increased the power consumption of the compressor (high compressor work) thus resulting in a reduction of COP (Elsayed and Hariri, 2011; Prapainop and Suen, 2012). Similar trends were observed by Mani et al. (2013), in the study of R12, R134a and R290/R600 for the development of the statistical model for predicting refrigerant performance as well as Elsayed and Hariri (2011), investigating the effects of condenser air flow on the performance of split air conditioner. This trend was the same as the one obtained in this study as illustrated in Figure 7.4. The commercial refrigerant R413a exhibited better performance than pure refrigerant R134a, as R413a has a higher COP value for a lower condensing temperature.

Hwang et al. (2004) in their study working with R-290, R404a and R410a in medium temperature applications observed that at very low condensing temperatures, low COP was obtained. COP increased with an increase in condenser temperature until it reached a maximum

value then it decreased. This variation was due to the reduction in the latent heat of evaporation as the condenser temperature increased whereas the compressor work kept on increasing. Hence the cooling capacity of the refrigerant increased until it reached a maximum point then thereafter decreased, resulting in the COP value decreasing as well.

7.4.5 Variation of Cooling Effect with COP

COP is a ratio of cooling effect to the compressor work. Therefore theoretically, COP is directly proportional to the cooling effect with compressor work held constant. The three refrigerants analysed in the study depict a trend which follows the theoretical postulation. This trend is illustrated in Figure 7.5, and it can be observed that COP increased as the cooling effect increased.

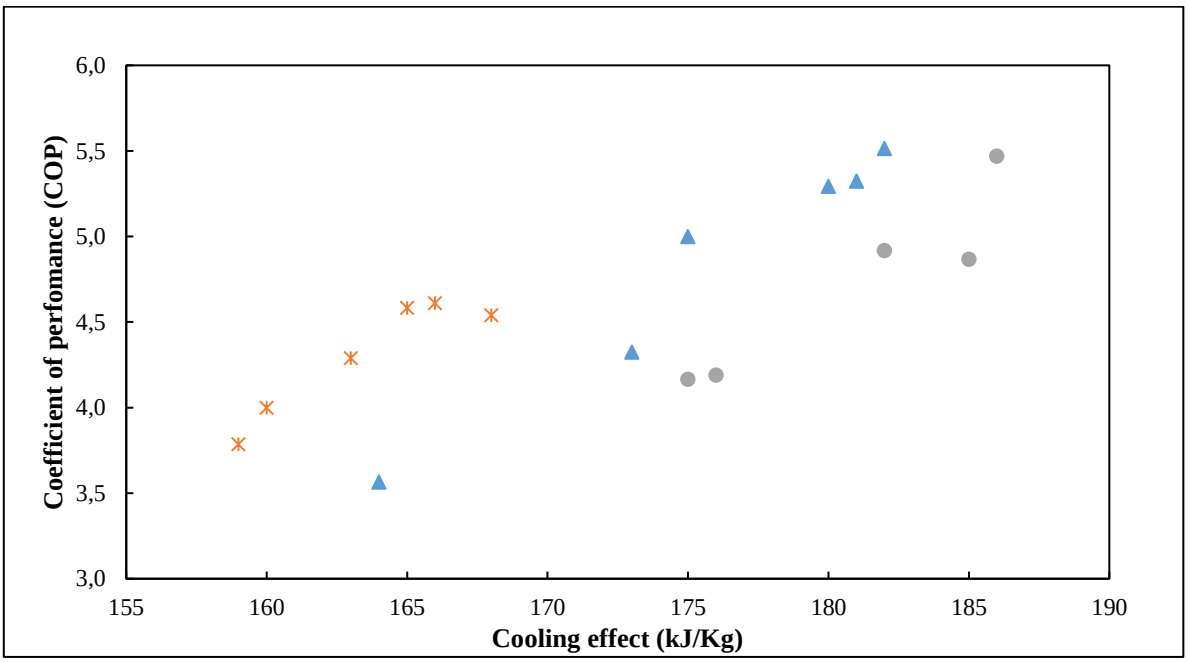

Figure 7-5 : Cooling effect vs. Coefficient of performance (COP), (*) R507, (▲) R413a, (●) R134a

The nonlinearity of the trend lines was due to the influences of the compressor work which was affected by several factors. R413a depicts the trend, but it was less explicit with R507 this was due to the limited range of application of this refrigerant on the refrigerant test rig used in the study.

7.4.6 Variation of Condenser Water Flowrate effect with COP

The relationship between condenser water flowrate and COP for pure refrigerant R134a and refrigerant blend R507 is shown in Figure 7.6, where the performance of the two refrigerants investigated was in a comparable range. Considering refrigerant blend R507 it is evident that initially COP increased with condenser water flow rate until a maximum value was reached thereafter COP decreased as the condenser flow rate increased at a low flowrate.

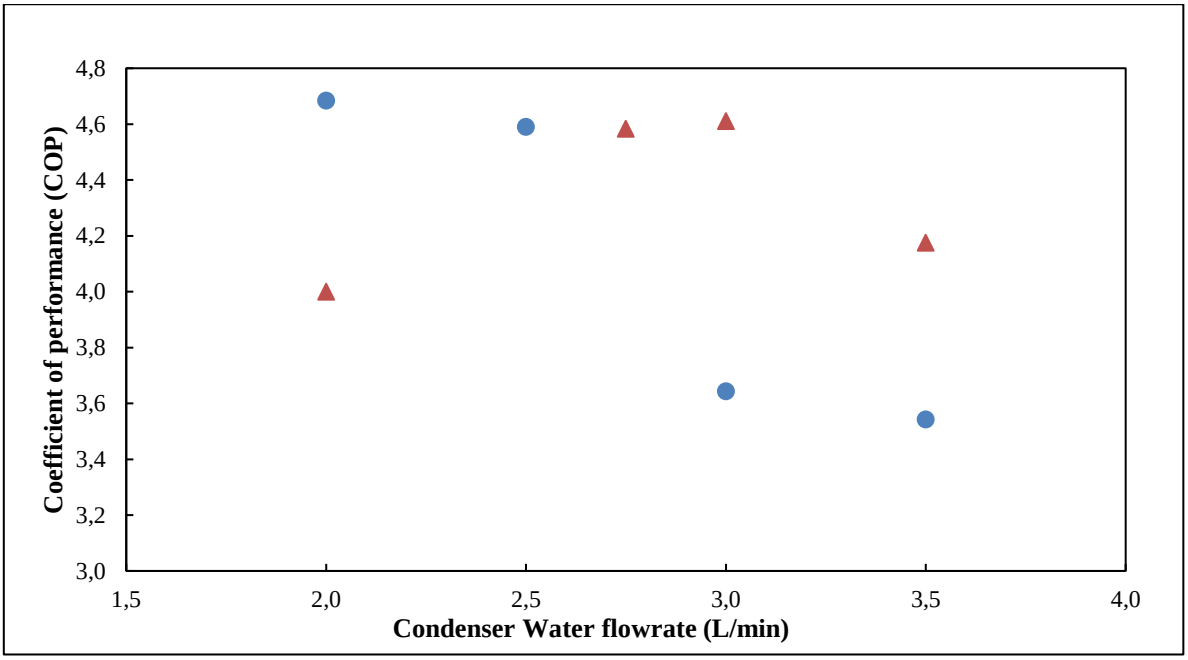

Figure 7-6 : Condenser Water flowrate vs. Coefficient of performance (COP), (▲) R507, (●) R134a

With refrigerant R134a, the COP decreased as the condenser flowrate increased. However, it may be the case that the R134a graph is similar to the second part of the R507 graph. Cooling of the refrigerant was affected when the condenser was *starved of the cooling fluid* (Datta et al., 2014).

7.4.7 Variation of Condenser water flowrate with Discharge Temperature

Datta et al. (2014) in the study on automobile air-conditioning observed that *starving* the condenser of the airflow (heat sink) leads to a decrease in the cooling of the refrigerant through it. Likewise, an increase in the condenser cooling water flowrate with its temperature held constant leads to improved refrigerant cooling. The throttling effect becomes more pronounced at the expansion valve. This throttling effect leads to excellent cooling which results in lower

evaporator exit temperatures consequently lower compressor discharge temperatures results. For this reason, discharge temperature decreases as condenser water increases. This trend is observed with both R134a and refrigerant blend R507 in Figure 7.7. Refrigerant blend R507 had a higher discharge temperature than R134a for a given condenser flow rate this was due to the difference in the refrigerant charge to the system and the interaction of the refrigerant with the compressor oil.

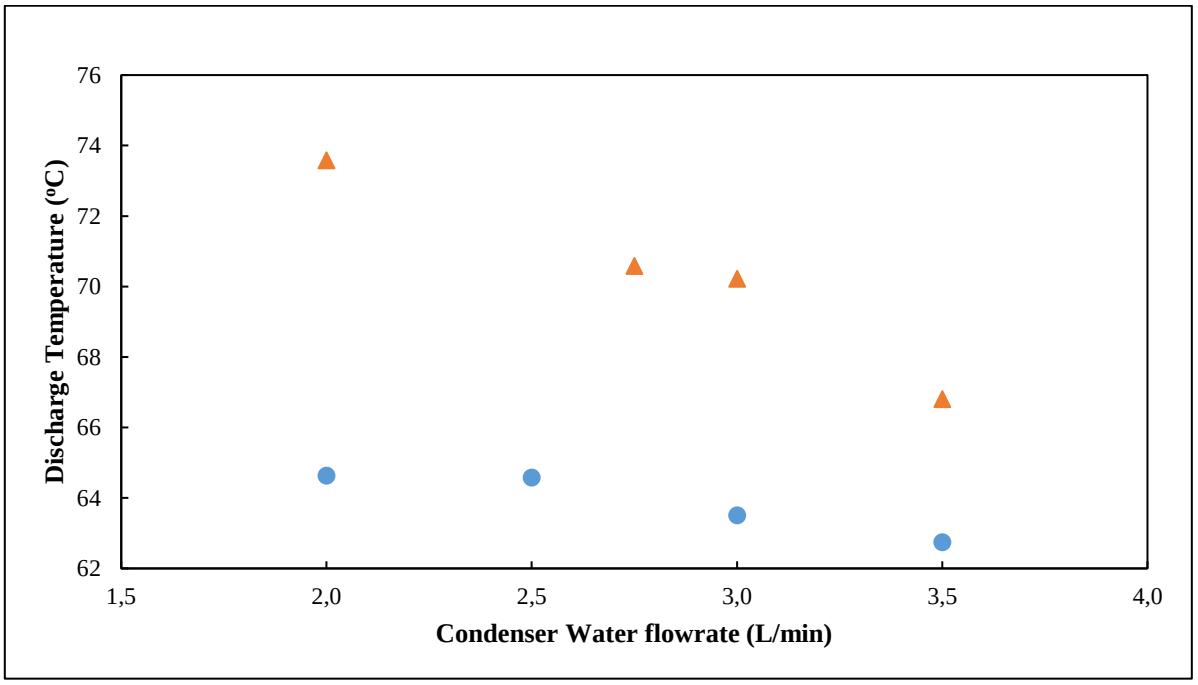

Figure 7-7 : Condenser water flowrate vs. Compressor discharge temperature, (▲) R507, (●) R134a.

7.4.8 Variation of Refrigerant Charge with Discharge Temperature

Illustrated in Figure 7.8 is the effect of refrigerant mass on the compressor discharge temperature for a set compressor frequency and power. It can be gathered from Figure 7.8 that the discharge temperature decreased as the refrigerant charge was increased. Datta et al. (2014) observed the same trend in the investigation of effects of charge on automotive air conditioning systems.

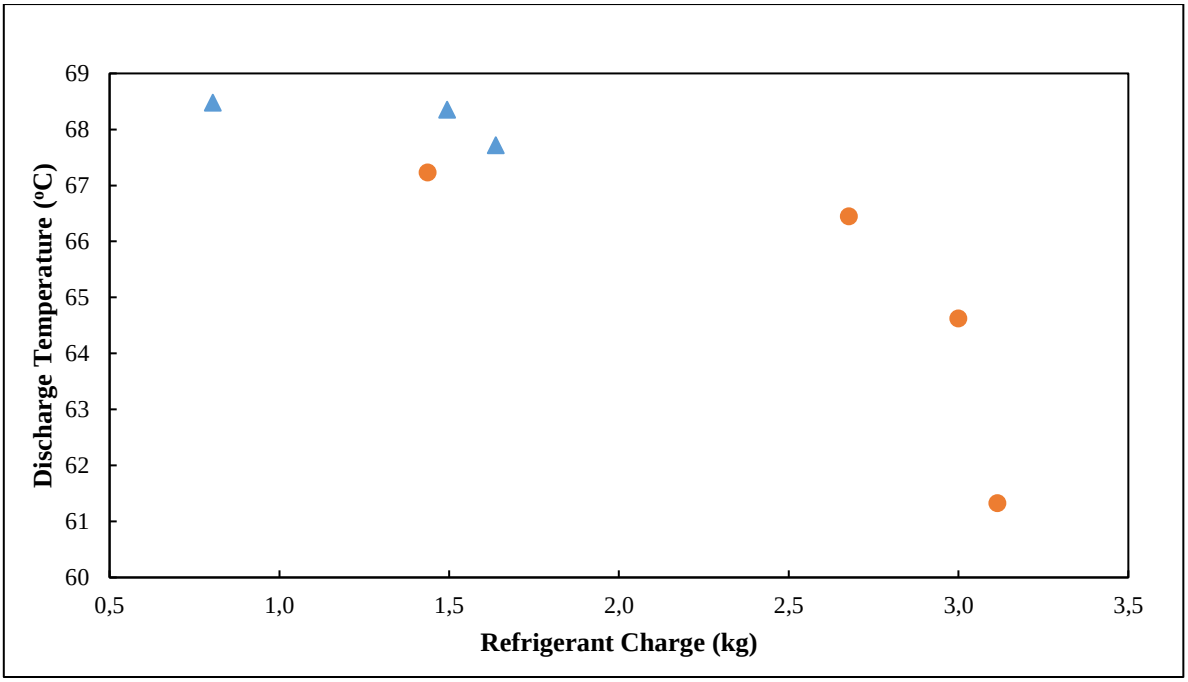

Figure 7-8 : Refrigerant charge vs. compressor discharge temperature, (▲) R413a, (●) R134a

7.4.9 Variation of Refrigerant Charge with Compressor Efficiency

Figure 7.9 shows the variation of refrigerant mass with the compressor efficiency. It can be observed that compressor efficiency decreased as the refrigerant charge was increased for R134a refrigerant. This change was as a result of the increase of vapour compressed in the

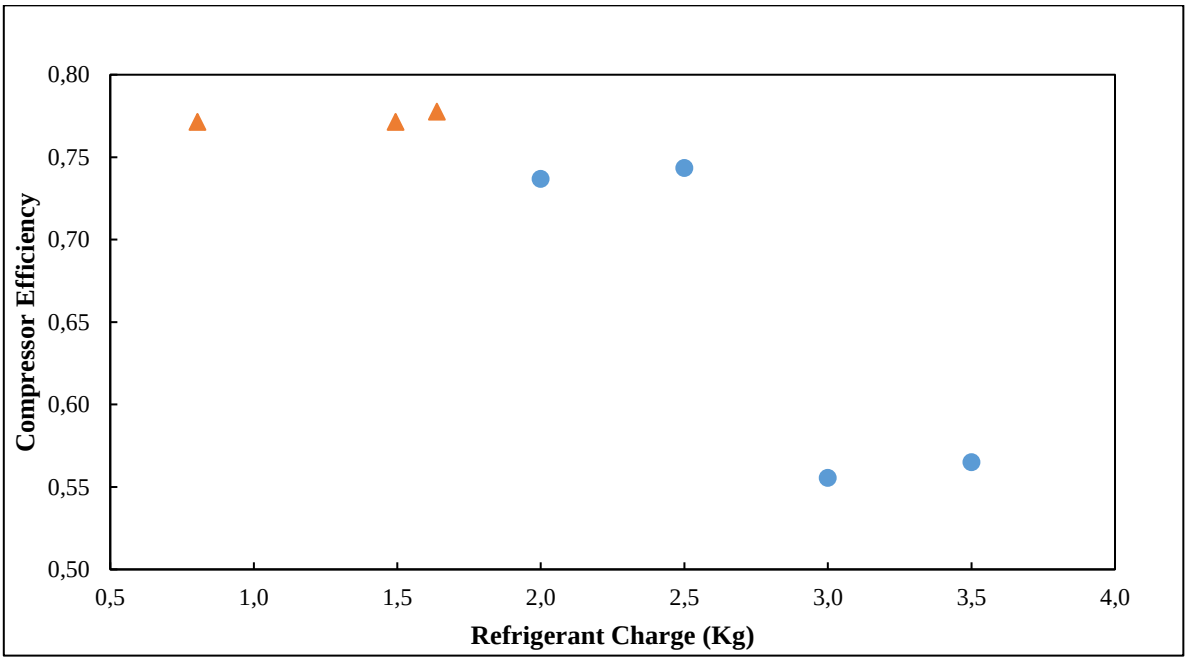

Figure 7-9 : Refrigerant charge vs Compressor Efficiency, (▲) R413a, (●) R134a.

compressor cylinder hence the effective work of the compressor was reduced. Starving the compressor might also lead to lower compressor efficiency. Thus there was an optimum value at which the compressor efficiency was at the highest. Refrigerant R413a had a relatively constant compressor efficiency for different amounts of refrigerant charged into the system. A higher charge of R413a could not be investigated due to the limitation in the maximum pressure rating of the test rig.

Akintunde (2013) in the experimental study of replacing R12 with R600a, R134a and R406a blends observed that for most refrigerant blends the compressor efficiency was constant regardless of the amount of refrigerant in the system. In his study, it was observed that only one refrigerant blend (laboratory synthesised) compressor efficiency had a sharp decrease over a small range of refrigerant charge.

7.4.10 Variation of Condenser and Evaporator water flowrate with Evaporator Refrigerant Temperature

A comparison between condenser water flowrate with the evaporator refrigerant inlet temperature, and evaporator water flow rate and evaporator refrigerant inlet temperature is shown in Figure 7.10.

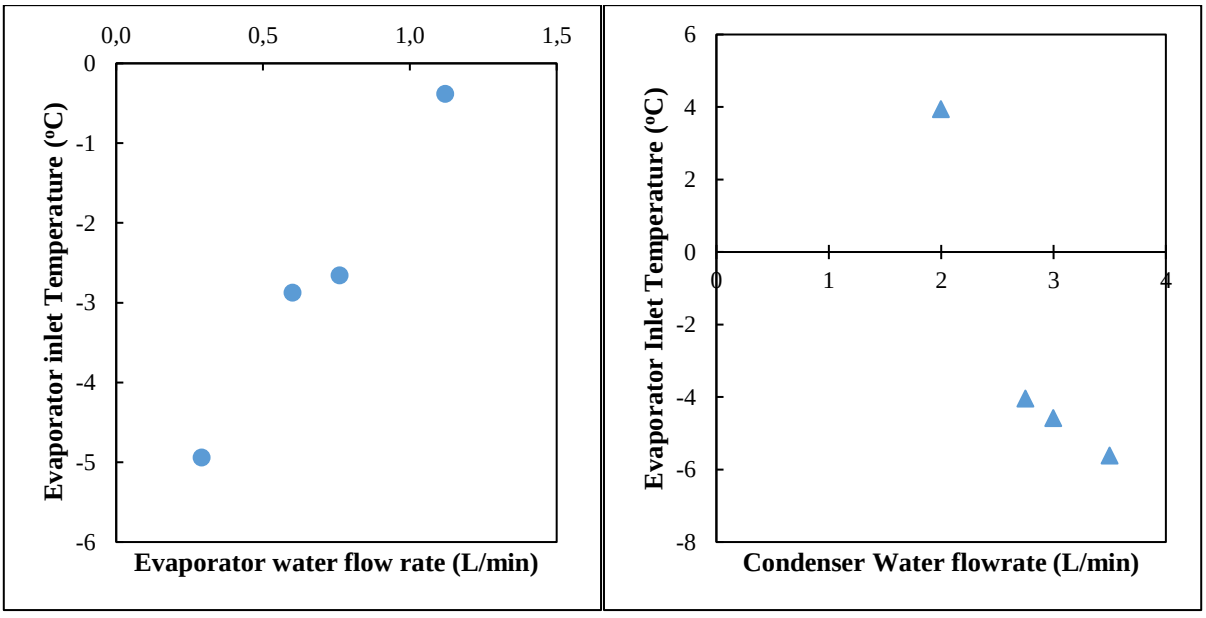

Figure 7-10 : Condenser and Evaporator water flowrate vs Evaporator Refrigerant Temperature. (right (●) R134a), left (▲) R507)

The refrigerant temperature at the evaporator inlet decreased with an increase in condenser water flowrate conversely it increased with the evaporator water flowrate. An increase in the condenser water flowrate increases the rate of heat rejection at the heat sink thus the refrigerant emerges with a lower temperature thus the throttling effect produced a vapour liquid mixture with higher liquid fraction which led to a lower temperature at the evaporator inlet.

At high evaporator temperatures, the amount of superheat was high hence the refrigerant exited the evaporator at higher temperature. Heat rejection was constant at the condenser since the condenser conditions were kept constant. Therefore, the outlet temperature of the refrigerant at the condenser increased with the increase in the flow rate through the evaporator. Consequently, the refrigerant returned to the evaporator at a higher temperature.

7.5 Simulations for the Vapour Compression Cycle

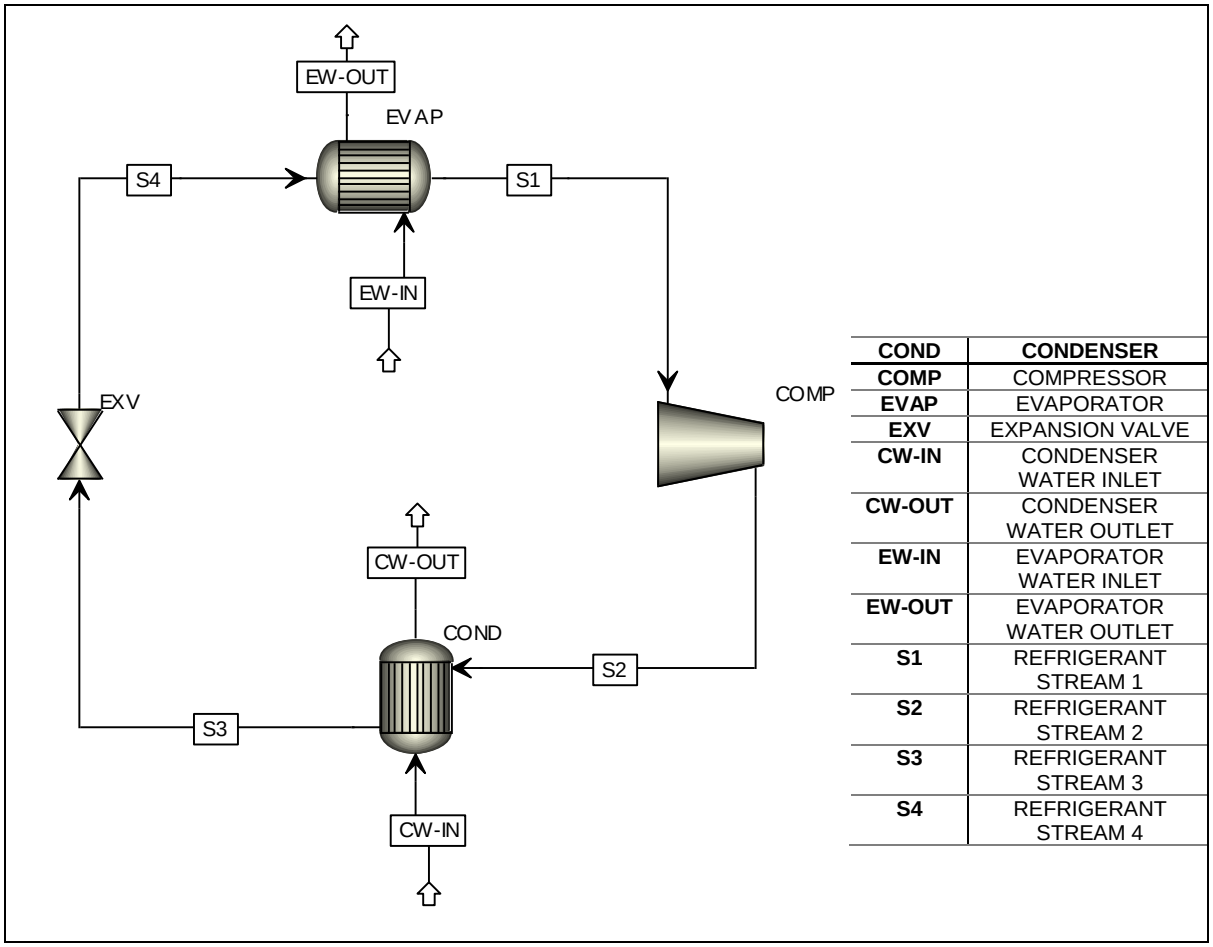

COND	CONDENSER
COMP	COMPRESSOR
EVAP	EVAPORATOR
EXV	EXPANSION VALVE
CW-IN	CONDENSER WATER INLET
CW-OUT	CONDENSER WATER OUTLET
EW-IN	EVAPORATOR WATER INLET
EW-OUT	EVAPORATOR WATER OUTLET
S1	REFRIGERANT STREAM 1
S2	REFRIGERANT STREAM 2
S3	REFRIGERANT STREAM 3
S4	REFRIGERANT STREAM 4

Figure 7-11 : Flowsheet of a single vapour compression cycle with Hot and Cold fluid cycles.

Aspen Plus ® V8.6 an engineering software was employed to simulate of the refrigeration cycle, the results obtained were compared to the results obtained from the experimental study. Figure 7.11 presents the simulated cycle developed using Aspen Plus ®. The simulation model consists of the four main components of a VC cycle, which are; the evaporator, the compressor, an expansion valve, a condenser, the connecting lines and water lines.

7.5.1 Components Selection for the vapour compression cycle

The unit operations forming the refrigeration cycle are the condenser, the evaporator, the compressor and an expansion valve. The evaporator and the condenser selected from the Exchangers, under the HeatX category, and of the Gen HT type this type chosen because it best simulates the evaporator and condenser used in the refrigerant test unit, with two inlet and outlet ports.

The compressor was selected from Pressure changers, under the Compr category and the ICON2 type. This simulated the reciprocating compressor utilised in the refrigerant test rig. Similarly, the expansion valve was selected from Pressure changers, in the Valves category. Specifically, VALVE2 was chosen as it best simulated the throttling effect produced by the expansion valve in the refrigerant unit.
Material lines were used to connect the various units in the sequence as shown in Figure 7.11.

7.5.2 Thermodynamics models employed in the study

REPROF **(***REFerence fluid PROPerties packag**e***)** method was utilised in evaluating the simulation performance the refrigeration cycle in this study. This method has been used successfully in refrigeration studies by, (Kim and Didion, 1995); (Satola, 2014), and (Tuta and Orozco, 2016).

REPROF was developed by NIST and contains 121 pure fluids some of which are binary mixtures. Its particular emphasis is on refrigerants and hydrocarbons. The REFPROP package describes fluids properties with an uncertainty of below 1% for most conditions (Satola, 2014). It is based on three accurate thermodynamics models for pure liquids and mixtures. It implements these models for the thermodynamic properties of pure fluids: the Modified Benedict-Webb-Rubin equation of state, Equations of State (EoS) explicit in Helmholtz energy and an extended corresponding states (ECS) model.

The fundamental equation of state explicit in the Helmholtz free energy *f* has the independent variables which are temperature *T* and density ρ. Several thermodynamics properties can be obtained from the Helmholtz free energy equation derivate (Equation 7.1) as a function of these two variables. Also, it is one of the four fundamental equations of state (Wagner and Pruß, 2002).

$$\phi(\delta,\tau) = \phi^{o}(\delta,\tau) + \phi^{r}(\delta,\tau), \tag{7.1}$$

where $\tau = T_c / T$ is the inverted reduced temperature and $\delta = \rho/\rho_c$ is the reduced density with T_c and ρ_c being the critical temperature and critical density respectively. The fundamental equation of state was established for Helmholtz free energy of refrigerant R134a by (Tillner-Roth and Baehr, 1994). Its temperature range is from -103.15 to 181.85 ^{o}C with pressure of up to 700 bars.

The modified Benedict-Webb-Rubin (mBWR) equation as described by Jacobsen and Stewart (1973), it is very accurate and flexible to be applied to the liquid, vapour and supercritical regions of the fluid. The mBWR equation represents the pressure *P* as a function of molar density ρ and the absolute temperature *T*:

$$P = \sum_{n=1}^{9} a_n \rho^n + \exp(-\delta^n) \sum_{n=10}^{15} a_n \rho^{2n-17} \tag{7.2}$$

where $\delta=\rho/\rho_c$, ρ_c is the critical density, and the temperature dependence of the coefficients is given by Outcalt and McLinden (1996). The data covers the temperature range from -103.15 to 251.85 ^{o}C with pressure of up to 350 bars in terms of the mBWR equation of state with 32 adjustable coefficients with refrigerant R152a (Outcalt and McLinden, 1996).

The Extended Corresponding-States Principle **(**ECS) is used to represent transport properties and thermodynamic of fluid with particular emphasis on fluids with limited data. This principle does not depend on the assumption that molecules are symmetric spheres with conformal intermolecular potentials as some refrigerants have non-spherical and polar molecules. The shapes factors of these substances are reduced and represented as functions of density and

temperature (Ely and Huber, 1990). This method was found to work well with R134a reference fluid for various fluids (McLinden et al., 2000). Furthermore, the implementation of extended corresponding states requires the molecular mass, critical point, and normal boiling point to be specified as these empirical relations can be used to obtain the shape factors (Huber et al., 1992).

In mixture calculations, a different rule applies which combines the Helmholtz energy of the components in the mixture; and a difference function is used to account for the deviation from ideal mixing. Thermal conductivity and viscosity modeled with either fluid-specific correlations, an ECS method or the friction theory method in some cases. REFPROP has three reference states on which the values of entropy and enthalpy are based. The analysis of the mixtures is also made complex by the composition of the equivalent substance reducing ratios. To simplify the system, an assumption is made that the composition dependence is offered by the van der Waals one-fluid mixing rules. The following equations illustrate the van der Waals mixing rules:

$$h_x = \sum_{i=1}^{n}\sum_{j=1}^{n} x_i x_j \, h_{ij} \tag{7.3}$$

$$f_x h_x = \sum_{i=1}^{n}\sum_{j=1}^{n} x_i \, x_j f_{ij} h_{ij} \tag{7.4}$$

The cross terms obtained from combining rules are;

$$f_{ij} = \sqrt{f_i} f_j \left(1 - k_{if}\right) \tag{7.5}$$

$$h_{ij} = \left(h_i^{1/3} + h_j^{1/3}\right)^3 \left(1 - l_{ij}\right)/8 \tag{7.6}$$

where x_i is the concentration of constituent *i* in the mixture, k_{ij} and l_{ij} are the binary interaction parameters and are nonzero when $i \neq j$ also h_x and f_x are the equivalent substance reducing ratios for the mixture (Ely and Huber, 1990). Application of the mixing formulas requires the derivatives of h_x and f_x with respect to composition, density and temperature. The arguments of the shape factors pertaining to the mixing rules and the definition of equivalence substance reducing ratios are shown to be the effective temperature and densities of the mixture's components. The scope of equations of state described here have been limited due to the substances covered in this study.

7.5.3 Specifications of Simulation Parameters

In running the simulation software, there was a need to specify variables for each component and stream shown in Figure 7.11. The simulation model computed the unspecified variables. The methodology of variable specification used is detailed in Table 7.12.

The inputs values used in the simulation were obtained from the experimental runs conducted in the test rig used in this study. The results obtained from the simulations were then compared with the experimental results to ascertain the deviation of experimental results from simulated results (ideal).

The model computes the properties of the refrigeration streams as they flow around the cycle. The outputs obtained were; enthalpy, entropy, density, liquid-vapour compositions, unspecified temperatures and pressure for the refrigerant and water streams. Typical results obtained from the simulation are presented in Appendix E, Table E.1 to Table E.7.

Table 7-12 : Specification of Simulation Variables.

Component	*Variables Specified*	*Variables Calculated*
Condenser	Flow direction-Counter current. Exchanger specification- Hot stream outlet temperature (^oC).	Refrigerant inlet temperature (^oC) and pressure (bar).
Compressor	Compressor type- Isentropic. Outlet specification- Discharge pressure (bar). Efficiencies – Isentropic.	Refrigerant inlet temperature (^oC) and pressure (bar).
Evaporator	Flow direction-Counter current. Exchanger specification- Cold stream outlet temperature (^oC)	Properties of the refrigerant stream flowing through it and the refrigeration capacity.
Expansion valve	Calculation type-Adiabatic flash for specified outlet (pressure changer). Outlet pressure (bar).	Vapour fraction in the liquid –vapour mixture at its outlet.
Condenser water inlet ***Condenser water outlet*** ***Evaporator water inlet*** ***Evaporator water outlet***	Temperature/^0C, (TCW-IN, PCW-IN, TEV-IN, PEV-IN) Pressure /bar, (TCW-OUT, PCW-OUT, TEV-OUT, PEV OUT) Composition of the streams in mass fractions of the components Total flow basis-mass (specify the mass flow rate, kg/hr).	Mass Flow (kg/hr), Mole Flow (kmol/hr), Volume Flow (L/min), Vapor Fraction, Liquid Fraction, Molar Enthalpy (kJ/kmol), Mass Enthalpy (kJ/K), Enthalpy Flow (kW), Mass Entropy (kJ/kg-K), Molar Entropy (kJ/kmol-K), Mass Density (kg/ cm^3), Molar Density (kmol/cm^3), Average Molecular Weight.
Refrigerant stream 1	Temperature (^oC), Pressure (bar), Composition of the stream in mass fractions of the components, Total flow basis-mass: specify the mass flow rate, (kg/hr).	
Refrigerant stream 2 ***Refrigerant stream 3*** ***Refrigerant stream 4***	No Inputs.	Mass Flow (kg/hr), Mole Flow (kmol/hr), Volume Flow (L/min), Pressure (bar), Temperature (^oC), Liquid Fraction, Vapor Fraction, Molar Enthalpy (kJ/kmol), Mass Enthalpy (kJ/K), Enthalpy Flow (kW), Molar Entropy (kJ/kmol-K), Molar Density (kmol/ cm^3), Mass Entropy (kJ/kg-K), Mass Density (kg/ cm^3), Average Molecular Weight.

The pure refrigerants and refrigerants blends analysed were: R134a, R507, R413a, R134a/R125 (66/34 wt %), and R134a/R125 (50/50 wt %).

7.5.4 Analysis of the simulated results

The results obtained from Aspen simulations of two pure refrigerants and four refrigerant blends are presented in Table 7.13.

Table 7-13 : Comparison of Simulated COP results for refrigerants and refrigerant blends.

Refrigerant/Refrigerant Blend (wt %)	***Compressor Work (kW)***	***Refrigeration Effect (kW)***	***COP***
R134a	0.09	0.43	4.78
R413a *R134a/R600a/R218* *(88/3/9)*	0.09	0.36	4.00
R134a\R125 *(50/50)*	0.05	0.24	4.80
R134a\R125 *(66/34)*	0.07	0.34	4.86
R507 *R143a/R125* *(50/50)*	0.08	0.40	5.0
R125	0.07	0.29	4.41

The commercial refrigerant blend R507 had the highest COP while R413a another commercial blend had the lowest COP value. R134a, a pure refrigerant had the highest refrigeration effect while R134a/R125 (50/50) had the lowest refrigeration effect as well as the compressor work. The high COP value for R507 was a result of both relatively high refrigeration effect and low power consumption at the compressor. Moreover, the high COP might have been due to high volumetric refrigeration capacity of the R507 refrigerant as a result of the high pressure of its vapour since it had the highest pressure in the study (Prapainop and Suen, 2012). R134a/R125 (66/34 wt %) a laboratory synthesised blend in this study had the second highest COP value. The overall performance of refrigeration blends was better than that of pure refrigerants in the simulation, with R125 a pure refrigerant gave the lowest COP value. R507 a commercial blend of R125/R143a in the ratio (50/50) showed better performance when compared to R134a/R125 in the same proportion.

7.5.4.1 Comparison of the performance of refrigerants

Pressure losses due to fluid flow and the heat exchange with the surroundings cause a performance deviation of the actual refrigeration cycle from the ideal one (Dalkilic and Wongwises, 2010). Additionally, in the practical cycle, significant refrigeration losses occurred in the evaporator, and pressure losses in the line connecting the condenser and the expansion valve. Furthermore, in this refrigerant unit system inefficiencies were experienced in the long pipeline joining the expansion valve and the evaporator (197 cm in length, with six bends and one valve along its length).

The comparison of experimental and simulation results from R134a refrigeration cycle is shown in Table 7.14. The following parameters have the same value in the simulation and experimental run as they were fixed. These were, the compressor efficiency, refrigerants' condenser and evaporator outlet temperatures and the compression ratio. The vapour fraction at the evaporator inlet and the discharge temperature are the dependent variables which depend on the set parameters. The formula used for calculating the percentage difference is;

$$Percentage\ difference = \frac{|x_1 - x_2|}{(x_1 + x_2)/2} \times 100 \qquad 7.7$$

where x_1 and x_2 are the two values of interest.

Table 7-14 : Comparison of the experimental and simulated results for R134a.

Variable	***Experimental***	***Simulation***	***% Difference***
COP	4.92	4.78	2.89
Refrigeration Effect (kW)	0.42	0.43	2.35
Compressor Efficiency	*0.69*	*0.69*	*0*
Vapour Fraction @ Evaporator Inlet	0.21	0,21	0
Compression Ratio	*3.11*	*3.11*	*0*
Discharge Temperature (^oC)	70.7	74.0	4.56
Refrigerant Evap Inlet Temp (^oC)	-2.9	-6.5	76.60
Refrigerant Evap Outlet Temp (^oC)	*23.6*	*23.5*	*0.42*
Refrigerant Cond Outlet Temp (^oC)	*25.2*	*25.0*	*0.79*

The refrigeration capacity was higher in the simulated results than in the experiments. A percentage difference of 2.35 % was observed between the experimental and theoretical study as shown in Table 7.14. This was within the uncertainty of 16.8 % and 4.472 % calculated by the uncertainty function *R* computed by Moffat (1988) as reported by Hoşöz (2005) and Datta et al. (2014) respectively. The difference was mainly due to the inefficiencies which occur in the experimental apparatus. The system inefficiencies were due to the loss of refrigeration capacity to the surroundings, the section worth mentioning being the long pipeline that exists between the expansion valve and the evaporator. The coefficient of performance was unexpectedly higher for the experimental than for the theoretical run due to the compressor effects and the exaggerated exit outlet evaporator temperature which increased the cooling effect in the experimental run. A 2.91 % difference in COP existed between the measured and simulated results. The inlet temperature of the evaporator was higher for the practical cycle than the simulated one (Rigola et al., 1996). This occurrence was expected due to irreversibility at the expansion valve in the practical cycle and the loss of the refrigeration capacity of the refrigerant as it cooled (heat load) the long pipeline which connects the expansion valve and the evaporator inlet**.** This section accounts for the large percentage difference that was observed in the evaporator inlet temperature (76.6 %).

Table 7.15, shows the values obtained from the experimental and simulated runs for a commercial refrigerant blend R507 under the same conditions. It can be noted that a difference of 9.64 % existed between the COP values for the two methods with the experimental run having a lower value.

Table 7-15 : Comparison of the Experimental and simulated results for R507.

Variables	***Experimental***	***Simulation***	***% Difference***
COP	4.54	5.0	9.64
Refrigeration Effect (kW)	0.34	0.40	16.22
Compressor Efficiency	*0.78*	*0.78*	*0*
Vapour Fraction @ Evaporator Inlet	0.28	0.31	10.17
Compression Ratio	*3.89*	*3.89*	*0*
Discharge Temperature (^oC)	71.4	79.2	10.36
Refrigerant Evap Inlet Temp (^oC)	-5.9	-21.2	112.92
Refrigerant Evap Outlet Temp (^oC)	*23.7*	*23.7*	*0*
Refrigerant Cond Outlet Temp (^oC)	*18.6*	*18.6*	*0*

The percentage difference in COP between the experimental run and the simulation was small, (within 10% difference), but the refrigeration effect was higher for the simulation than the experimental run. As expected the COP value simulated results are greater than in the experimental run. This observation was due to the inefficiencies that exist in the experimental equipment. The percentage difference was within the 16.8% uncertainty computed by Hoşöz (2005), using Moffat's uncertainty function *R*.

Refrigerant R507 is a high-pressure refrigerant. Therefore, the test rig pressure limitations affected its analysis, as a little amount of refrigerant R507 produced a high-pressure value. It is also a low-temperature refrigerant, but the apex temperature it can reach is limited or influenced by the external ambient temperature. The huge percentage difference of the refrigerant temperature at the evaporator inlet was due to the fact that R507 is a higher-pressure refrigerant. Thus its performance in the experimental unit was limited. Also, the systems' inefficiencies affected the performance of the refrigerant in the unit.

Tabulated in Table 7.16 is the comparison of the experimental and simulated results obtained with refrigerant blend R413a. Commercial R413a was intended to replace the Freon 12 refrigerant (R12). Therefore it was expected to have excellent refrigerant properties. As expected the simulation produced better results than the experimental due to the effects of the surroundings and system inefficiencies on the experimental runs.

Table 7-16 : Comparison of the experimental and simulated results for R413a.

Variables	***Experimental***	***Simulation***	***% Difference***
COP	3.57	4.0	11.36
Refrigeration Effect (kW)	0.20	0.36	57.14
Compressor Efficiency	*0.65*	*0.65*	*0*
Vapour Fraction @ Evap Inlet	0.22	0.23	4.44
Compression Ratio	*3.79*	*3.80*	*0.26*
Discharge Temperature (^oC)	67.4	66.2	1.80
Refrigerant Evap Inlet Temp (^oC)	-5.8	-8.0	31.88
Refrigerant Evap Outlet Temp (^oC)	*6.9*	*6.9*	*0*
Refrigerant Cond Outlet Temp (^oC)	*23.9*	*23.9*	*0*

The percentage difference in COP between the experimental result and the simulated results was again less the 16.8 % uncertainty determined by Hoşöz (2005) using Moffat's uncertainty

function *(R)*. A higher compressor discharge temperature occurred in the experimental run due to the inefficiency in the compressor, which generated much energy. This occurrence was a result of some factors such as; friction between the moving parts in the compressor and the incompatibility of the oil and the refrigerant investigated. One can observe that while the difference in the values reported for the refrigeration effects is not huge, there is a significant difference, in the inlet temperature of the evaporator which is attributed to the lengthy pipeline between the expansion valve and the evaporator which introduces the heat load along the pipeline. Close agreement was observed in the refrigerant condenser temperatures due to a large bath in the condenser which ensures complete condensation of the refrigerant when it exits the condenser.

7.5.4.2 Comparison of R134a, R125, and R134a/R125 blends

The analysis of the performance of the R134a/R125 blends could not be analysed using a P-H diagram since this was not available for these laboratory synthesised blends and the different composition utilised in the experiments made the construction of the P-H diagram difficult. Therefore, derived results such as COP, compressor efficiency, and work, cooling effect and the vapour fraction at the evaporator inlet could not be obtained for experimental work. Consequently, simulations were used to analyse the performance of the blends, using the same input values as used in the experimental study.

The results for these refrigerant blends display improved refrigeration performance in the simulated study over the pure refrigerant counterparts. The blends had higher COP values than the pure refrigerants as can be seen in Table 7.17. This result was to a large part due to lower compression power rather than the cooling effect.

Table 7-17 : Comparison of simulated results for R134a, R125, and R134a/R125 blends.

Variables	***R134a***	***R134a\R125 (wt %)***		***R125***
		(66/34)	**(50/50)**	
COP	4.78	4.88	4.80	4.41
Refrigeration Effect (kW)	0.43	0.34	0.24	0.29
Compressor Efficiency	0.69	0.75	0.75	0.69
Compressor Power (kW)	0.09	0.05	0.07	0.07
Vapour Fraction @ Evaporator Inlet	0.21	0.23	0.23	0.32
Compression Ratio	3.13	3.16	3.24	3.25
Discharge Temperature (^oC)	74.0	68.3	67.6	68.34
Refrigerant Evap Inlet Temp (^oC)	-6.5	-12.7	-12.7	-15.35
Refrigerant Evap Outlet Temp (^oC)	23.5	22.0	20.3	20.0
Refrigerant Cond Outlet Temp (^oC)	25.0	19.0	18.3	21.0

Considering pure refrigerants, the refrigeration effect and compressor power of the R134a was higher than that of R125 therefore overall the coefficient of performance for R134a was greater than that of R125. Furthermore, R134a had a higher discharge temperature which was due to a high-power consumption at the compressor. For the refrigerant blends, (R134a/R125) blends had low discharge temperatures. Hence they are safe for the operation of the compressor and the compressor life. In general, the blends had superior compressor properties which are low compressor work and low discharge temperature. The efficiency values used in the simulation were obtained from the experimental runs hence the blends operate at a higher compressor efficiency.

It is evident from the analysis in this section that blend formation improves the performance of pure refrigerants. The R134a/ R125 blend in the ratio studied (66/34 by wt %) had a high refrigeration effect and the low compressor power consumption consequently a high-value COP. The refrigeration effect of the (50/50 by wt %) R134a/ R125 had the lowest refrigeration effect. However, its compressor power was relatively low thus its COP was higher than that of R134a and R125.

Refrigerant R134a expanded most favorable at the expansion valve as it existed with the largest percentage of the liquid phase in the two-phase mixture whereas R125 had the lowest proportion of liquid. However, R125 gave the lowest temperature at the evaporator inlet than R134a thus it is an excellent low-temperature refrigerant.

From the analysis carried out above, the R134a/R125 (66/34 by wt %) blend is the best performing blend in the refrigerant unit operating conditions investigated in this study and can be utilised in medium temperature applications.

Chapter 8

8 Conclusions

The main objective of this study was to commission a refrigerant test rig and investigate the performance of various refrigerant blends. The apparatus was successfully commissioned using refrigerant R134a.

The operating range of the refrigeration unit is within -20 to 100 ^{o}C, sealing under vacuum pressures of 26.6 kPa at room temperature and a maximum pressure limit of 1.9 MPa.
Results from the trial runs carried out with refrigerant R134a indicate that the equipment could produce accurate and reliable refrigeration effect, therefore, deeming it to be suitable for refrigeration studies.

The commercial refrigerant blends studied in the project included R413a and R507 whereas the blend synthesised in this study were R134a/R125 (66/34 by wt %) and R134a/R125 (50/50 by wt %). In comparing the performance of commercial refrigerant blends, refrigerant blend R507a performed better than refrigerant R413a in both the experimental and simulation analyses. The COP values for R507a and R143a in the experimental studies were 4.54 and 3.57 respectively, whereas in the simulation the COP values were 5.00 and 4.00 respectively. However, the performance of refrigerant R413a is comparable to that of refrigerant R134a, used as the reference refrigerant in this study. For this reason, refrigerant blend R413a is a potential candidate to be applied as a replacement of refrigerant R134a.

The results from the simulations performed using Aspen Plus® V8.6 utilising REFPROP method to evaluate the performance of the refrigerants. The generated COP results deviated from the experimental data for the refrigerants R134a, R413a and R507a as per the following percentage differences, 2.89%, 9.64% and 11.36% respectively. Thus, it can be concluded that the unit performance is close to the simulation (ideal) based on the COP values which are the overall performance measurement of a refrigerant.

Considering the blends synthesised for this study, refrigerant blend R134a/R125 (66/34 by wt %) displayed better performance than R134a/R125 (50/50 by wt %). The former had a COP value of 4.88, refrigeration effect of 0.34 kW and compressor power of 0.05 kW whereas the latter had COP value of 4.80, refrigeration effect of 0.24 kW and compressor power of 0.07 kW. This outcome is favorable since R134a, with a lower GWP, constitutes a larger percentage

in the blend. Thus, the R134a/R125 (66/34 by wt %) blend has a minimal environmental impact compared to the R134a/R125 (50/50 by wt %) blend. Moreover, the synthesised R134a/R125 blends displayed better performance than the pure refrigerants (R134a, COP value of 4.78 and R125, COP value of 4.41) in the comparative analysis of the simulation results.

Overall, of all the refrigerants investigated in this study R507A (R134A/R143a, 50/50 wt %) a commercial blend and R134a/R125 (66/34 by wt %) a laboratory synthesised blend were the better performing refrigerants from those investigated. The refrigeration effect for R507 was 0.4 kW whereas for R134a/R125 (66/34 by wt %) was 0.34 kW. However, the compression work of R507a was 0.08 kW which is higher than that of R134a/R125 (66/34 by wt %) which was 0.07 kW. The COP values for R507a a commercial blend and R134a/R125 (66/34 by wt %) the synthesised blend were 5.00 and 4.88 respectively. Incorporating the environmental factors R134a/R125 (66/34 by wt %) with GWP value of just above 1300 had an overall more desirable performance than R507 with a GWP value of 3900.

Chapter 9

9 Recommendations

To improve the performance and versatility of the refrigerant unit and obtain accurate data it is imperative to carry out the following modifications in the unit:

1. The distance between the expansion valve and the evaporator inlet should be reduced because it lowers the refrigerating capacity of the refrigerant in the evaporator as there is extra heat load along the pipeline.
2. The water valve at the evaporator water bath needs to be replaced with a smaller flowmeter graduated in the range 0.1 -1 litre.
3. Improvement in the method of cooling the water in the condenser water bath, so as to keep the condenser temperature constant, thus maintain a steady temperature in the unit for prolonged periods.
4. Installation of a pressure sensor at the expansion valve to report the conditions accurately at the expansion valve.
5. The configuration at the T-junction at the SA-01 inlet should be changed as it is suspected to be the cause of a large refrigerant loss at high operating pressures.
6. The operation of other cycles (Two stage Vapour–Compression Cycle, Cascade System, and Vapour –Compression Cycle with a Suction-line Heat Exchange) so as to utilise the equipment to the maximum of its design capabilities.

References

Abdelaziz, O., Fricke, B. and Vineyard, E. A. 2012. Development of Low Global Warming Potential Refrigerant Solutions for Commercial Refrigeration Systems using a Life Cycle Climate Performance Design Tool. *International Refrigeration and Air Conditioning Conference* Purdue: Oak Ridge National Laboratory, Energy and Transportation Science Division, Oak Ridge, TN, USA.

Ahamed, J., Saidur, R. and Masjuki, H. 2011. A review on exergy analysis of vapor compression refrigeration system. *Renewable and Sustainable Energy Reviews,* 15**,** 1593-1600.

Air-Conditioning Heating and Refrigeration Institute, A. 2007. 2007 Performance Rating of Commercial and Industry Unitary Air-Conditioning and Heat Pump Equipment. *ANSI/AHRI Standard 340/360-2007 with Addenda 1and 2.* Wilson Boulevard, Suite 500 ARLINGTON ,USA: Air-Conditioning Heating and Refrigeration Institute.

Akintunde, M. 2013. Experimental Study of R134a, R406A and R600a Blends as Alternative To Freon 12. *IOSR Journal of Mechanical and Civil Engineering,* 7**,** 40-46.

Angell, J. 1988. An update through 1985 of the variations in global total ozone and north temperate layer-mean ozone. *Journal of Applied Meteorology,* 27**,** 91-97.

Arora, A. and Kaushik, S. 2008. Theoretical analysis of a vapour compression refrigeration system with R502, R404A and R507A. *International Journal of Refrigeration,* 31**,** 998-1005.

Arora, C. P. 2009. *Refrigeration and Air Conditioning,* New Dehli, Tata McGraw-Hill Companies.

Baskaran, A. and Mathews, P. K. 2012. A Performance comparison of vapour compression refrigeration system using Eco friendly refrigerants of low global warming potential. *International journal of scientific and research publications,* 2**,** 1-8.

Baxter, V., Fischer, S. and Sand, J. R. 1998. Global warming implications of replacing ozone-depleting refrigerants. *ASHRAE journal,* 40**,** 23.

Bhatkar, V. W., Kriplani, V. and Awari, G. 2013. Alternative refrigerants in vapour compression refrigeration cycle for sustainable environment: a review of recent research. *International Journal of Environmental Science and Technology,* 10**,** 871-880.

Bitzter 2014. Refrigerant Report 18. 17th ed. www.bitzer.de/shared_media/documentation/a-501-18.pdf [29 Feb 2016].

Bolaji, B. O. 2011. Performance investigation of ozone-friendly R404A and R507 refrigerants as alternatives to R22 in a window air-conditioner. *Energy and Buildings,* 43**,** 3139-3143.

Breidenich, C., Magraw, D., Rowley, A. and Rubin, J. W. 1998. The Kyoto protocol to the United Nations framework convention on climate change. *The American Journal of International Law,* 92**,** 315-331.

Brijendra, K. Y., Suresh, K. B. and Rohit, C. 2017. Replacement of R22 in Vapour Compression Refrigeration Cycle with Mixture of Environment Friendly Refrigerant - did not match any articles. *International Journal of Engineering Technology and Applied Science,* Vol. 3.

Calm, J. M. 2008. The next generation of refrigerants–Historical review, considerations, and outlook. *International Journal of Refrigeration,* 31**,** 1123-1133.

Çengel, Y. A. and Boles, M. A. 2006. *Thermodynamics: An Engineering Approach*, McGraw-Hill, New York.

Chesi, A., Ferrara, G., Ferrari, L. and Tarani, F. 2012. Setup and characterisation of a multi-purpose test rig for R744 refrigerating cycles and equipment. *International Journal of Refrigeration,* 35**,** 1848-1859.

Coggins, C. L. 2007. *Single-and multiple-stage cascaded vapor compression refrigeration for electronics cooling.* Georgia Institute of Technology.

Dalkilic, A. and Wongwises, S. 2010. A performance comparison of vapour-compression refrigeration system using various alternative refrigerants. *International Communications in Heat and Mass Transfer,* 37**,** 1340-1349.

Datta, S. P., Das, P. K. and Mukhopadhyay, S. Effect of refrigerant charge, compressor speed and air flow through the evaporator on the performance of an automotive air conditioning system. 15th International Refrigeration and Air Conditioning Conference July 14-17, 2014 2014 Purdue.

Dennis, L. O. N., William, J. M., Roberto, R. A., Daniel, J. D. and Cecily, M. G. 2010. *ASHRA Handbook of Refrigeration,* 1791 Tullie Circle, N.E., Atlanta, GA 30329, American Society of Heating, Refrigerating and Air-Conditioning Engineers, Inc.

Domanski, P. A. Comparable performance evaluation of HC and HFC refrigerants in an optimized system. 7th IIR Gustav Lorentzen Conference on Natural Working Fluids May 28-31, 2006 Trondheim, Norway.

Donald, M. E., Harold, G. L., Ramon, P. and Brian, C. K. 1997. *ASHRA Handbook of Refrigeration,* 1791 Tullie Circle, N.E., Atlanta, GA 30329, American Society of Heating, Refrigerating and Air-Conditioning Engineers, Inc.

Elsayed, A. O. and Hariri, A. S. Effect of condenser air flow on the performance of split air conditioner. World Renewable Energy Congress-Sweden; , 8-13 May; 2011; 2011 Linköping; Sweden. Linköping University Electronic Press, 2134-2141.

Ely, J. F. and Huber, M. L. 1990. A predictive extended corresponding states model for pure and mixed refrigerants.

Emerson 1969. Refrigeration Manual Part-4 System Design. *In:* PRODUCTS, C. B. (ed.) *Emerson Climate Technology.*

Emerson Climate Technologies Ae4-1299 R9 2010. Application Guidelines for K4 Refrigeration Copeland Scroll® Compressors 2 - 6 Horsepower. *In:* PRODUCTS, C. B. (ed.). Printed in the U.S.A.

Goetzler, W., Sutherland, T., Rassi, M. and Burgos, J. 2014. Research & development roadmap for next-generation low global warming potential refrigerants. *In:* ENERGY (ed.) *Energy Efficiency and Renewable Energy.* Washington, DC: U.S.A: Navigant Consulting, Inc.

Gomaa, A. 2015. Performance Characteristics of Automotive Air Conditioning System with Refrigerant R134a and Its Alternatives. *International Journal of Energy and Power Engineering*.

Gupta, M., Aftab Anjum*, Ansari, N. A. and Rs, M. 2017. Performance Analysis of a Two Stage Vapour Compression Refrigeration System Utilizing the Waste Heat of the Intercooler for Water Heating. *Journal of Fundamentals of Renewable Energy and Applications,* 7.

Halimic, E., Ross, D., Agnew, B., Anderson, A. and Potts, I. 2003. A comparison of the operating performance of alternative refrigerants. *Applied Thermal Engineering,* 23**,** 1441-1451.

Heldon 2009a. Suction Accumulators. www.henrytech.com.au *[24 Mar 2016]*.

Heldon 2009b. Vibrator Eliminators. www.heldon.com.au *[23 Mar 2016]*.

Hesselgreaves, J. E. 2011. *Compact Heat Exchangers Selection , Design and operation,* Lockport, NY, USA, Elsevier Science & Technology Books.

Hoşöz, M. 2005. Performance comparison of single-stage and cascade refrigeration systems using R134a as the working fluid. *Turkish Journal of Engineering and Environmental Sciences,* 29**,** 285-296.

Huber, M. L., Friend, D. G. and James F. Ely 1992. Prediction of the Thermal Conductivity of Refrigerants and Refrigerant Mixtures. *Fluid Phase Equilibria, 80:249-261*.

Hundy, G. F., Trott, A. R. and Welch, T. 2008. *Refrigeration and Air-conditioning,* Butterworth-Heinemann.

Hwang, Y., Jin, D.-H. and Radermacher, R. 2004. Comparison of hydrocarbon R-290 and two HFC blends R-404A and R-410A for medium temperature refrigeration applications. *Final Interim Report to ARI, Global Refrigerant Environmental Evaluation Network (GREEN) Program, CEEE Department of Engineering, University of Maryland, USA.*

Hwang, Y., Jin, D.-H. and Radermacher, R. 2007. Comparison of R-290 and two HFC blends for walk-in refrigeration systems. *International Journal of Refrigeration,* 30**,** 633-641.

Isceon Refrigerants 1998. R413A (ISCEON 49) Drop-In Replacement for R12, ODP Zero Compatible with traditional lubricants. *In:* RHODIA LIMITED, I. H. (ed.) *Bristol BS11 9YF England.* www.kemikaal.ee/lie/failid/brochure49.pdf [19 Apr 2017].

Jain, V., Kachhwaha, S. S. and Mishra, R. S. 2011. Comparative performance study of vapour compression refrigeration system with R22/R134a/R410A/R407C/M20. *International Journal of Energy and Environment,* 55**,** 297-310.

Jeong, J. H., Park, S.-G., Sarker, D. and Chang, K. S. 2012. Numerical simulation of the effects of a suction line heat exchanger on vapor compression refrigeration cycle performance. *Journal of Mechanical Science and Technology,* 26**,** 1213.

Jerald, L. A. and Kumaran, D. S. 2014. Investigations on the performance of vapour compression system retrofitted with zeotropic refrigerant R404a. *American Journal of Environmental Sciences,* 10**,** 35.

Jung, D., Kim, C.-B., Hwang, S.-M. and Kim, K.-K. 2003. Condensation heat transfer coefficients of R22, R407C, and R410A on a horizontal plain, low fin, and turbo-C tubes. *International Journal of Refrigeration,* 26**,** 485-491.

Jung, D., Song, Y. and Park, B. 2000. Performance des mélanges de frigorigènes utilisés pour remplacer le HCFC22. *International Journal of Refrigeration,* 23**,** 466-474.

Kakac, S., Liu, H. and Pramuanjaroenkij, A. 2012. *Heat exchangers: Selection, Rating, and Thermal design*, Boca Raton, Florida, CRC press.

Karagoz, S., Yilmaz, M., Comakli, O. and Ozyurt, O. 2004. R134a and various mixtures of R22/R134a as an alternative to R22 in vapour compression heat pumps. *Energy conversion and management,* 45**,** 181-196.

Kim, J. H., Cho, J. M., Lee, I. H., Lee, J. S. and Kim, M. S. 2007. Circulation concentration of CO 2/propane mixtures and the effect of their charge on the cooling performance in an air-conditioning system. *International Journal of Refrigeration,* 30**,** 43-49.

Kim, M. and Didion, D. 1995. Simulation of isothermal and adiabatic leak processes of zeotropic refrigerant mixtures. *HVAC&R Research,* 1**,** 3-20.

Klein, S., Reindl, D. and Brownell, K. 2000. Refrigeration system performance using liquid-suction heat exchangers. *International Journal of Refrigeration,* 23**,** 588-596.

Kumar, S. S., Sivaram, A. and Rajavel, R. 2015. Thermodynamic Analysis of a Cascade Refrigeration System with R744/R290 Mixtures. *Indian Journal of Science and Technology,* 8.

Lavelle, J. 2006. Understanding Refrigerant Blend Performance Part 1. *In:* INC, N. R. (ed.).

Mani, K. and Selladurai, V. 2008. Experimental analysis of a new refrigerant mixture as drop-in replacement for CFC12 and HFC134a. *International Journal of Thermal Sciences,* 47**,** 1490-1495.

Mani, K., Selladurai, V. and Murugan, N. 2013. Development of Mathematical Models for Predicting Performance of CFC12, HFC134a and R290/R600 Mixture Refrigerants using Design of Experiments. *International Journal of Thermodynamics,* 16**,** 43-53.

Mcgeorge, H. D. 1998. *Marine auxiliary machinery,* Linacre House, Jordan Hill, Oxford 0X2 BDP, Butterworth-Heinemann.

Mclinden, M. O., Klein, S. A. and Perkins, R. A. 2000. An extended corresponding states model for the thermal conductivity of refrigerants and refrigerant mixtures. *International Journal of Refrigeration,* 23**,** 43-63.

Mishra, R. 2014. Thermodynamic Performance Evaluation of Multi-Evaporators Single Compressor and Single Expansion Valve and Liquid Vapour Heat Exchanger in Vapour Compression Refrigeration Systems using Thirteen Ecofriendly Refrigerants for Reducing Global Warming and Ozone depletion. *International Journal,* 2**,** 325-332.

Moffat, R. J. 1988. Describing the uncertainties in experimental results. *Experimental Thermal and Fluid Science,* 1**,** 3-17.

Mohanraj, M., Muraleedharan, C. and Jayaraj, S. 2011. A review on recent developments in new refrigerant mixtures for vapour compression-based refrigeration, air-conditioning and heat pump units. *International Journal of Energy Research,* 35**,** 647-669.

Molina, M. J. and Rowland, F. S. 1974. Stratospheric sink for chlorofluoromethanes: chlorine atom-catalysed destruction of ozone. *Nature,* 249**,** 810-812.

Moran, M. J. and Shapiro, H. N. 2006. *Fundamentals of Engineering Thermodynamics,* West Sussex, England, John Wiley & Sons Ltd, .

Mulroy, W., Domanski, P. and Didion, D. 1994a. Glide matching with binary and ternary zeotropic refrigerant mixtures Part 2. A computer simulation. *International Journal of Refrigeration,* 17**,** 226-230.

Mulroy, W., Domanski, P. A. and Didion, D. 1994b. Glide matching with binary and ternary zeotropic refrigerant mixtures Part 1. An experimental study. *International Journal of Refrigeration,* 17**,** 220-225.

Narayan, L., Arya, A. and Khare, S. 2013. A comparative study for retrofitting of R-12 vapour compression refrigeration system by eco-friendly refrigerants R-134a, R-413a, R-423a. *International Journal of Application of Engineering and Technology,* 2.

Outcalt, S. L. and Mclinden, M. O. 1996. A Modified Benedict–Webb–Rubin Equation of State for the Thermodynamic Properties of R152a (1, 1-difluoroethane). *Journal of Physical and Chemical Reference Data,* 25**,** 605-636.

Padilla, M., Revellin, R. and Bonjour, J. 2010. Exergy analysis of R413A as replacement of R12 in a domestic refrigeration system. *Energy Conversion and Management,* 51**,** 2195-2201.

Park, K.-J., Shim, Y.-B. and Jung, D. 2009. A ‘drop-in’refrigerant R431A for replacing HCFC22 in residential air-conditioners and heat pumps. *Energy Conversion and Management,* 50**,** 1671-1675.

Parker Hannifin Corporation 2015. Combination Moisture & Liquid Indicators for Refrigerants R134a, R22, R404A, R407C, R407F, R410A or R507. *In:* EUROPE, I. G. R. A. A. C. (ed.). Cortonwood Drive, Brampton Barnsley S73 OUF - United Kingdom.

Pelchem 2014. Pelchem SOC Ltd Overview. *In:* PELCHEM (ed.) *Fluorochemical excellence.*

Prapainop, R. and Suen, K. 2012. Effects of refrigerant properties on refrigerant performance comparison: A review. *International Journal of Engineering and Research and Applications (IJERA),* 2**,** 486-493.

Rajapaksha, L. 2007. Influence of special attributes of zeotropic refrigerant mixtures on design and operation of vapour compression refrigeration and heat pump systems. *Energy Conversion and Management,* 48**,** 539-545.

Rasti, M., Hatamipour, M. S., Aghamiri, S. F. and Tavakoli, M. 2011. Experimental study of R600a and R436a to replace R134a in a domestic refrigerator and freezer. *7th International Chemical Engineering Congress & Exhibition.* Kish, Iran.

Rigola, J., Escanes, F., Oliva, A. and Pérez-Segarra, C. 1996. Numerical study of a single stage vapor compression refrigerant unit using non-contaminant refrigerants.

Rigola, J., Pérez-Segarra, C., Garcia-Valladares, O., Serra, J., Escriba, M. and Pons, J. 1998. Numerical study and experimental validation of a complete vapor compression refrigerating cycle.

Sami, S. M. and Desjardins, D. E. 2000. Performance comparative study of new alternatives to R-502 inside air/refrigerant enhanced surface tubing. *International Journal of Energy Research,* 24**,** 177-186.

Sapali, S. 2009. *Refrigeration and Air conditioning,* PHI Learning Pvt. Ltd.

Satola, B. J. 2014. Molecular Targeting of Refrigerant Mixtures,. University of KwaZulu-Natal, School of Engineering, Howard College Campus, For the degree Doctor of Philosophy in Engineering (Chemical Engineering).

.

Satyanarayana, M. D. V. and Kotaiah, B. 2012. Impact of CFCs on Ozone layer and Global warming. *IOSR Journal of Engineering (IOSRJEN),* Vol. 2 059-069.

Sekiya, A. and Misaki, S. 2000. The potential of hydrofluoroethers to replace CFCs, HCFCs and PFCs. *Journal of Fluorine Chemistry,* 101**,** 215-221.

Sivasakthivel, T. and Reddy, K. S. K. 2011. Ozone layer depletion and its effects: a review. *International Journal of Environmental Science and Development,* 2**,** 30.

Smith, J. M., Ness, H. C. V. and Abbott, M. M. 2005. *Introduction to Chemical Engineering Thermodynamics,* Boston, McGraw-Hill Higher Education.

South African Government Press Release. 2009. *Fluorochemical Expansion Initiative launch* [Online]. http://www.gov.za/m-mangena-fluorochemical-expansion-initiative-launch. [Accessed 17 May 2017].

Stanciu, C., Gheorghian, A., Stanciu, D. and Dobrovicescu, A. 2011. Exergy analysis and refrigerant effect on The operation and performance limits of a One stage vapor compression Refrigeration system. *Termotehnica,* 1**,** 36-42.

Swagelok Company 2013. Swagelok Metering Valves MS-01-142. *Kalrez—TM DuPont.* USA: www.swagelok.com [Accessed 02 Apr 2016].

Szymurski, S. R. 2005. Refrigerant Blends, 9th Annual Financial Agent Workshop the World bank. *In:* INSTITUTE, A.-C. R. (ed.) *Air-Conditioning & Refrigeration Institute.*

Taylor, B. N. and Kuyatt, C. E. 1994. *Guidelines for evaluating and expressing the uncertainty of NIST measurement results*, US Department of Commerce, Technology Administration, National Institute of Standards and Technology Gaithersburg, MD.

Tillner-Roth, R. and Baehr, H. D. 1994. An international standard formulation for the thermodynamic properties of 1, 1, 1, 2-Tetrafluoroethane (HFC-134a) for temperatures from 170 K to 455 K and pressures up to 70 MPa. *Journal of Physical and Chemical Reference Data,* 23**,** 657-729.

Tuta, E. C. and Orozco, M. R. Computational tool for simulation of power and refrigeration cycles. IOP Conference Series: Materials Science and Engineering, 2016. IOP Publishing, 012017.

United Nations Epa 2014. Benefits of Addressing HFCs under the Montreal Protocol. *Stratospheric Protection Divivsion Office of Atmospheric Programs Office of Air and Radiation.*

United Nations Montreal Protocol. 1 January 1989. Montreal Protocol on Substances that Deplete the Ozone Layer. Montreal Protocol, 1987 Montreal, Canada.

United States Epa 2007. Achievements in Stratospheric Ozone Protection Progress Report. *In:* AGENCY, U. S. E. P. (ed.) *Office of Air and Radiation.* Washington,DC 20460.

Venkatarathnam, G. and Murthy, S. S. 2012. Refrigerants for vapour compression refrigeration systems. *Resonance,* 17**,** 139-162.

Wagner, W. and Pruß, A. 2002. The IAPWS formulation 1995 for the thermodynamic properties of ordinary water substance for general and scientific use. *Journal of Physical and Chemical Reference Data,* 31**,** 387-535.

Whitman, B., Johnson, B., Tomczyk, J. and Silberstein, E. 2013. *Refrigeration and Air Conditioning Technology*, Clifton Park ,USA, Delmar Cengage Learning.

Wongwises, S., Kamboon, A. and Orachon, B. 2006. Experimental investigation of hydrocarbon mixtures to replace HFC-134a in an automotive air conditioning system. *Energy Conversion and Management*, 47**,** 1644-1659.

Yadav, R. 2007. *Thermodynamics and Heat Engines* Central Publishing House.

Yataganbaba, A., Kilicarslan, A. and Kurtbaş, İ. 2015. Exergy analysis of R1234yf and R1234ze as R134a replacements in a two evaporator vapour compression refrigeration system. *International Journal of Refrigeration,* 60**,** 26-37.

Appendices

Appendix A: Temperature Glide

Table A.1: Azeotropic Refrigerant blends temperature glide for selected CFCs/HCFCs replacements determined at 100kPa. (Rajapaksha, 2007).

Mixture	**Components and mass fraction (%)**	**Replaced CFC/HCFC**	**TG (^{0}G)**
R409A	R22/R124/R142b (60/25/15)	R12 (CFC)	7,89
R401A	R22/R152a/R124 (53/13/34)	R12 (CFC)	5,59
R407C	R32/R125/R134a (23/25/52)	R22 (HCFC)	7,09
R410A	R32/R125 (50/50)	R22 (HCFC)	0,05
R401B	R22/R152A/R124 (61/11/28)	R500 (CFC +HFC)	4,95

A.1: Temperature glide matching

Refrigerant Mixtures having a temperature glide (about 5^0C or greater) ideally present a potential can be utilised in the performance improvement and energy efficiency of vapour compression refrigeration systems. Temperature glide matching is done by matching the refrigerant with the HTF temperature profile in the counter flow configuration as shown in Figure A.1. This is meant to keep a constant and small temperature variance between the HTF and the refrigerant.

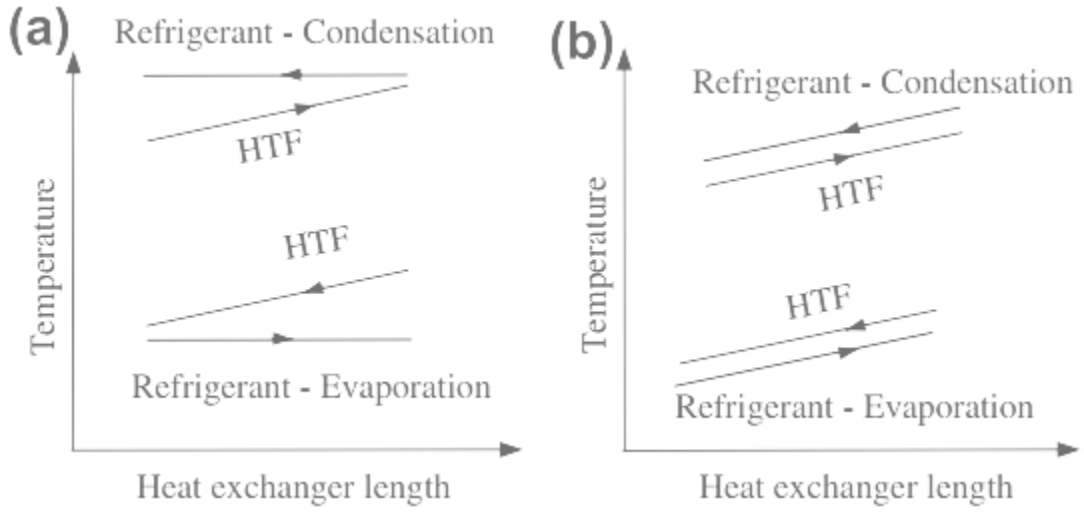

Figure A.1 : Temperature profiles of heat exchanger during the phase change of (a) pure refrigerant, (b) zeotropic refrigerant mixture with glide matching. (Rajapaksha, 2007).

Glide matching improves the efficiency of the system by reducing irreversibility of the heat transfer process Glide matching is only achievable in heat exchangers with certain geometries where counter-flow of fluids is possible, such as concentric tubes, shell and tube and flat heat exchangers. Glide matching reduces the entropy generated in the heat exchanger during the phase change thus increasing the efficiency of the system. Moreover, it improves the COP as the compressor will be operating under reduced pressure. Atmospheric air and water/glycol mixture and are a good example of HTFs for glide matching in the condenser and evaporator and for vapour compression systems (Mulroy et al., 1994a; Mulroy et al., 1994b).Glide matching is best suited for liquid-liquid systems and is affected by changes in operating pressure. Understanding glide properties of refrigerants are essential in identifying problems in retrofitting systems and in new refrigeration design and hardware improvements to incorporate temperature glide and composition change so as to improve the efficiency of the system (Rajapaksha, 2007). Mixtures exhibiting a glide of / less than 2K are termed 'near-azeotropes' and are often treated as a pure substance for the purposes of design (Hundy et al., 2008).

A.2: Effects of Phase Change of Zeotropic blends on Heat Transfer Coefficients (HTC)

Due to preferential boiling or condensation, composition shifts occur within the different phases of the fluid. Consider the condensation of a binary mixture of components A and B on a cold surface. Component A with a higher boiling point will condense first reducing its vapour concentration (and consequently its partial pressure) closer to the wall. This results in the formation of a vapour diffusion film (with concentration gradient) between the condensate and bulk vapour (Figure A.2).

This vapour diffusion film acts as an additional thermal resistance. The reduction of interfacial temperature from T_b to T_i (and consequently reduction of the temperature driving force for conduction in the condensate film) results in lower heat transfer coefficients when compared to an azeotropic mixture.

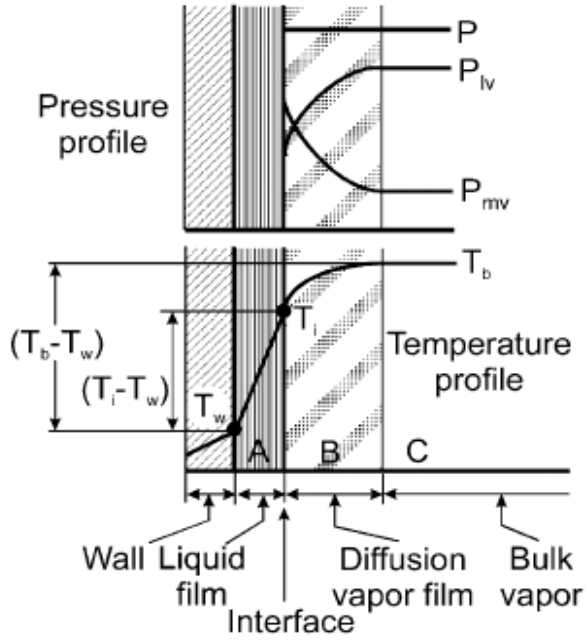

Figure A.2 : Pressure and temperature profile for condensation of a non-azeotropic mixture. (Jung et al., 2003).

Jung et al. (2003) investigated the heat transfer coefficients for condensation of R22, R407C, and R410A on different tube surfaces. The HTC's of zeotropic R407C were up to 50 % lower than those of R22. This was attributed to the presence of the diffusion vapour film.

Appendix B: Technical Information of the Equipment Components

The technical specifications for the suction accumulator, compressor and the valves are stated below:

B.1: Suction Accumulators

Manufactured in accordance with AS 2971, AS1210 and UL207.

General Safe Working Pressure for Heldon Suction Accumulators is 2.500 kPa.

General minimum burst Pressure for Heldon Accumulators is 12500 kPa.

Design temperature range of all Heldon Accumulators is -30 ^{0}C to +50 ^{0}C.

Copper tubing and fittings in accordance with AS 1571-1995 or ASTM B28.

Table B.1 : Compressor Specifications

Type	Reciprocating
Model	Bitzer 2KES-05(Y)
No. cylinder x bore x stroke	2 x 30 mm x 33 mm
Cooling	Air
Refrigerant	HFC (spec. R134a, R404A, R407A/C/F, R507A
Oil type	POE (Emkarate 32)
Oil charge	1.00 dm^3
Maximum pressure (LP/HP)	1.9/2.8 MPa
Displacement at 50Hz (1450 RPM)	4.06 m^3/hr
Displacement at 60Hz (1750 RPM)	4.90 m^3/hr
Motor	230/400 V-3-50 Hz
Drive	3 phase motor
Capacity adjustment	Variable frequency drive (30 -70 Hz)
Maximum operating current	2.8 A(Y)
Maximum power consumption	1.5 kW

Table B.2 : Valves Specifications (Swagelok Company, 2013).

	Expansion Valves	**Metering Valves**
Code on the Unit	SS-4L-BU-MH	SS-4MG-BU-MH
Description	Metering Valve Buna O-rings , MH Handle	Metering Valve L-SERIES, Buna O-rings, MH
Orifice	0.128 inch/3.25 mm	0.0056 inch/1.42 mm
Working Pressure/bars	68.9	68.9
Temperature/^{0}C	-23 to 148	-23 to 148
C_v	0.004 to 0.16	0.004 to 0.16

Appendix C: Refrigeration Cycle

A schematic representation and description are presented for each cycle to be investigated in the unit in Figures below. The red/green and blue lines are indicative of the refrigerant flow, and heat transfer fluid flow paths, respectively.

Simple Vapour Compression Cycle (VCC)

The VCC is the simplest cycle. It utilizes an evaporator, condenser, and expansion valve and one (or both) compressors. Figure 2 represents a simple VCC cycle, in which the second expansion valve (EX-02) and compressor (CM-02) are bypassed. EX-02 is bypassed by directing the refrigerant flow, after the condenser, through valves V-10 and V-4, directly to the evaporator. A flexible hose fixed between CP-01 and CP-02, and the correct orientation of switching valves V-1 and V-2, effectively bypass CM-02.

The compressors may be used in series for large refrigerant flow rates or pressure differentials between the evaporation and condensation sides. This cycle is illustrated in Figure C.1.

VCC with Suction Line Heat Exchanger

A suction line heat exchanger (SLHX), or flash cooler, is included as a means of increasing system efficiency. Its effectiveness is, however, dependent on the refrigerant in use.

Klein et al. (2000), investigated the impact of SLHXs on overall system performance. In contrast to other researchers, they considered the effect of pressure drop across the SLHX. They further identified a dimensionless group that would allow correlation of these impacts. They reported that systems with low SLHX pressure drops on the low-pressure side improved system performance for a range of refrigerants, whilst degrading the performance of other systems.

Jeong et al. (2012), developed a computer program based on momentum, mass, and energy conservation equations to investigate the influence of an SLHX on the performance of an R134a VCC. Their simulations revealed that the system cooling capacity, as well as COP, is dependent on both the location and of the length SLHX. They also indicated that the system performance could deteriorate under certain conditions. With the inclusion of this cycle, the benefits of an SLHX, with a specific refrigerant, can be gauged. This configuration is illustrated in Figure C.3.

Cascade Refrigeration Cycle

The cascade VCC is represented in Figure C.4, where the green and red lines indicate the respective refrigerant flows through the two cycles of the cascade system. By facilitating both these cycles on a single unit, a direct comparison can be made for refrigerants and operating conditions.

Hoşöz (2005), conducted an experimental comparison of R134a single stage and cascade VCCs. He found that, for a given refrigerating capacity, the cascade system exhibited lower evaporating temperatures. The required compressor power and refrigerant flowrates were also reduced, as compared to the single stage. Although this implies a higher COP for the lower temperature cycle, the overall system COP is lower, due to the additional power requirement of the second compressor. The cascade VCC leads to lower operating pressure ratios for the compressor, higher volumetric efficiencies, and lower discharge temperatures that should lengthen compressor life. (Kumar et al., 2015).

Multistage Refrigeration Cycle

A two-stage VCC is illustrated in Figure C.5. Splitting the condensate stream is accomplished by two Swagelok fine metering valves (EX-01 and MV-2). The valves are equipped with Vernier handles to allow reproducibility as well as fine control. Manipulating this will allow identification of the optimal split ratio for a specific refrigerant.

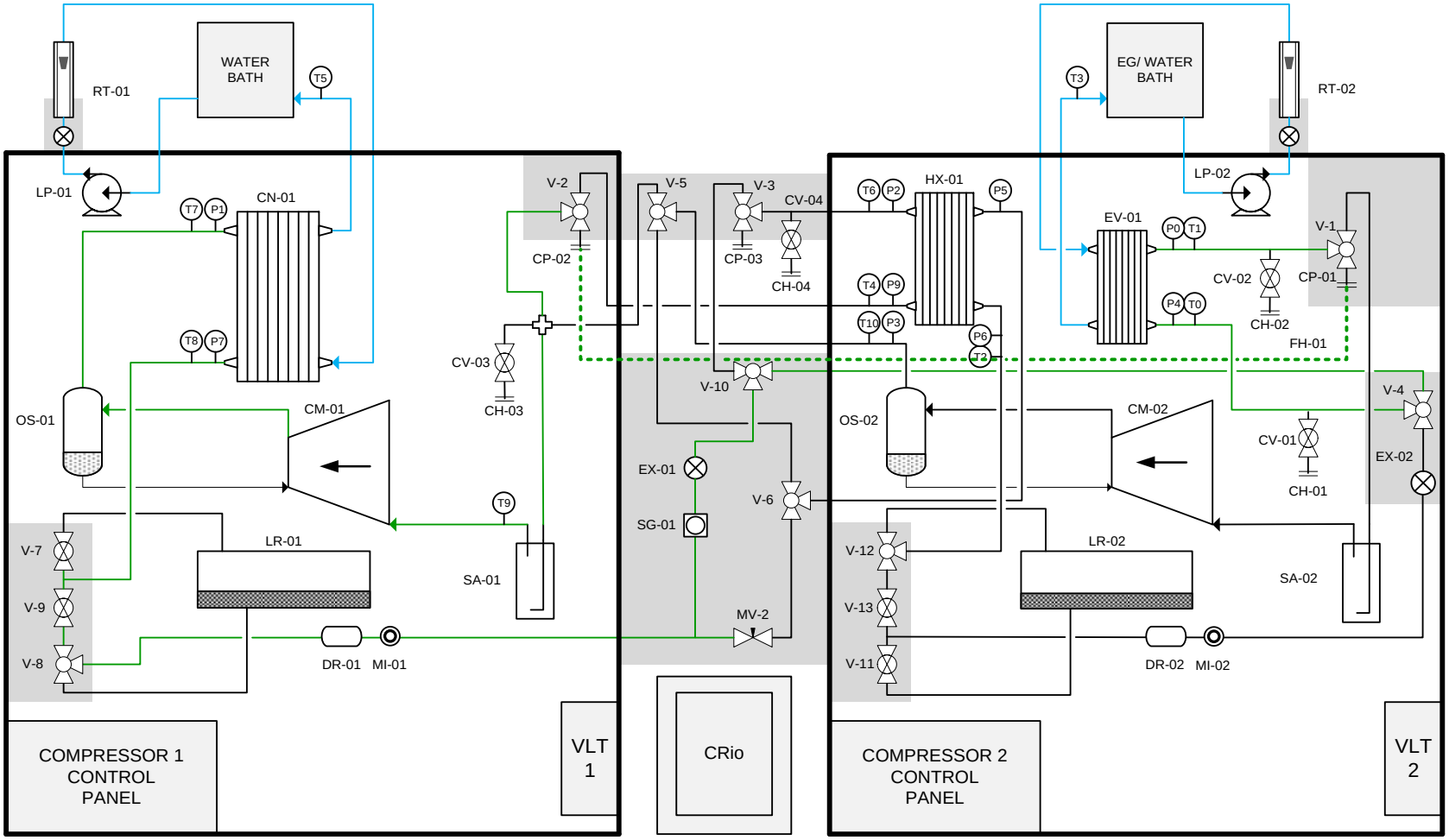

Figure C.1 : Simple VC configuration.

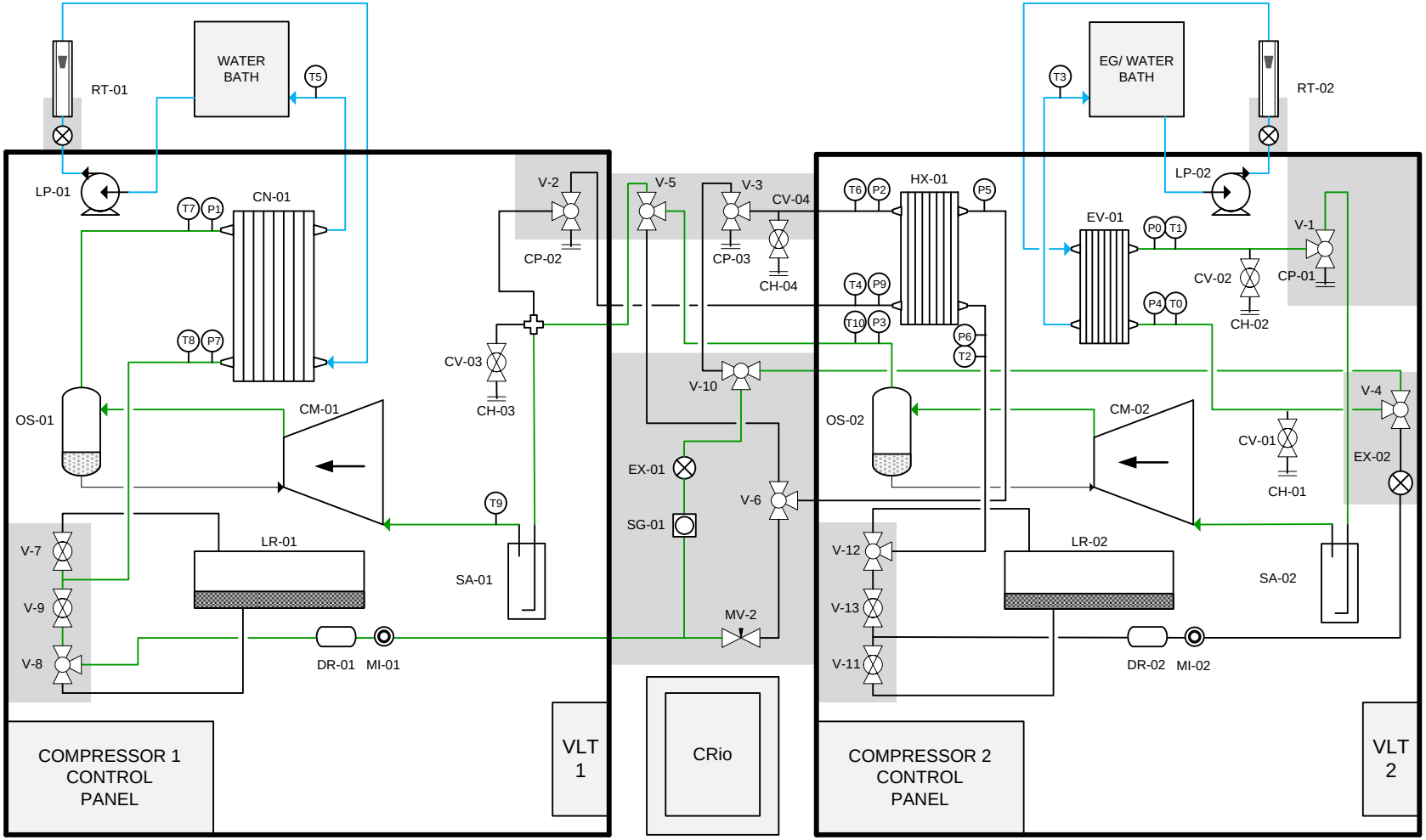

Figure C.2 : VC configuration using two compressors.

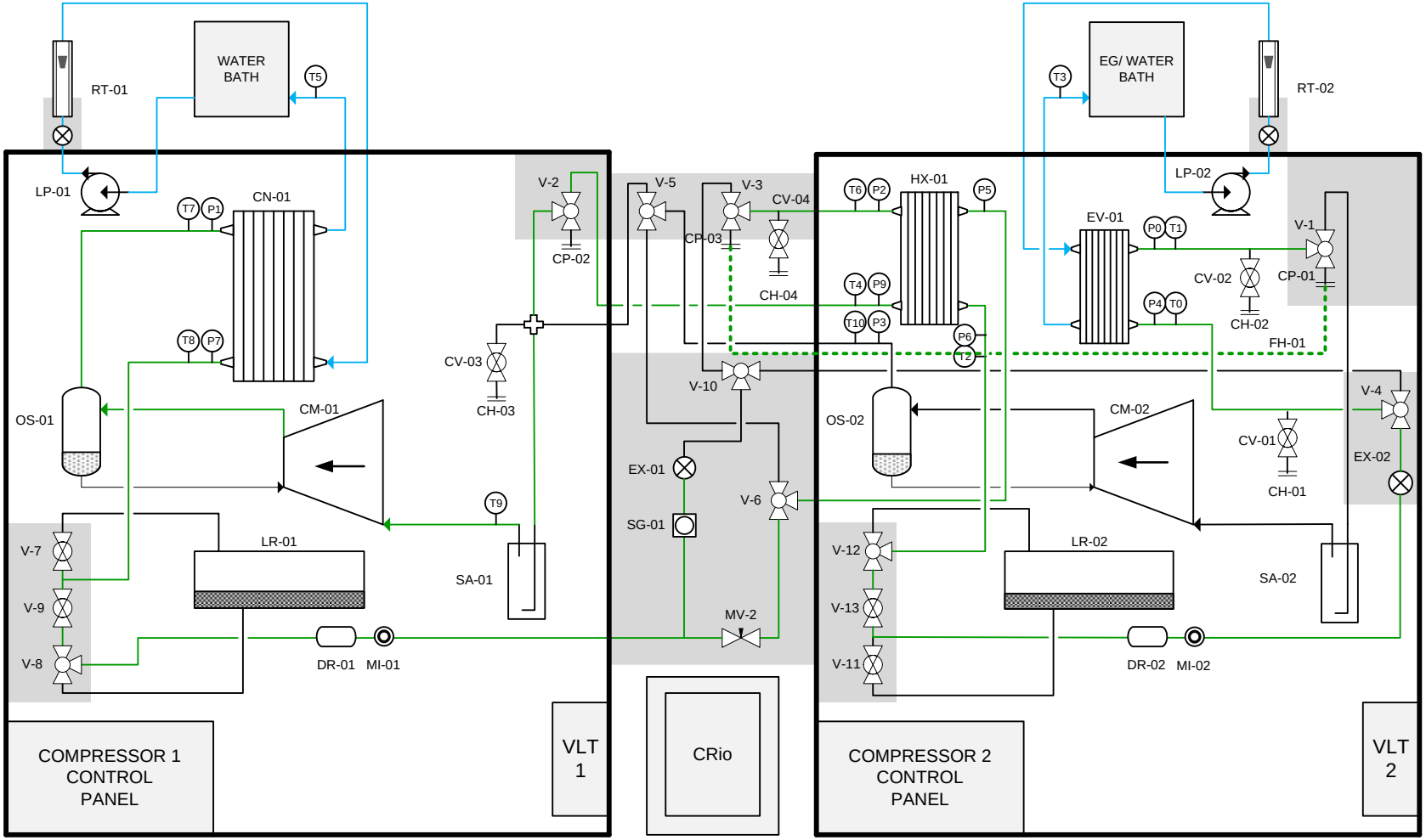

Figure C.3 : Configuration for VC with suction line heat exchanger.

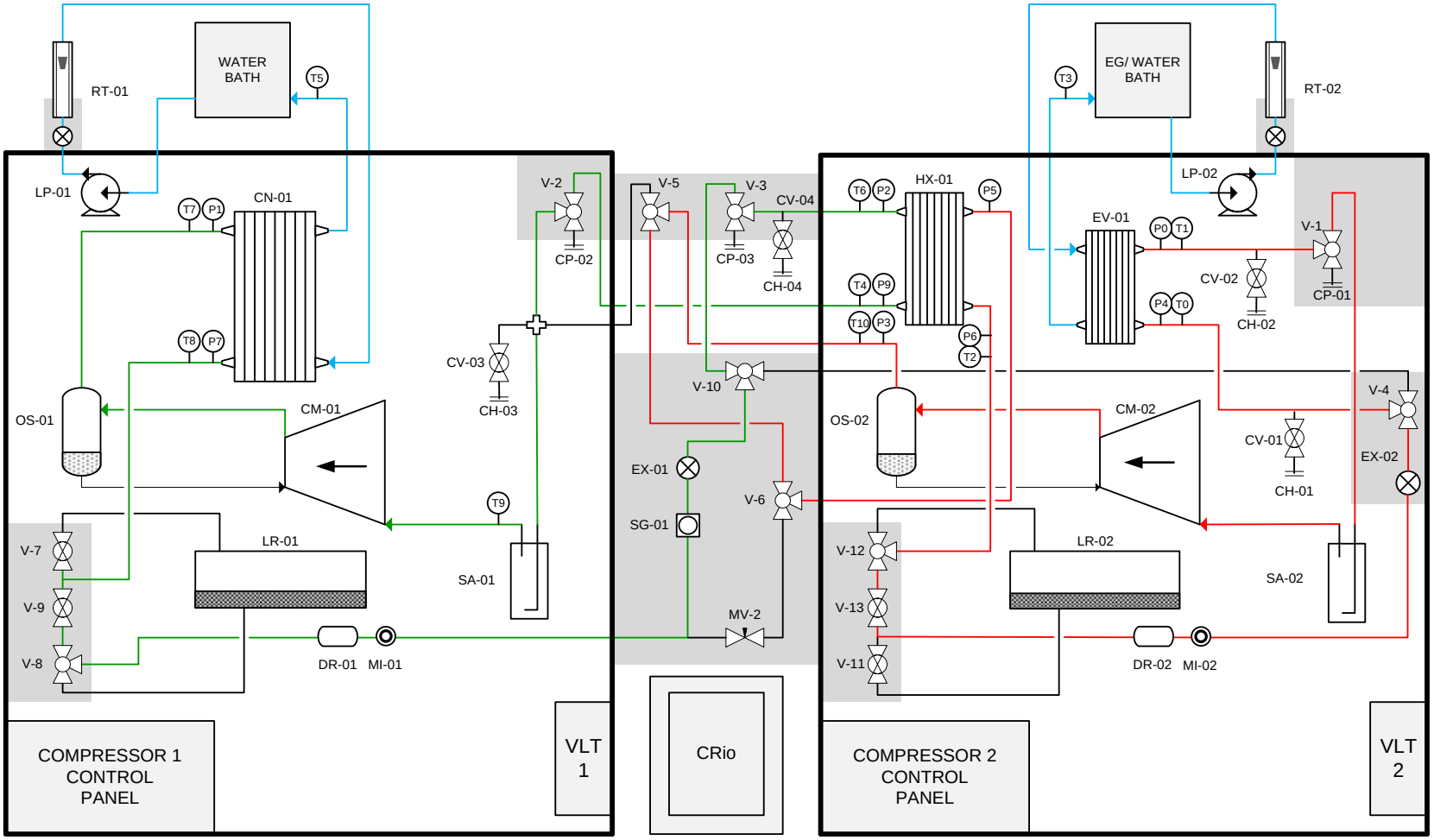

Figure C.4 : Cascade VC cycle configuration

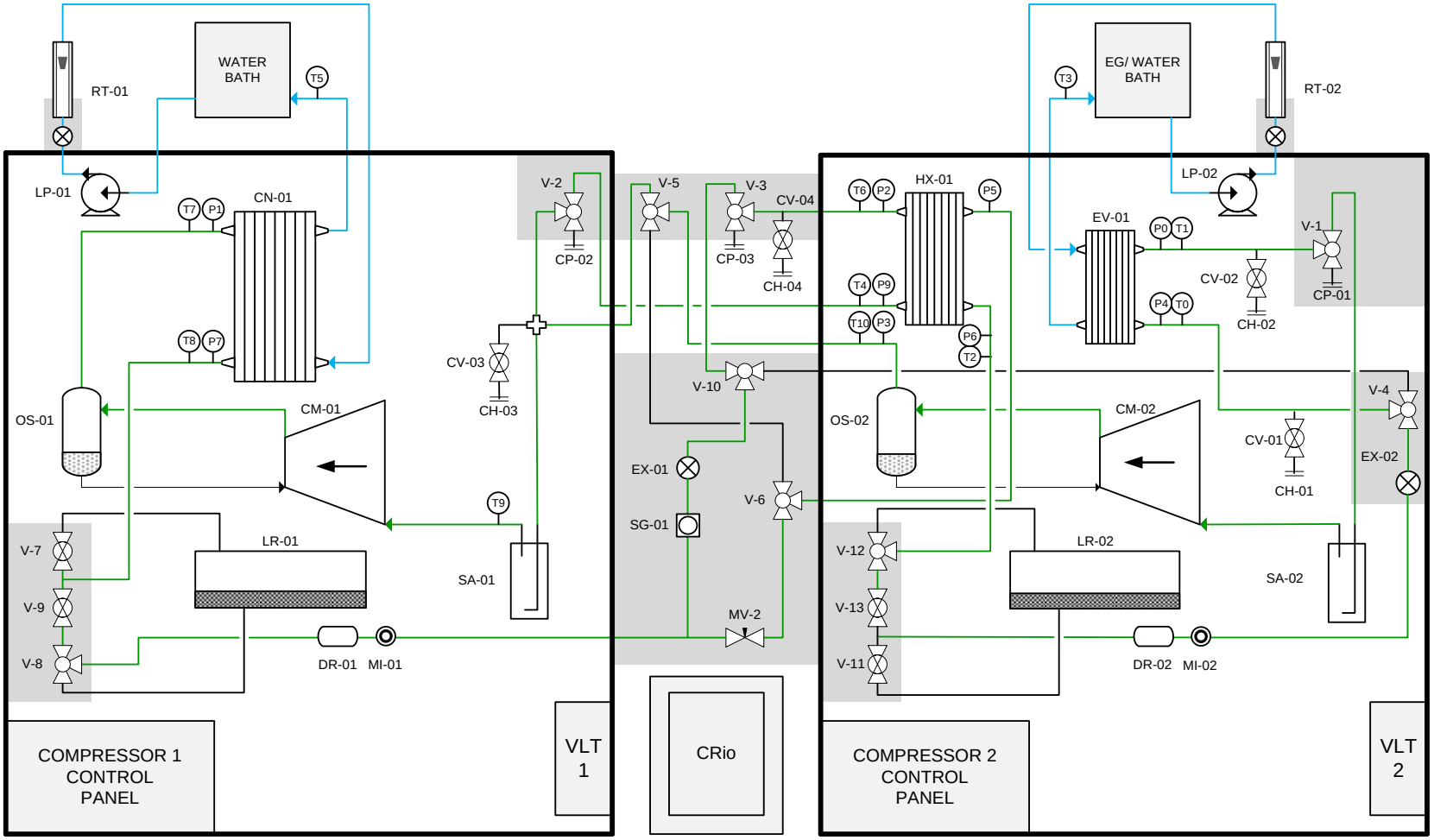

Figure C.5 : Two-stage VC cycle configuration.

Appendix D: Uncertainty in Measurements

D.1: Experimental Uncertainty

There are several components which constitute to the uncertainty of a measurement, however, these components are usually categorised in accordance with the method used to estimate their numerical values: Type A and Type B.

An alternative nomenclature that is commonly used to classify the uncertainty in measurements is as either the part of uncertainty from random effect or the element of uncertainty from a systematic effect. (NIST) (Taylor and Kuyatt, 1994).

The CSU of a measurement is obtained by combining the individual standard uncertainties Regardless of whether they are from a type A evaluation or a type B using the method of combined standard deviations. The expanded uncertainty is the measure of certainty intended to meet the required measurement. It is obtained by multiplying the CSU by the coverage factor, *k*, to give combined expanded uncertainty represented by $U(x)$. Hence the combined expanded uncertainty is given by:

$$U(x) = ku_c(x) \qquad \text{D.1}$$

where *k* is the coverage factor with a typical value of 2 is used to define an interval, having a level of confidence of approximately 95 percent. (NIST) (Taylor et al 1994). This can be expressed as:

$$u_c(x) = \pm\sqrt{\sum_i u_i\,(x)^2} \qquad \text{D.2}$$

where $u_i(x)$ is the standard uncertainty for a value *x*, such as uncertainty due to calibration correlation or standards or uncertainty due to the instrument manufacturer and uncertainty due to the repeatability of the measurement.

The combined uncertainty $u_c(x)$ is calculated from the uncertainty which arises from any of the two classes of uncertainty Type A or Type B. The Type A uncertainty is calculated by statistical methods in which the mean is taken to represent the true value. It is calculated by:

$$u_i(x) = \frac{\sigma}{\sqrt{N}} \qquad \text{D.3}$$

where σ the standard deviation of the data and N is the number of data points. Type B uncertainty is computed by a number of methods and information related to the measurements. The uncertainty can lie anywhere between the distribution and such distributions are known as rectangular. They are represented by:

$$u_i(x) = \frac{b}{\sqrt{3}} \qquad \text{D.4}$$

where b is the half the width of the interval. The rectangular distribution model is always the default model in the absence of any other information.

D.2: Temperature and Pressure Uncertainty

In refrigeration studies, temperature and pressure are the two most important parameters measured. The combined uncertainty of temperature is given by:

$$u_c(T) = \pm\sqrt{u_{calib}(T)^2 + u_{rep}(T)^2 + u_{instr}(T)^2} \qquad \text{D.5}$$

where $u_{rep}(T)$ denotes the standard uncertainty because of repeatability of a measurement (Type A), $u_{instr}(T)$ is the uncertainty of the Pt-100 standard temperature probe and $u_{calib}(T)$ denotes the standard uncertainty as a result of temperature calibration and is determined by:

$$u_{calib}(T) = \pm\sqrt{u_{std}(T)^2 + u_{corr}(T)^2} \quad \text{D.6}$$

where $u_{corr}(T)$ denotes the standard uncertainty because of the temperature calibration correlation (Type B) and $u_{std}(T)$ denotes the standard uncertainty inherent in the standard temperature probe (Type B).

Likewise, the combined standard uncertainty in pressure is calculated by:

$$u_c(P) = \pm\sqrt{u_{corr}(P)^2 + u_{rep}(P)^2 + u_{std}(P)^2 + u_{atm}(P)^2} \quad \text{D.7}$$

where $u_{corr}(P)$ is the standard uncertainty due to the pressure calibration correlation (Type B), $u_{std}(P)$ is the standard uncertainty of the pressure transducer (Type B), and $u_{rep}(P)$ is the standard uncertainty due to the repeatability of the pressure measurement (Type A).

D.3: Rotameter Uncertainty

The water flowrates across the evaporator and condenser were gauged by rotameters. The combined uncertainty of flowrate is given by:

$$u_c(F) = \pm\sqrt{u_{corr}(F)^2 + u_{rep}(F)^2} \quad \text{D.8}$$

where $u_{rep}(F)$ is the standard uncertainty due to the repeatability of the flowrate measurement (Type A) and $u_{corr}(P)$ is the standard uncertainty due to flowrate calibration correlation (Type B).

Appendix E: Simulation results

Table E.1 : Simulation Results for R413a

	Units	S1	S2	S3	S4	WC-IN	WC-OUT	WE-IN	WE-OUT
From		EVAP	COMP	COND	EXV	COND	COND	EVAP	EVAP
To		COMP	COND	EXV	EVAP				
Sub stream: MIXED									
Phase:		Vapor	Vapor	Liquid	Mixed	Liquid	Liquid	Liquid	Liquid
Component Mole Flow									
H20	KMOL/HR	0	0	0	0	9,992	9,992	1,499	1,499
C2H2F4	KMOL/HR	0,069	0,069	0,069	0,069	0	0	0	0
C3F8	KMOL/HR	0,004	0,004	0,004	0,004	0	0	0	0
C4H10	KMOL/HR	0,004	0,004	0,004	0,004	0	0	0	0
Mole Flow	KMOL/HR	0,077	0,077	0,077	0,077	9,992	9,992	1,499	1,499
Mass Flow	KG/HR	8	8	8	8	180	180	27	27
Volume Flow	L/MIN	10,71	3,17	0,11	2,48	3,01	3,01	0,45	0,45
Temperature	C	6,90	66,24	24,30	-7,97	20,00	22,18	25,00	13,61
Pressure	MPa	0,26	0,99	0,99	0,26	0,07	0,07	0,04	0,04
Vapor Fraction		1	1	0	0,24	0	0	0	0
Liquid Fraction		0	0	1	0,76	1	1	1	1
Solid Fraction		0	0	0	0	0	0	0	0
Molar Enthalpy	KJ/KMOL	-901360	-896760	-918080	-918080	-286210	-286040	-285830	-286690
Mass Enthalpy	KJ/KG	-8670,74	-8626,50	-8831,59	-8831,59	-15886,94	-15877,82	-15866,05	-15913,72
Enthalpy Flow	KW	-19,27	-19,18	-19,63	-19,63	-794,35	-793,89	-119,00	-119,35
Molar Entropy	KJ/KMOL-K	-259,71	-254,86	-323,58	-322,31	-164,51	-163,95	-163,23	-166,17
Mass Entropy	KJ/KG-K	-2,50	-2,45	-3,11	-3,10	-9,13	-9,10	-9,06	-9,22
Molar Density	KMOL/CUM	0,12	0,41	11,18	0,52	55,41	55,38	55,34	55,47
Mass Density	KG/CUM	12,45	42,11	1162,00	53,86	998,19	997,72	997,02	999,27
Average Molecular Weight		103,95	103,95	103,95	103,95	18,02	18,02	18,02	18,02

Table E.2 : Simulation Results for R134a

	Units	S1	S2	S3	S4	WC-IN	WC-OUT	WE-IN	WE-OUT
From		EVAP	COMP	COND	EXV				
To		COMP	COND	EXV	EVAP	COND	COND	EVAP	EVAP
Sub stream: MIXED									
Phase:		Vapor	Vapor	Liquid	Mixed	Liquid	Liquid	Liquid	Liquid
Component Mole Flow									
C2H2F4	KMOL/HR	0,082	0,082	0,082	0,082	0	0	0	0
H20	KMOL/HR	0	0	0	0	6,66	6,66	2,00	2,00
Mole Flow	KMOL/HR	0,082	0,082	0,082	0,082	6,66	6,66	2,00	2,00
Mass Flow	KG/HR	8	8	8	8	120	120	36	36
Volume Flow	L/MIN	13,91	4,98	0,12	2,67	2,00	2,01	0,60	0,60
Temperature	C	23,53	73,78	25	-6,48	20	23,74	25	14,69
Pressure	MPa	0,23	0,72	0,72	0,23	0,07	0,07	0,04	0,04
Vapor Fraction		1	1	0	0,21	0	0	0	0
Liquid Fraction		0	0	1	0,79	1	1	1	1
Molar Enthalpy	KJ/KMOL	-896360	-892360	-915340	-915340	-286210	-285930	-285830	-286610
Mass Enthalpy	KJ/KG	-8785,10	-8745,95	-8971,18	-8971,18	-15886,94	-15871,28	-15866,05	-15909,19
Enthalpy Flow	KW	-20,36	-20,27	-20,80	-20,80	-529,56	-529,04	-158,66	-159,09
Molar Entropy	KJ/KMOL-K	-239,39	-235,81	-311,13	-310,06	-164,51	-163,55	-163,23	-165,88
Mass Entropy	KJ/KG-K	-2,35	-2,31	-3,05	-3,04	-9,13	-9,08	-9,06	-9,21
Molar Density	KMOL/CUM	0,10	0,27	11,83	0,51	55,41	55,36	55,34	55,46
Mass Density	KG/CUM	10,00	27,93	1206,57	52,00	998,19	997,35	997,02	999,12

Table E.3 : Simulation Results for R134a/R125 (50/50 wt %)

	Units	S1	S2	S3	S4	WC-IN	WC-OUT	WE-IN	WE-OUT
From		EVAP	COMP	COND	EXV				
To		COMP	COND	EXV	EVAP	COND	COND	EVAP	EVAP
Sub stream: MIXED									
Phase:		Vapor	Vapor	Liquid	Mixed	Liquid	Liquid	Liquid	Liquid
Component Mole Flow									
C2H2F4	KMOL/HR	0,032	0,032	0,032	0,032	0	0	0	0
C2HF5	KMOL/HR	0,014	0,014	0,014	0,014	0	0	0	0
H2O	KMOL/HR	0	0	0	0	9,99	9,99	0,67	0,67
Mole Flow	KMOL/HR	0,047	0,047	0,047	0,047	9,99	9,99	0,67	0,67
Mass Flow	KG/HR	5	5	5	5	180	180	12	12
Volume Flow	L/MIN	7,18	2,44	0,07	1,45	3,00	3,00	0,20	0,20
Temperature	C	20,25	67,55	18,29	-12,72	14,90	16,27	25,00	7,86
Pressure	MPa	0,25	0,81	0,81	0,25	0,07	0,07	0,04	0,04
Vapor Fraction		1	1	0	0,23	0	0	0	0
Liquid Fraction		0	0	1	0,77	1	1	1	1
Molar Enthalpy	KCAL/KMOL	-229050	-228150	-233470	-233470	-68451	-68427	-68270	-68579
Mass Enthalpy	KJ/KG	-8919,81	-8884,89	-9092,10	-9092,10	-15908,29	-15902,53	-15866,05	-15937,84
Enthalpy Flow	KW	-12,39	-12,34	-12,63	-12,63	-795,41	-795,13	-52,89	-53,13
Molar Entropy	KJ/KMOL-K	-242,06	-239,27	-313,29	-312,14	-165,83	-165,47	-163,23	-167,70
Mass Entropy	KJ/KG-K	-2,25	-2,23	-2,91	-2,90	-9,20	-9,19	-9,06	-9,31
Molar Density	KMOL/CUM	0,11	0,32	11,52	0,53	55,46	55,45	55,34	55,50
Mass Density	KG/CUM	11,61	34,11	1238,51	57,33	999,10	998,89	997,02	999,83
Average Molecular Weight		107,51	107,51	107,51	107,51	18,02	18,02	18,02	18,02

Table E.4 : Simulation Results for R134a/R125 (66/34 wt %)

		S1	S2	S3	S4	WC-IN	WC-OUT	WE-IN	WE-OUT
From		EVAP	COMP	COND	EXV				
To		COMP	COND	EXV	EVAP	COND	COND	EVAP	EVAP
Sub stream: MIXED									
Phase:		Vapor	Vapor	Liquid	Mixed	Liquid	Liquid	Liquid	Liquid
Component Mole Flow									
C2H2F4	KMOL/HR	0,045	0,045	0,045	0,045	0	0	0	0
C2HF5	KMOL/HR	0,020	0,020	0,020	0,020	0	0	0	0
H2O	KMOL/HR	0	0	0	0	9,99	9,99	1,53	1,53
Mole Flow	KMOL/HR	0,07	0,07	0,07	0,07	9,99	9,99	1,53	1,53
Mass Flow	KG/HR	7	7	7	7	180	180	27,6	27,6
Volume Flow	L/MIN	10,12	3,53	0,09	2,08	3,00	3,00	0,46	0,46
Temperature	C	22	68,30	19	-12,70	14,9	16,82	25	14,53
Pressure	MPa	0,25	0,79	0,79	0,25	0,07	0,07	0,04	0,04
Vapor Fraction		1	1	0	0,23	0	0	0	0
Liquid Fraction		0	0	1	0,77	1	1	1	1
Molar Enthalpy	KJ/KMOL	-958810	-955110	-977390	-977390	-286590	-286450	-285830	-286620
Mass Enthalpy	KJ/KG	-8918,32	-8883,90	-9091,12	-9091,12	-15908,29	-15900,23	-15866,05	-15909,88
Enthalpy Flow	KW	-17,34	-17,27	-17,68	-17,68	-795,41	-795,01	-121,64	-121,98
Molar Entropy	KJ/KMOL-K	-241,52	-238,77	-312,93	-311,74	-165,83	-165,33	-163,23	-165,93
Mass Entropy	KJ/KG-K	-2,25	-2,22	-2,91	-2,90	-9,20	-9,18	-9,06	-9,21
Molar Density	KMOL/CUM	0,11	0,31	11,49	0,52	55,46	55,44	55,34	55,46
Mass Density	KG/CUM	11,52	33,06	1235,37	56,09	999,10	998,79	997,02	999,14
Average Molecular Weight		107,51	107,51	107,51	107,51	18,02	18,02	18,02	18,02

Table E.5 : Simulation Results for R507

	Units	S1	S2	S3	S4	WC-IN	WC-OUT	WE-IN	WE-OUT
From		EVAP	COMP	COND	EXV				
To		COMP	COND	EXV	EVAP	COND	COND	EVAP	EVAP
Sub stream: MIXED									
Phase:		Vapor	Vapor	Liquid	Mixed	Liquid	Liquid	Liquid	Liquid
Component Mole Flow									
C2HF5	KMOL/HR	0,029	0,029	0,029	0,029	0	0	0	0
C2H3F3	KMOL/HR	0,042	0,042	0,042	0,042	0	0	0	0
H20	KMOL/HR	0	0	0	0	9,99	9,99	1,50	1,50
Mole Flow	KMOL/HR	0,071	0,071	0,071	0,071	9,99	9,99	1,50	1,50
Mass Flow	KG/HR	7	7	7	7	180	180	27	27
Volume Flow	L/MIN	9,18	2,62	0,11	2,34	3,0	3,0	0,45	0,45
Temperature	C	23,73	79,20	18,63	-21,17	14,9	16,82	25	14,83
Pressure	MPa	0,30	1,17	1,17	0,30	0,07	0,07	0,04	0,04
Vapor Fraction		1	1	0	0,31	0	0	0	0
Liquid Fraction		0	0	1	0,69	1	1	1	1
Molar Enthalpy	KJ/KMOL	-886870	-882630	-903090	-903090	-286590	-286450	-285830	-286600
Mass Enthalpy	KJ/KG	-8971,01	-8928,15	-9135,12	-9135,12	-15908,29	-15900,24	-15866,05	-15908,60
Enthalpy Flow	KW	-17,44	-17,36	-17,76	-17,76	-795,41	-795,01	-119,00	-119,31
Molar Entropy	KJ/KMOL-K	-244,37	-241,69	-309,34	-307,50	-165,83	-165,33	-163,23	-165,85
Mass Entropy	KJ/KG-K	-2,47	-2,44	-3,13	-3,11	-9,20	-9,18	-9,06	-9,21
Molar Density	MOL/CC	0,00	0,00	0,01	0,00	0,06	0,06	0,06	0,06
Mass Density	KG/CUM	12,71	44,47	1078,97	49,90	999,10	998,79	997,02	999,10
Average Molecular Weight		98,86	98,86	98,86	98,86	18,02	18,02	18,02	18,02

Table E.6 : Simulation Results for R125

Updated									
	Units	S1	S2	S3	S4	WC-IN	WC-OUT	WE-IN	WE-OUT
From		EVAP	COMP	COND	EXV				
To		COMP	COND	EXV	EVAP	COND	COND	EVAP	EVAP
Sub stream: MIXED									
Phase:		Vapor	Vapor	Liquid	Mixed	Liquid	Liquid	Liquid	Liquid
Component Mole Flow									
H2O	KMOL/HR	0	0	0	0	6,66	6,66	1,33	1,33
C2HF5	KMOL/HR	0,067	0,067	0,067	0,067	0	0	0	0
Mole Flow	KMOL/HR	0,067	0,067	0,067	0,067	6,66	6,66	1,33	1,33
Mass Flow	KG/HR	8	8	8	8	120	120	24	24
Volume Flow	CUM/HR	0,38	0,13	0,007	0,11	0,12	0,12	0,024	0,024
Temperature	C	20	68,34	21	-15,35	20	22,55	25	14,89
Pressure	MPa	0,4	1,30	1,30	0,4	0,07	0,07	0,04	0,04
Vapor Fraction		1	1	0	0,32	0	0	0	0
Liquid Fraction		0	0	1	0,68	1	1	1	1
Solid Fraction		0	0	0	0	0	0	0	0
Molar Enthalpy	KJ/KMOL	-1101400	-1097500	-1116700	-1116700	-286210	-286020	-285830	-286590
Mass Enthalpy	KJ/KG	-9177,03	-9144,02	-9303,96	-9303,96	-15886,94	-15876,28	-15866,05	-15908,37
Enthalpy Flow	KW	-20,39	-20,32	-20,68	-20,68	-529,56	-529,21	-105,77	-106,06
Molar Entropy	KJ/KMOL-K	-265,41	-261,75	-325,37	-323,66	-164,51	-163,85	-163,23	-165,83
Mass Entropy	KJ/KG-K	-2,21	-2,18	-2,71	-2,70	-9,13	-9,10	-9,06	-9,21
Molar Density	KMOL/CUM	0,18	0,53	10,11	0,63	55,41	55,38	55,34	55,46
Mass Density	KG/CUM	21,11	63,33	1213,51	75,77	998,19	997,63	997,02	999,09
Average Molecular Weight		120,02	120,02	120,02	120,02	18,02	18,02	18,02	18,02

Appendix F: Simulation Procedure

Aspen Refrigeration Cycle Simulation Procedure

Getting Started

- Open the Aspen user interface, click on file then on new.
- With the Installed Templates highlighted on the left and blank simulation to the right, select Create. Component selection platform pops up.

Properties

- On the component specification tab, specify all components to be used in the simulation. On the third column with heading Component name type the chemical name for the substance to be used in the simulation. Then click on find to recall the component from the Aspen Database.
- If the component (substance) does not exist in the databank it can be added using User Defined option.
- The sequence in which the components are specifications does not matter, they can be specified in any order. When all the components have been entered then click next.
- Method specification template comes up, then selected the method to be used in the simulation.In this case, REFPROP method is selected from a list of methods available in Aspen database as it is the method selected for this study.
- The physical properties of the components selected can be viewed by clicking the Retrieve Parameters Icon.

Simulation

- At the bottom left-hand corner of the user interface, a statement that notifies that Required Properties Input Complete. Then click on Simulation Icon situated on the at the bottom left corner.
- A blank Flowsheet comes up with a components bar at the bottom labeled model palette. Then from the model palette select the four components of a refrigeration cycle and drag them to the main-flowsheet.
- For the evaporator and the condenser –Click on Exchangers, Select HeatX then Gen HT. Then rename the blocks as EVAP and COND respectively.
- For the compressor –Click on Pressure Changers, Select Compr, then ICON2
- For the expansion valve-Click on Pressure Changers, Select Valve, then VALVE2.

- For the connecting line click the arrow on the material, then on the Material Icon. Connect on the component to the next to produce a closed cycle with HTF lines flowing into and out of the heat exchange.
- Rename the streams and produce a complete flowchart as shown in Figure 7.11.
- To set the fix parameters on the component Right click on the component then select Input or double click.

Appendix G: Lists of Refrigerants utilised in this study

Table G 1: List of Refrigerants used in this study.

ASHRAE Number	IUPAC CHEMICAL NAME	Molecular Formula	Type
R12	Dichlorodifluoromethane	CCl_2F_2	CFC
R22	Chlorodifluoromethane	$CHClF_2$	HCFC
R32	Difluoromethane	CH_2F_2	HFC
R125	Pentafluoroethane	C_2HF_5	HFC
R134a	1,1,1,2-Tetrafluoroethane	C2H2F4	HFC
R152	1,2-Difluoroethane	$C_2H_4F_2$	HFC
R152a	1,1-Difluoroethane	$C_2H_4F_2$	HFC
R600	Butane	$CH_3CH_2CH_2CH_3$	HC
R600a	Isobutane	$CH(CH_3)_2CH_3$	HC
R404A	R-125/143a/134a (44/52/4)	$C_2HF_5/C_2H_3F_3/C_2H_2F_4$	HFC
R407A	R-32/125/134a (20/40/40)	$CH_2F_2/C_2HF_5/C_2H_2F_4$	HFC
R407B	R-32/125/134a (10/70/20)	$CH_2F_2/C_2HF_5/C_2H_2F_4$	HFC
R407C	R-32/125/134a (23/25/52)	$CH_2F_2/C_2HF_5/C_2H_2F_4$	HFC
R407F	R-32/125/134a (30/30/40)	$CH_2F_2/C_2HF5/C_2H_2F_4$	HFC
R408A	R-125/143a/22 (7/46/47)	$C_2HF_5/C_2H_3F_3/CHClF_2$	HCFC
R410A	R-32/125	CH_2F_2/C_2HF_5	HFC
R413a	R-218/134a/600a (9/88/3)	$C_3H_8/C_2H_2F_4/C_4H_{10}$	HFC
R507a	R-125/143a (50/50)	$C_2HF_5/C_2H_3F_3$	HFC
R744	Carbon dioxide	CO_2	
R1270	Propene (Propylene)	$CH_3CH=CH_2$	HO
R1234yf	2,3,3,3-Tetrafluoropropene	$C_3H_2F_4$	HFO
R1234ze	1,3,3,3- Tetrafluoropropene	$C_3H_2F_4$	HFO